Doctor of Engineering Thesis

Study and research for high-moisture refuse incinerator using biomass gas derived from gasification as a fuel source

(バイオマスガスを利用した高含水廃棄物の焼却炉に関する研究)

Yaowateera Achawangkul
Division of Systems Engineering,
Graduate School of Engineering, Mie University
Tsu, Mie, Japan

September, 2014

ABSTRACT

High-moisture refuse incineration has recently presented several problems, such as consuming a great deal of petroleum fuel and releasing pollution after the process if the incinerator has a low efficiency. This research, therefore, purposes to study biomass-producing gas derived from the gasification process to incinerate high-moisture materials by conducting a laboratory scale experiment. Then, a Computational Fluid Dynamics analysis was carried out by referring to the experimental results in order to investigate the combustion and flow characteristics inside the actual scale of the incinerator.

In Chapter 1, overviews of recent problems regarding high-moisture refuse incineration, advantages of biomass energy resource and significant objectives of this research are introduced.

In Chapter 2, details about literature are reviewed for both biomass gasification and incineration technologies. In addition, the principal calculations used for an experimental apparatus (gasifier and incinerator) design are described.

Chapter 3 explains the methodology to calculate and design a biomass gasifier and incinerator prototype used for experimental conduction. The existing capacity of the gasifier is equal to 30 kilowatts-thermal. The designed incinerator contains a double chamber, in which the volume for the primary and secondary chamber is 0.104 and 0.03 m^3, respectively.

Chapter 4 describes the details about setting up the experimental apparatus with the biomass property and sampled material. Four kinds of biomasses were examined for proper fuel to produce biomass fuel gas. Five kilograms with a 60% moisture content of fresh meat were selected as a high moisture sample. During the experimental conduction, necessary data were measured and recorded, such as the temperature, electricity consumption, gas and air volumetric flow rate, and the opacity of the combustion exhaust gas. In addition, some biomass producer gas was sampled and analyzed by Gas Chromatography.

In Chapter 5, the experimental conduction procedures are presented with the experimental results. It was found that the biomass gas quality became best when the temperature of the gasifier's reduction zone achieved more than 900 deg-C with a rich constituent of CO and the highest calorific value. The temperature of the incinerator's primary and secondary combustion chambers achieved the highest temperature at approximately 750 deg-C if the combustion equivalent ratio in the gas burner was set to 0.9, and the temperature decreased gradually if the equivalent ratio was lower than 0.9. In addition, the best result for high moisture material combustion inside the primary chamber occurred when the amount of excess air was 100% of the meat's stoichiometric air. By this condition, the temperature of both primary and secondary combustion chambers was 500 and 750 deg-C, respectively, and the pollution release was 10% of the opacity exhaust gas. In contrast, the overall temperature decreased if there was a large amount of air in the combustion chamber, which was 150% and 230% excess air, and there was a tendency towards the instability of the combustion chamber's temperature. Moreover, an evaluation system energy balance was also carried out. It was found that the efficiency of the incinerator was 15% when both primary and secondary combustion chambers were operated.

In Chapter 6, the CFD analysis was implemented in the standard model of a high-moisture refuse incinerator in order to investigate the temperature profile and combustion characteristics. A standard k-epsilon model, SIMPLE algorithm, and the first-order upwind method were used to solve the fluid flow numerical problem. The simulation results showed that the maximum temperature occurring from fuel gas-air combustion became highest at 1,700 K, which is close to the theoretical flame temperature of biomass producer gas. The modified model simulation resulted in a more efficient heat distribution and turbulent intensity compared with the traditional model. In addition, it was discovered that the rate of NO formation became highest if there was only primary burner in operation and the rate decreased when both primary and secondary chambers were in operation. These simulation results also support the advantages of the double-chambered incinerator for pollution reduction.

Chapter 7 explains the conclusion of this research, summarizing how the biomass producer gas derived from the gasification process can be applied to high-moisture refuse incineration using the double-chambered incinerator, because significant combustion properties, such as maximum temperature and emission preventing availability, are similar to those using petroleum as a fuel source. Accordingly, the benefit of biomass utilization for high-moisture refuse incineration is not only able to replace petroleum fuel, but it is also able to reduce the environmental impact from petroleum fuel combustion.

In conclusion, the results obtained from this research will be available for other combustion applications concerning biomass producer gas use as a fuel, as well as for the possibility of research and development of gasification and incineration technology in order to gain a higher effectiveness in the future.

ACKNOWLEDGEMENTS

First of all, I would like to record my heartfelt gratitude to my supervisor Associate Professor Maruyama Naoki for his invaluable guidance, cordial advice and constant encouragement throughout this research since I have started as a Ph.D. student at Mie University. I feel very fortunate to have this opportunity to work with him and I shall always remain obliged to his greatness in devoting a large share of his valuable time and knowledge to this work.

I would like to express my sincere gratitude to Assistant Professor Chatchawan Chaichana of the Faculty of Engineering, Chiang Mai University of Thailand, for his kind support during I have conducted my experiments at Chiang Mai University until I obtained enough perfect experimental results to prepare my dissertation, as well as comments to prepare the international journals and dissertation.

I truly would like to acknowledge to Professor Hirota Masafumi and Associate Professor Nishimura Akira of the Mechanical Engineering Department, Mie University for their every valuable comments given to me, in order to conduct the efficient experiment, and the suggestions to improve the quality of my research papers and dissertation.

I also wish to acknowledge to the Dean of Faculty of Engineering, Chiang Mai University, for the great favor I have obtained to conduct my experiment at the faculty. I also thank to all member staffs of the Renewable Energy and Energy Conservation Laboratory and the Energy Technology for Environment Research center (ETERC) for their kind support when I have stayed and carried out my experiment. Likewise, I hope to thank to Associate Professor Kulachate Pienthong of Ubon Rachathani University for many suggestions about how to conduct the effectively research concerning to biomass gasification, as well as Mr. Thanadej Kanthachote, the Managing Director of J.E.N. Construction Co. Ltd. for his kind support for the perfect experimental apparatuses construction.

I would like to acknowledge the deputy director general of the Department of Alternative Energy Development and Efficiency (DEDE), Dr. Twarath Sutabutr, to give me the great opportunity to study for Ph.D. program in Japan, and the staffs of the Energy Research Bureau of DEDE to give me much valuable information for my dissertation conduction. I also hope to acknowledge to the Committee of Thailand Petroleum Development Support Fund for my scholarship and financial supports.

I sincerely hope to mention the students at the Energy System Design Laboratory of Mie University for their assisting during I have been at this laboratory. Moreover, I wish to thank to Thai students at Mie University for the good memory during my staying.

Finally, I would like to take this opportunity to thank my father and mother, my brother and sister, including all of my cousins, for their constant affections, encouragements, and supports since I have come to Japan until I can finish my task as a Ph.D.

Yaowateera Achawangkul

September, 2014

Table of Contents

Abstracts i
Acknowledgements iii
List of Figures viii
List of Tables x
Nomenclatures xi

1. Introduction

1.1 Backgrounds 1
1.2 Recent situation of high-moisture refused incineration and common problems 1
1.3 Research's objectives 2
1.4 Thesis's organizations 2

2. Theory of Gasification and Incineration

2.1 Philosophy of gasification 4
2.2 Types of gasifiers 5
2.3 Prediction of the producer gas composition 8
2.4 Type of the conventional gasifiers 9
2.4.1 The Imbert Downdraft Gasifier
2.4.2 The Stratified Downdraft Gasifier
2.4.3 Tar-Cracking Gasifiers
2.4.4 Susanto and Beenackers' gasifier
2.4.5 Three Stages Fluidized-Bed Gasifier
2.5 Literature reviewing on biomass gasification researches 18
2.6 Calculation of the significant parameters of gasification 20
2.6.1 Mass balance in gasifier
2.6.2 Equivalence ratio
2.6.3 Energy balance in gasifier
2.6.4 Gasifier efficiency
2.6.5 Significant equations of thermochemical processes inside the downdraft gasifier
2.6.6 Fluid flow equation of the downdraft biomass gasifier
2.6.7 Heat transfer
2.6.8 Properties of biomass producer gas
2.7 Producer gas treatment systems 26
2.7.1 Cyclone separator

2.7.2 Condenser (Tar extraction unit)
2.7.3 Fabric filter
2.8 Overview of incineration technology 28
2.9 Classification of incinerators 28
2.9.1 Multiple-chamber incinerator
2.9.2 Controlled-air incinerators
2.9.3 Rotary kiln incinerator
2.10 Combustion process calculations in the incinerator 32
2.10.1 Heat balance
2.10.2 Specific heat and enthalpy
2.10.3 Temperature calculation
2.10.4 Adiabatic flame temperature
2.10.5 Stoichiometry and combustion equivalent ratio
2.11 Concepts of high-moisture material incineration process 35
2.12 Combustion residence time 35
2.13 Characteristics of turbulent nonpremixed flame 36
2.14 Theory and calculation of gas burner 37
2.14.1 Calculation for partially-aerated burner

3. Calculation and Design for the Experimental Apparatuses

3.1 Design on downdraft biomass gasification system 43
3.2 Calculation and design on double-chambered incinerator prototype 44
3.3 Calculation and design on biomass producer gas burner 47
3.3.1 Burner's orifice
3.3.2 Mixing room
3.3.3 Burner throat
3.4 Design of the producer gas treatment systems 48
3.4.1 Cyclone
3.4.2 Condenser (Tar extraction unit)

4. Apparatuses Preparation and Experiment Conduction

4.1 Biomass fuels 52
4.2 High-moisture material sampling 53
4.3 Experiment measurements 53
4.3.1 Gas and air volumetric flow rate
4.3.2 Temperature measurement
4.3.3 Electricity consumption

4.3.4 Exhaust gas property
4.3.5 Opacity of exhaust gas
4.4 Experimental apparatuses set up …… 56
4.4.1 Prototype of high-moisture material incinerator
4.4.2 Producer gas tube and flow control
4.4.3 Electrical devices
4.5 Conduction for the experiment ……... 57
4.6 Biomass producer gas sampling ……. 59

5. Evaluations on Experimental Results and Discussions
5.1 Biomass producer gas analysis ……... 60
5.2 Combustion temperature of biomass producer gas at any equivalence ratio ……. 61
5.3 Flame shape and theoretical flame length calculation ……... 62
5.4 Temperature accuracies inside the double-chambered incinerator prototype …… 65
5.5 Results on pollution investigation ……... 68
5.6 Energy balance evaluations …… 69
5.6.1 Energy input
5.6.2 Energy output
5.6.3 Results on energy balance evaluation and discussions
5.7 Chapter's conclusions …… 75

6. Investigation of actual scale incinerator's combustion characteristics by using CFD analysis
6.1 Philosophy of Computational Fluid Dynamics Analysis ……... 77
6.2 Literature reviewing for CFD analysis in combustion and incineration schemes ……... 77
6.3 Related equations used for CFD analysis …… 78
6.3.1 Governing equations
6.3.2 Partial differential equation for heat transfer analysis
6.3.3 Turbulence equations
6.3.4 Standard $k-\varepsilon$ model
6.3.5 Finite volume method
6.3.6 Diffusion and heat transfer solution
6.3.7 Convection and diffusion problem
6.3.8 Flow field problem
6.4 Three-Dimensions model implementations ……... 91
6.5 Grid sensitivity study …… 93
6.6 Initial conditions of simulation ……..…….... 94
6.7 Boundary conditions and chemical kinetics of biomass gas combustion ……. 95

6.8 Results on CFD analysis and discussions …….. 96
6.8.1 Temperature profiles
6.8.2 Turbulent intensity
6.8.3 Results on prediction of nitrogen oxide (NO) formation
6.9 Analysis of combustion chamber's shape effect to residence time …… 104
6.8.1 Differential equations
6.8.2 Chamber's model implementation
6.8.3 Residence time analysis results
6.10 Chapter's conclusions …… 109

7. Conclusions

7.1 Summary of major conclusions …….. 110
7.2 Highlights of study and further works ……..… 111

References

Appendix A Experimental Apparatuses' Drawings

Appendix B Specific Properties of Materials

List of Publications

List of Figures

Figures	Page
1-1 Schematic diagram of the commercial double-chambered incinerator	2
2-1 Diagram for Updraft Gasifier	6
2-2 Diagram for Downdraft Gasifier	6
2-3 Diagram for Crossdraft Gasifier	7
2-4 Fluidized-bed Gasifier	8
2-5 Schematic diagram for stratified downdraft gasifier	12
2-6 Schematic diagram for the DeLaCotte tar-recycling gasifier	13
2-7 Principle process of Susanto and Beenackers' gasifier with internal recycle and separate combustion of pyrolysis gas	14
2-8 Schematic layout of the three stages gasifier	15
2-9 Cyclone cut size versus inlet width	27
2-10 Retort type multiple-chamber pathological waste incinerator	30
2-11 In-line type multiple-chamber incinerators	30
2-12 Diagram of a Rotary Kiln with a Secondary Combustion Chamber	32
2-13 General layout of an atmospheric injection aerated burner	38
3-1 Drawing of gasifier prototype	44
3-2 Drawing of designed double-chambered incinerator prototype	46
3-3 Dimension of designed gas burner	48
3-4 Significant dimension for high efficiency cyclone design	49
3-5 Designed producer gas's cyclone	50
3-6 Three dimension drawing of tar extraction unit	51
3-7 Schematic drawing of the tar extraction unit used in this research	51
4-1 Selected biomass fuel	52
4-2 Photography of Venturi flow meters and manometers used in the experiment	54
4-3 Schematic diagram of the data loggers and power meters arrangement	54
4-4 Data loggers and power meters set up	55
4-5 Ringelmann's chart	55
4-6 Prototype of high-moisture material's double-chambered incinerator	56
4-7 Schematic diagram of experimental apparatuses	57
4-8 Gasifier's reduction zone	58
4-9 Introduction of biomass fuel into the gasifier	58
4-10 Ignition of biomass producer gas at the primary burner	59

Figures **Page**

4-11 Biomass producer gas sampling 59
5-1 Maximum temperature occurring when adjust any equivalence ratio 61
5-2 Shape of flame when adjust any equivalence ratio 62
5-3 Estimation results of producer gas flame length at any equivalence ratio 64
5-4 Relationship between flame length with ratio of fuel gas and air density 64
5-5 Temperature accuracies of primary and secondary chamber when adjust any excess air condition 66
5-6 Exhaust gas opacity 69
5-7 Evaluated energy loss through exhaust gas 72
6-1 Position of 2-dimension control volume 83
6-2 Staggered grid arrangement 86
6-3 Arrangement of the control volume p-cell 86
6-4 Arrangement of the control volume u-cell 86
6-5 Arrangement of the control volume v-cell 87
6-6 Flow chart of SIMPLE method 90
6-7 Schematic dimension of the double-chambered incinerator model 91
6-8 Double-chambered incinerator's model with arrangement of air nozzle and angle 92
6-9 Combusted material model implementation in the incinerator 93
6-10 Classification of grid type in sensitivity study 93
6-11 Temperature contours inside the primary chamber with a material model 97
6-12 Temperature contours inside the secondary chamber model 99
6-13 Turbulent intensity (%) contour of the primary chamber 100
6-14 Turbulent intensity (%) contour of the secondary chamber 100
6-15 NO prediction if operating only primary chamber 101
6-16 NO prediction if operating both primary and secondary chamber 102
6-17 NO prediction simulation results at any fuel-gas equivalent ratio 103
6-18 Rate of NO formation at gas burner when adjusting any fuel-gas equivalent ratio 103
6-19 Models for residence time analysis 105
6-20 Simulation results of the residence time of the rectangular chamber type (Model A) 106
6-21 Simulation results of the residence time of the cylinder type (Model B) 106
6-22 Simulation results of the residence time of the cylinder type (Model C) 107
6-23 Simulation results of the residence time when increasing the chamber's height 108

List of Tables

Tables	Page
2-1 Comparison for each type of conventional downdraft gasifiers	16
2-2 Coefficients for Antoine equation for saturation vapour pressure	22
2-3 Chemical reactions in oxidation zone	23
2-4 Chemical reactions in reduction zone	24
2-5 Combustion mechanisms of solid material	35
3-1 Composition of producer gas generated from wood	43
3-2 Determined parameters for gasifier design	44
4-1 Proximate and ultimate analysis of selected biomasses	52
4-2 Ultimate analysis for high-moisture material	53
5-1 Biomass producer gas analysis results	60
5-2 Heating value of biomass producer gas	60
5-3 Evaluation results of heat loss through incinerator's wall	73
5-4 Results of energy balance calculation if operate only primary chamber	74
5-5 Results of energy balance calculation if operate both primary and secondary chambers	75
6-1 Constants used in the standard $k-\varepsilon$ model	81
6-2 Comparison between transport equations of 2-dimension turbulent flow with the ordinary equations	82
6-3 Dimension of each double-chambered incinerator model	91
6-4 Grid sensitivity study results	94
6-5 Boundary conditions values	95
6-6 Pre-exponential factors and activation energy values of biomass gas combustion reactions	96

Nomenclatures

A	area (m^2), pre-exponential factor
A/F	air-fuel ratio
B_h	hearth load ($Nm^3\ h^{-1}cm^{-2}$)
C_d	coefficient of discharge
C_p	specific heat ($kJ\ kg^{-1}K^{-1}$)
D_p	cyclone cut side
d_j^*	momentum diameter
E_A	activation energy
E_a	energy in the reaction air (MJ)
E_g	energy in the producer gas (MJ)
F/A	fuel-air ratio
Fr_f	Froude number
f	friction factor
g	acceleration due to gravity ($m\ s^{-2}$)
h	relative humidity ratio
h_f	enthalpy of formation
$\overline{h}_i$	standardized enthalpy
$\overline{h}_{f,i}^0$	enthalpy of formation at standard reference state
$\Delta\overline{h}_{s,i}$	sensible enthalpy change
k	thermal conductivity ($W\ m^{-1}K^{-1}$), turbulent kinetic energy ($m^2\ s^{-2}$)
k_{dev}	pressure drop parameter
L^*	dimensionless flame length
MW	molecular weight
$\dot{m}$	mass flow rate ($kg\ s^{-1}$)
N_e	number of cyclone's centrifugal round
P	pressure (Pa)
p_v	saturated vapour pressure of water (Pa)
$Q_{H.E.}$	heat transfer rate of heat exchanger
Q_{net}	net heat generation
$(Q_R)_V$	heat release ($MJ\ m^{-3}\ hr^{-1}$)
$\dot{Q}$	heat transfer rate (Watt)

$(R_{A/C})_r$	air-fuel real relation
$(R_{A/C})_s$	air-fuel stoichiometric relation
Re	Reynolds number
R_u	Universal gas constant (J kmol^{-1} K^{-1})
r	entrainment ratio
SG	specific gravity
T	temperature (^{o}C, K)
T_{ad}	adiabatic flame temperature (^{o}C, K)
t_{res}	residence time (s)
U	Overall heat transfer coefficient (W m^{-2} K^{-1}), standardized internal energy of the mixture
V	velocity (m s^{-1})
V_s	superficial velocity (m s^{-1})
W	mass flow rate of gas (mol h^{-1})
X	Molar concentration (kmol kmol^{-1})
Y	mass concentration (kg kg^{-1})

Greek letters

β	thermal decomposition parameter
γ	specific heat ratio
ΔH	heat of reaction (kJ kg^{-1})
ξ	gasifier equivalence ratio
ε	porosity, Void fraction, turbulent dissipation rate (m2 s^{-3})
μ	viscosity (N s m^{-2})
η	dimensionless pressure efficiency
η_{th}	thermal efficiency (%)
Φ	equivalence ratio
ρ	density (kg m^{-3})
ρ_∞	density of ambient gas (kg m^{-3})
ρ_e	density of fluid at nozzle (kg m^{-3})
$\overline{\sigma_{ji}}$	deviatoric part of the viscous stress tensor
τ_{ij}	shear stress (N m^{-2})
ω	humidity ratio

Abbreviations

Biomass	biomass
LHV	low heating value (MJ kg^{-1}), (MJ m^{-3})
HHV	high heating value (MJ kg^{-1}), (MJ m^{-3})
RSM	Reynolds stress model
FVM	finite volume method

Subscript

res	residence time

Chapter 1
Introduction

1.1 Backgrounds

High-moisture refused elimination is still a serious problem in many countries such as Thailand, Japan and India, especially, a cremation, or municipal waste incineration. However, the traditional incineration process has mainly used charcoal and fuel wood as fuels, whereas the original incinerator was a simple type and has no pollution treatment. Consequently, there were many environmental impacts to the nearest people. In order to prevent the pollution emission, the Pollution Control Department has established for the standard of emission released from incineration process. In fact, the modern type of incinerator usually uses commercial fuels such as diesel and liquefied petroleum gas (LPG) to make completely combustion, and the operation cost for 60 kg of high moisture waste per one time is about 2,000-3,000 baht (67-100 USD) [(1)]. However, if the global petroleum price is increased in future, the operation cost for cremation will be increased and people will unavoidably pay the expensive. Thus, it is necessary to research and develop for alternative energy utilization in the incineration process which contains low operation cost and emitting low pollution.

Biomass gasification is an incomplete combustion of biomass resulting in production of combustible gases consisting of Carbon monoxide (CO), Hydrogen (H_2) and traces of Methane (CH_4). This mixture is called producer gas [(2)]. Producer gas can be used to run internal combustion engines (both compression and spark ignition). Otherwise, it also can be used as substitute for furnace oil in direct heat applications. Hence, it is necessary to study and research for the application of biomass producer gas-derived from gasification utilization as a fuel in double-chambers incinerator, including studying for the parameters to achieve possibly highest efficiency, are significant issue to introduce a new biomass application, and also reduce petroleum utilization.

1.2 Recent situation of high-moisture refused incineration and common problems

In the past, high-moisture refused was eliminated by outdoor method, or using of traditional incinerator, which contained low efficiency and neglecting the pollution control. In case of complete combustion, product occurred after combustion process usually theoretically are water and carbon dioxide. However, in actual process, some combustion products are generated such as carbon monoxide, sulfur dioxide, dioxin furan, hydrogen sulfide and etc., which are harmful pollutant and may cause of nuisance to the nearest people [(3)]. According to the studying of waste incineration, it was found that the pollution usually occurred when the flame directly contacts with the waste, moisture content is evaporated and makes the combustion temperature decrease rapidly. Moreover, the disintegration of organic composition mainly cause of smell and pollutant, especially when there is inefficient pollution control system [(4)].

Accordingly, a double-chambered incinerator has been introduced and become popular instead of the old type incinerator. The commercial double-chambered incinerator mainly composes of two main combustion chambers. The primary chamber is used to combusted high-moisture waste. After the primary combustion process, dust particle and decomposed gaseous substance is drafted into the secondary chamber and combusted again at high temperature

before releasing to the atmosphere. Figure 1-1 shows the simply diagram of the commercial double-chambered incinerator.

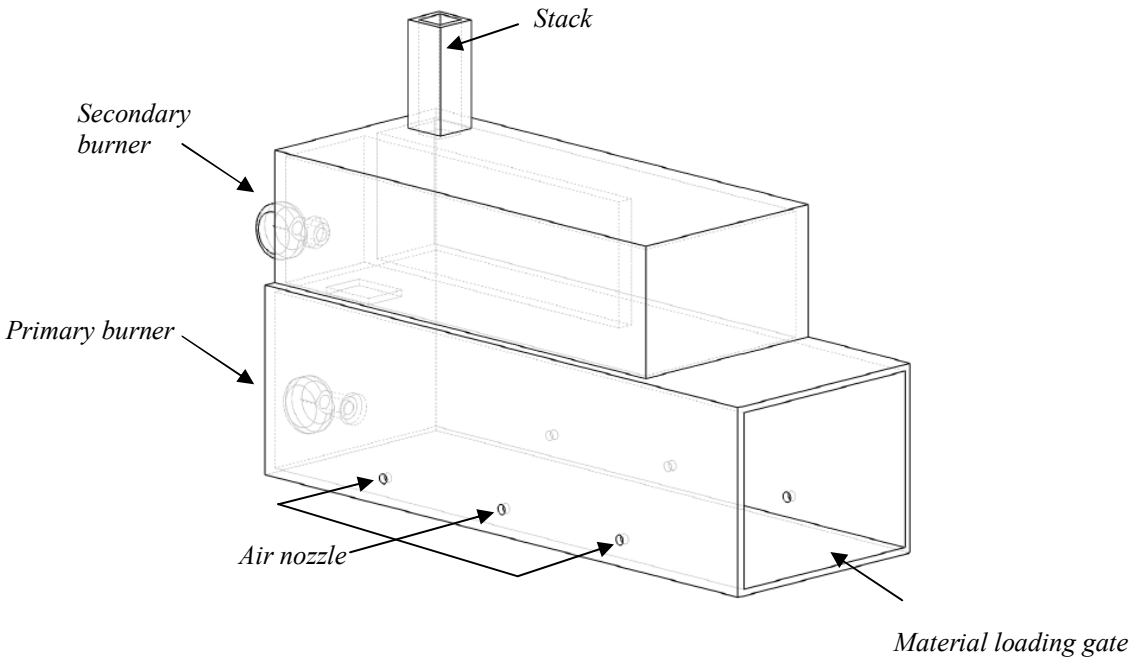

Fig. 1-1 Schematic diagram of the commercial double-chambered incinerator

1.3 Research's objectives

1) To study and research for availability of biomass producer gas-derived from gasification process which proper for using in high moisture materials incineration.
2) To study for the significant combustion behaviors of gasification system and high moisture materials incineration.
3) To evaluate for the efficiency of biomass gas-derived utilization in prototype incinerator, compare to the traditional incinerator.
4) To simulate for combustion characteristics of high moisture materials incineration inside the actual double-chambered incinerator by applying Computational Fluid Dynamics analysis.

1.4 Thesis's organizations

In chapter 1, overviews on recent problem of high moisture materials incineration, advantage of biomass energy resource and significant objectives of this research are introduced.

In chapter 2, this chapter contains of detail about literature reviewing for both of biomass gasification and incineration technologies. In addition, the principal calculations used for experimental apparatus (gasifier and incinerator) design are described.

In chapter 3, this chapter explains for the methodology to calculate and design for biomass gasifier and incinerator prototype used for experimental conduction.

In chapter 4, this chapter describes the details about experimental apparatus setting up, with the property of biomass and sampled material.

In chapter 5, this chapter describes for the detail of experiment conduction procedure. Then, the experimental results and evaluations such as temperature, emission and system energy balance, are reported.

In chapter 6, this chapter explains for the methodology of CFD analysis implemented to the actual model of high moisture material incinerator, in order to investigate temperature distribution, combustion characteristics, including simulation of chamber's residence time in order to examine an adequate time to eliminate combustible toxic gas released from high moisture material combustion.

In chapter 7, this chapter explains for the conclusion of this research.

Chapter 2
Theory of Gasification and Incineration

2.1 Philosophy of gasification

Biomass gasification means incomplete combustion of biomass resulting in production of combustible gases consisting of Carbon monoxide (CO), Hydrogen (H_2) and Methane (CH_4) [(2)]. This mixture is called producer gas. Producer gas can be used to run internal combustion engines (both compression and spark ignition), can be used as substitute for furnace oil in direct heat applications. The process of gasification to produce combustible from organic feeds was used in blast furnaces over 180 years ago. The possibility of using this gas for heating and power generation was soon realized and there emerged in Europe producer gas systems, which used charcoal and peat as feed material. At the turn of the century petroleum gained wider use as a fuel, but during both world wars and particularly World War II, shortage in petroleum supplies led to widespread re-introduction of gasification.

The production of generator gas (producer gas) called gasification, is partial combustion of solid fuel (biomass) and takes place at temperatures of about 1,000^{o}C. The reactor is called a gasifier [(5)]. The combustion products from complete combustion of biomass generally contain nitrogen, water vapor, carbon dioxide and surplus of oxygen. However in gasification where there is a surplus of solid fuel (incomplete combustion) the products of combustion are combustible gases like Carbon monoxide (CO), Hydrogen (H_2) and traces of Methane and non-useful products like tar and dust. The production of these gases is by reaction of water vapor and carbon dioxide through a glowing layer of charcoal. Thus, the key to gasifier design is to create conditions such that a) biomass is reduced to charcoal and, b) charcoal is converted at suitable temperature to produce CO and H_2.

In any gasification system, there are four important reactions that take place.

1) Combustion zone

The combustible substance of a solid fuel is usually composed of elements carbon, hydrogen and oxygen. In complete combustion carbon dioxide is obtained from carbon in fuel and water is obtained from the hydrogen, usually as steam. The combustion reaction is exothermic and yields a theoretical oxidation temperature of 1,450^{o}C.

$$C + O_2 \rightarrow CO_2 \quad (+ 393 \text{ MJ/kg mole}) \qquad (2.1)$$

$$2H_2 + O_2 \rightarrow 2H_2O \quad (- 242 \text{ MJ/kg mole}) \qquad (2.2)$$

2) Reduction zone

The products of partial combustion (water, carbon dioxide and uncombusted partially cracked pyrolysis products) now pass through a red-hot charcoal bed where the following reduction reactions take place.

$$C + CO_2 \rightarrow 2CO \quad (- 164.9 \text{ MJ/kg mole}) \qquad (2.3)$$

$$C + H_2O \rightarrow CO + H_2 \quad (- 122.6 \text{ MJ/kg mole}) \qquad (2.4)$$

CO	+	H_2	→	$CO + H_2O$	(+ 42 MJ/kg mole)	(2.5)
C	+	$2H_2$	→	CH_4	(+ 75 MJ/kg mole)	(2.6)
CO_2	+	H_2	→	$CO + H_2O$	(- 42.3 MJ/kg mole)	(2.7)

3) Pyrolysis zone

Wood pyrolysis is an intricate process that is still not completely understood. The products depend upon temperature, pressure, residence time and heat losses. However following general remarks can be made about them. Up to the temperature of 200°C only water is driven off. Between 200 to 280°C carbon dioxide, acetic acid and water are given off. The real pyrolysis, which takes place between 280 to 500°C, produces large quantities of tar and gases containing carbon dioxide. Besides light tars, some methyl alcohol is also formed. Between 500 to 700°C the gas production is small and contains hydrogen.

$$\textit{Dry biomass (DB)} \xrightarrow{kdry} \textit{Char + Volatiles (CO, } H_2\textit{, } CO_2\textit{, } H_2O\textit{, } CH_4\textit{-equivalent, tar)} \quad (2.8)$$

4) Drying zone

The main process is drying of biomass. Fuel entering the gasifier has moisture content of 10-30%. Various experiments on different gasifiers in different conditions have shown that on an average the condensate formed is 6-10% of the weight of gasified biomass. Some organic acids also come out during the drying process. These acids give rise to corrosion of gasifiers.

2.2 Types of gasifiers

Since there is an interaction of air or oxygen and biomass in the gasification reactor (gasifier), they are classified according to the way air or oxygen is introduced in it. There are three types of gasifiers ; Downdraft, Updraft and Crossdraft. And as the classification implies updraft gasifier has air passing through the biomass from bottom and the combustible gases come out from the top of the gasifier. Similarly in the downdraft gasifier the air is passed from the tuyers in the downdraft direction [6].

1) Updraft Gasifier

An updraft gasifier is widely used for making producer gas from a coal and nonvolatiles fuel such as charcoal. This gasifier type has been the principle used for coal for 150 years.

During operation, biomass is fed into the top while air and steam are fed through a grate, which often is covered with ash. The grated is at the base of the gasifier, and the air and steam react there with charcoal from the biomass to produce very hot carbon dioxide (CO_2) and water (H_2O). In turn, the CO_2 and H_2O react endothermically with the char to form carbon monoxide (CO) and hydrogen (H_2). The temperatures at the grate must be limited by adding either steam or recycled exhaust gas to prevent damage to the grate and slagging from the high temperatures generated when carbon reacts with the air.

The ascending, hot, reducing gases pyrolyze the incoming biomass and cool down in the process. Usually, 5% to 20% of the tars and oils are produced at temperatures too low for significant cracking and air carried out in the gas stream. The remaining heat dries the incoming wet biomass, so that almost none of the energy is lost as sensible heat in the gas.

The updraft gasifier throughput is limited to about 10 GJ/h-m^2 either by bed stability or by incipient fluidization, slagging, and overheating. Large updraft gasifiers are sometimes operated in the slagging mode, in which all the ash is melted on a hearth. This is particularly useful for high-ash fuels such as municipal solid waste (MSW).

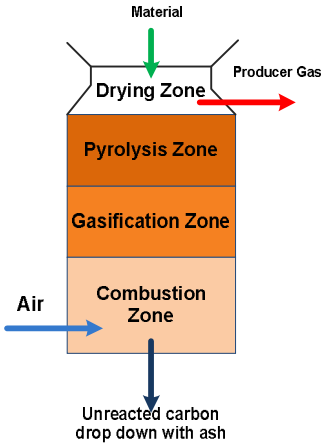

Fig. 2-1 Diagram for Updraft Gasifier

2) Downdraft Gasifier

A downdraft gasifier (or co-current gasifier) was developed to convert high volatile fuels (wood, biomass) to low tar gas, and therefore has proven to be the most successful design for power generation. The producer gas is removed at the bottom of the apparatus, so that fuel and gas move in the same direction. On their way down the acid and tarry distillation products from the fuel must pass through a glowing bed of charcoal and therefore are converted into permanent gases hydrogen, carbon monoxide and methane.

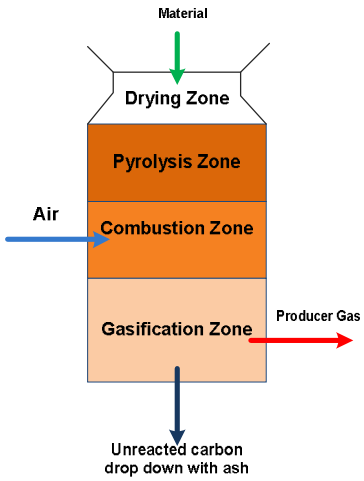

Fig. 2-2 Diagram for Downdraft Gasifier

3) Crossdraft Gasifier

For crossdraft gasifier, it is a simplest and lightest gasifier. Air enters the system at high velovity through a single nozzle, induces substantial circulation, and flows across the bed of fuel and char. Thid produces very high temperatures in a very small volume and results in production of a low-tar gas, permitting rapid adjustment to engine load changes. The fuel and ash serve as insulation for the walls of the gasifier, permitting mild-steel construction for all parts except the nozzles and grates, which may require refractory alloys or some cooling. Air-cooled or water cooled nozzles are often required. The high temperatures reached require a low-ash fuel to prevent slagging.

The crossdraft gasifier is generally considered suitable only for low-tar fuels. Some success has been observed with unpyrolyzed biomass, but the nozzle-to-grate spacing is critical. Unscreened fuels that do not feed into the gasifier freely are prone to bridging and channelling, and the collapse of bridges fills the hearth zone with unpyrolyzed biomass, leading to momentarily high rates of tar production. The fuel size also is very important for proper operation. Crossdraft gasifiers have the fastest response time and the smallest thermal mass of any gas producers because there is a minimum inventory of hot charcoal. In one design, a downdraft gasifier could be operated in a crossdraft scheme during start up in order to minimize the startup time.

Furthermore, the crossdraft gasifier has adopt for the use of charcoal, so it results in very high temperatures (1,500^{o}C and higher) in the oxidation zone which can lead to materials problems.

Advantages of this system lie in the very small scale at which it can be operated. Installations below 10 kW (shaft power) can under certain conditions be economically feasible. The reason is the very simple gas-cleaning train (only a cyclone and a hot filter) which can be employed when using this type of gasifier in conjunction with small gas engines. Nonetheless, there is a disadvantage that the minimal tar-converting capabilities and the consequent need for high quality (low volatile content) charcoal.

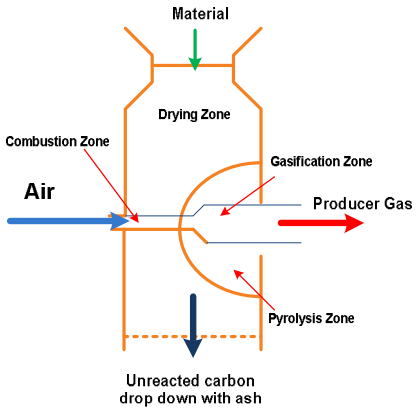

Fig. 2-3 Diagram for Crossdraft Gasifier

4) Fluidized Bed Gasifier

Air is blown through a bed of solid particles at a sufficient velocity to keep these in a state of suspension. The bed is originally externally heated and the feedstock is introduced as soon as a sufficiently high temperature is reached. The fuel particles are introduced at the bottom of the reactor, very quickly mixed with the bed material and almost instantaneously heated up to the bed temperature. As a result of this treatment, the fuel is pyrolyzed very fast resulting in a component mix with a relatively large amount of gaseous materials. Further gasification and tar-

conversion reactions occur in the gas phase. Most systems are equipped with an internal cyclone in order to minimize char-blow out as much as possible. Ash particles are also carried over the top of the reactor and have to be removed from the gas stream if the gas is used in engine applications.

The major advantages of fluidized bed gasifiers, as reported by Van der Aarsen et.al. (1982) [7], stem from their feedstock flexibility resulting from easy control of temperature, which can be kept below the melting or fusion point of the ash (rice husk), and their ability to deal with fluffy and fine grained materials (sawdust and etc.) without the need of pre-processing. Problems with feeding, instability of the bed and fly-ash sintering in the gas channels can occur with some biomass fuel.

Other drawback of the fluidized bed gasifier lies in the rather high tar content of the product gas (up to 500 mg/m^3 gas), the incomplete carbon burn-out, and poor response to load changes.

Particular because of the control equipment needed to cater for the latter difficulty, very small fluidized bed gasifiers are not foreseen and the application range must be tentatively set at about 500 kW (shaft power).

At present, fluidized bed gasifiers are currently available on a semi-commercial basis from several manufacturers in Europe and USA.

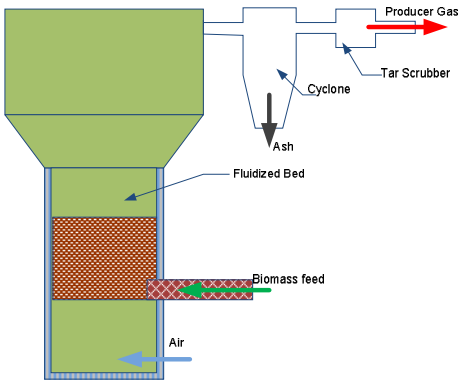

Fig. 2-4 Fluidized-bed Gasifier

2.3 Prediction of the producer gas composition

Tobler and Schelaepfer [8] have introduced the water-gas equilibrium concept, in order to provide the opportunity to calculate the gas composition theoretically from a gasifier which has reached equilibrium at a given temperature.

The procedure is to derive from mass balances of the four main ingoing elements (carbon, hydrogen, oxygen and nitrogen), an energy balance over the system and the relation given by the water-gas equilibrium. By further assuming that the amounts of methane in the producer gas per kilogram of dry fuel are constant (as is more or less the case of gasifiers under normal operating conditions) a set of relations becomes available permitting the calculation of gas compositions for a wide range of input parameters (fuel moisture content) and system characteristics (heat losses through convection, radiation and sensible heat in the gas).

2.4 Type of the conventional gasifiers

2.4.1 The Imbert Downdraft Gasifier

The nozzle (tuyere) and constricted hearth downdraft gasifier is sometimes called the "Imbert" gasifier (after its entrepreneurial inventor, Jacques Imbert) [9]. An air gasifiers can be operated either by forcing air through the fuel (pressurized) or by drawing the air through the fuel (suction). The upper cylindrical part of the inner chamber is simply a magazine for the wood chips or other biomass fuel. During operation, this chamber is filled every few hours as required. The spring-loaded cover is opened to charge the gasifier, and then it is closed during system operation. The spring permits the cover to pop open to relieve pressure in the case of gas explosion.

About one-third of the way from the bottom, there is a set of radially directed air nozzles that permit air to be drawn into the fuel as it moves down to be gasified. Typically, there are an odd number of nozzles so that the hot gases from one nozzle do not impinge on the opposite nozzle. The nozzles are attached to a distribution manifold that in turn is attached to the outer surface of the inner can. This manifold is connected through the outer can to a large air-entry port. One air nozzle is in line with this port, allowing the operator to ignite the charcoal base through this nozzle.

During operation, the incoming air burns and pyrolyzes some of biomass, most of tars and oils and some of the charcoal that fills the gasifier below the nozzles. Most of the mass of biomass is converted to gas within this flaming combustion zone since biomass contains more than 80% volatile matter.

The gasifier is in many ways self-adjusting. If there is insufficient charcoal at the air nozzles, more biomass burned and pyrolyzed to make more charcoal. If too much char forms during high-load conditions, then the char level rises above the nozzles so that incoming air burns the char to reduce the char level. Thus, the reaction zone is maintained at the nozzles.

Below the air nozzle zone lies the gas-reduction zone, usually consisting of a classical Imbert hearth or in later years, of the "V" hearth. Most recently, the flat plate hearth constriction has been introduced. The latter two hearth designs accumulate a layer of retained ash to form a high-quality, self repairing insulation.

In addition, improved insulation in the hearth results in lower tar production and a higher efficiency over a wider range of operating conditions.

After the combustion/pyrolysis of biomass and hot char at the nozzle level, the resulting hot combustion gas (CO_2 and H_2O) pass into the hot char where they are partially reduced to the fuel gas CO and H_2 according to Eq. 2.3 and 2.4. This procedure results in a marked cooling of the gas, and sensible-gas is converted into chemical energy. This removes most of charcoal and improves the quality of the gas. Eventually, the charcoal is dissolved by these gases and disintegrated to smaller chunks and a fine powder that either is swept out with the gases to the cyclone separator of falls through the grate. Tars that have escaped combustion at the nozzle may crack further in the hot char although tar cracking is now thought to occur only above 850^{o}C.

The space between the nozzles allows some unpyrolyzed biomass to pass through. The hearth constriction then causes all gases to pass through the hot zone at the constriction, thus giving maximum mixing and minimum heat loss.

The fine char-ash dust can eventually clog the charcoal bed and will reduce the gas flow unless the dust is removed. The charcoal is supported by a movable grate that can be shaken at intervals. Ash builds up below the grate and can be removed during cleaning operations. However, as the charcoal is consumed, it eventually collapses to

form a powdered char-ash that may represent 2% to 10% of the total biomass, in turn containing 10% to 50% ash. Ash contents depend on the char content of the biomass and the degree of agitation, the greater the degree of char reduction, the smaller the resulting particles and the higher the ash.

The Imbert type gasifier requires a low moisture (<20% moisture) and uniformly blocky fuel in order to allow easy gravity feeding through the constriction hearth. The reduction in area at the hearth and the protruding nozzles present hazards at which the passage of the fuel can be restricted, thus causing bridging and channelling followed by high tar output, as unpyrolyzed biomass falls into the reaction zone.

Superficial velocity, hearth load and gasifier sizing

A superficial velocity, Vs is the important factor for any gasifier dimension choosing. This factor is the gas calculation where it passes through the narrowest part of the gasification zone. The unit of the superficial velocity is usually length/time (e.g. m/s), or gas volume/cross section area-time (m^3/m^2-s), a specific gas production rate. It is called a superficial velocity since actual velocities will be three to six times higher due to the present of the charcoal and the high temperatures existing at the throat. A closely related term is the maximum hearth load, B_h, expressed in gas volume / hearth area-h, expressed in practical units.

In generator gas, a maximum hearth load ($B_{h,max}$) value for an Imbert gasifier type is about 0.9 $Nm^3/h\text{-}cm^2$. In other words, 0.9 m^3 of gas is produced for each square centimetre of cross-sectional area at the constriction. This corresponds to a superficial gas velocity V_s of 2.5 m/s calculated at NTP from the throat diameter and ignoring the presence fuel. This corresponds to a specific gas production rate of 9,000 m^3 of gas per square meter of cross-sectional area per hour.

The maximum hearth load is limited by many factors, such as the mechanical integrity of the char bed structure within the gasifier, degree of agitation, and the time available for conversion. High velocity can disturb the char and fuel bed, causing instability. If char fragments become dislodged and airborne, they may plug the bed or form channels. Therefore, a little agitation can effectively increase the maximum specific hearth load.

Turndown ratio

Turndown ratio is a ratio of the highest practical gas generation rate to the lowest practical rate. For an example, the turndown ratio of World War II gasifiers varied between 3 for Imbert-style gasifiers with uninsulated V-hearthy gasifiers and 18 for highly insulated V-hearth gasifiers. Furthermore, vehicle operation requires turndown ratio of at least 8:1.

Disadvantages of the Imbert design

The Imbert type gasifier has a number of disadvantages. The hearth constriction seriously limits the range of biomass fuel shapes which can be successfully gasified without expensive cubing or pelletizing pretreatment. This gasifier type requires a high-grade, usually hardwood, fuel, generally at least 2 cm along the smallest dimension with no more than 20% moisture.

In addition, the Imbert gasifier cannot be scaled-up to larger sizes because the air enters at the sides and it incapable of penetrating a large-diameter fuel bed unless the fuel size is increased proportionally. The tar level, while low (usually 5,000 ppm), is still high enough to require extensive scrubbing and disposal procedures.

2.4.2 The Stratified Downdraft Gasifier

Stratified downdraft gasifier (or "open-top" or "topless" gasifier) has been developed through cooperative efforts among researchers at Solar Energy Research Institute (SERI) of USA, the University of California in Davis, the Open University in London, the Buck Rogers Co. in Kansas, and in Florida [11]. The stratified downdraft gasifier overcomes many of the difficulties of the Imbert gasifier and may ultimately be the basis for improved gasifier designs.

System description

The stratified downdraft gasifier consists of a cylindrical vessel with a hearth on the bottom. During the operation of this gasifier, air and biomass pass uniformly downward through four zones. The open top ensures uniform access of air or oxygen to the flaming pyrolysis zone, as opposed to the Imbert gasifier. The uppermost layer is composed of *unreacted* biomass fuel through which air enters. In the second layer, biomass reacts with air in *flaming pyrolysis*. The third layer, which is made up of char from the second layer, reduces the pyrolysis gas. *Inert char*, which constitutes the fourth layer, normally is too cool to cause further reactions. However, since the fourth layer is available to absorb heat or oxygen if conditions change, it serves both as buffer as a charcoal storage zone.

The top zone of this gasifier may be adjusted to any depth during air operation and serves the same function as the fuel magazine in the Imbert gasifier. Fuel is added through the open top of the gasifier and should be replenished before the advancing pyrolysis front consumes all of the available fuel.

During oxygen operation, the advancing pyrolysis front moves much faster and it stabilized at the top of the second zone so there is no first zone of fuel storage. Biomass must then be fed regularly onto the top of the flaming pyrolysis zone, and the second zone must be closed and insulated above, forming a burner section.

Air reacts with pyrolyzing biomass in the second zone, and most of the volatile wood oil is burned to supply heat for this pyrolysis which is called "flaming pyrolysis" process, and distinguish it from "flaming combustion", which occurs in the absence of solids with excess air or oxygen. At the bottom of the second zone, the biomass has been converted to charcoal, and all of the oxygen from the air has reacted. The final gas leaving the second zone contains CO and H_2, as well as the CO_2 and H_2O produced in the earlier stages of combustion. The CO and H_2 mixture already is sufficiently concentrated to be a combustible gas at this point.

The hot gas produced in the flaming pyrolysis zone react with the charcoal in the third, or char gasification zone to convert more of the CO_2 and H_2O to CO and H_2, through the Boudouard and water-gas reactions, which is called *"adiabatic char gasification"* process (no heat flows into or out of this section). During the reaction, sensible heat of the gas is converted into chemical energy of the fuel gas. This results in cooling the gas to about 800^{o}C, a temperature at which no further reaction is possible.

Finally, there sometimes may be a zone of *unreacted charcoal* below the char gasification zone through which the gas must pass before it reaches the grate. This last zone has the disadvantage that char and ash from the char gasification zone also must pass through it to reach the grate.

Compare to the Imbert gasifier, the stratified gasifier has a number of advantages that the open top permits fuel to be fed more easily and allows easy access for instruments to measure conditions within the bed. The uniform passage of sir and fuel down the gasifier keeps local temperatures from becoming too high or too low while the average temperature is high. The cylindrical construction is easy to fabricate and permits continuous flow for otherwise troublesome fuels without causing bridging or channelling. The various strata are more accessible for measuring compositions and temperatures within the bed. Moreover, the stratified downdraft gasifier is both conceptually and mathematically easier to comprehend.

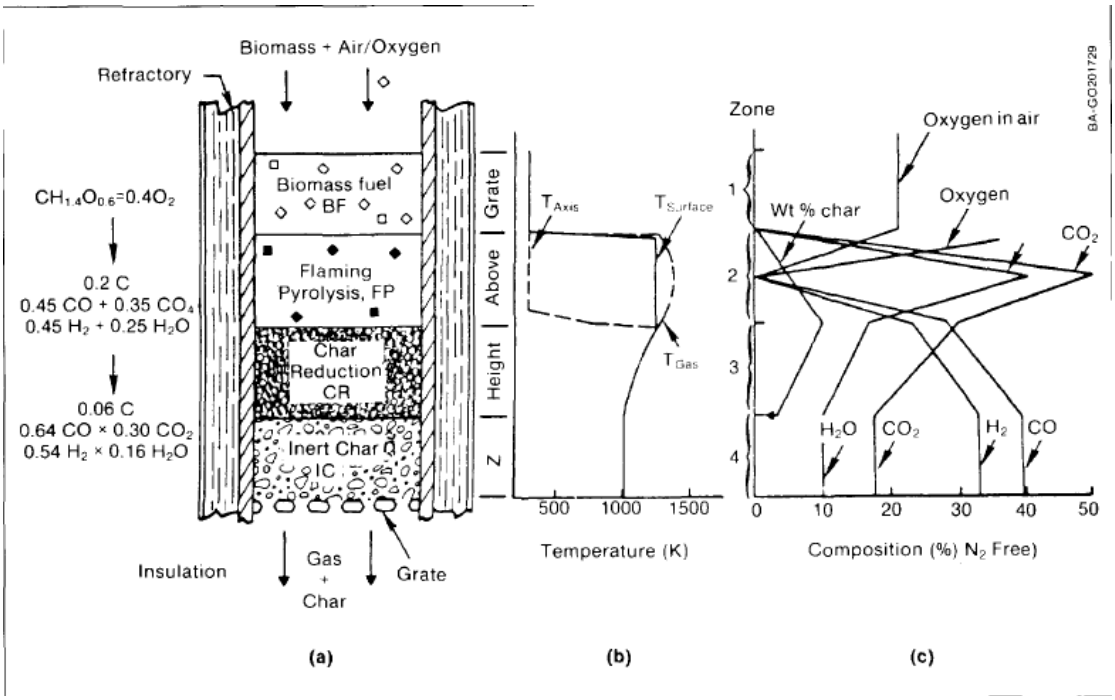

Source: Solar Energy Research Institute, U.S. Department of Energy, 1988

Fig. 2-5 Schematic diagram for stratified downdraft gasifier with
a) system schematic diagram
b) temperature profiles and
c) composition

Although the stratified downdraft gasifier has more advantages compare to the Imbert gasifier, nevertheless, there is some unanswered questions for this gasifier type which expressly on char and ash removal. As the charcoal reacts with the gases in the char gasification zone, it eventually reaches a very low density and breaks up into a dust containing all of the ash as well as a percentage of the original carbon. This dust may be carried away partially by the gas. However, it will begin to plug the gasifier so it must be removed by shaking or stirring.

2.4.3 Tar-Cracking Gasifiers

Due to the fact that the ordinary biomass gasifier usually produces a lot of unpleasant tar in producer gas content which takes effect for utilizing as fuel in an internal combustion engine. Consequently, the tar-cracking gasifiers have been researched and developed in order to convert the maximum quantity of tar to gas during gasification.

Combustion of tars

The downdraft gasifiers produce tar in amounts at least an order of magnitude lower than the updraft gasifiers, and new developments in present are reducing tars less than 100 ppm (1 mg/m^3) level.

The DeLaCotte tar-recycling gasifier (Fig. 2-6) was the first tar-burning gasifier. It has two solid-fuel chambers and a gas-combustion chamber on the side. Fuel is pyrolyzed in the upper part of the fuel chamber. Pyrolysis products are aspirated out the top to the side combustion chamber using the flow of combustion air in an ejector, where they burn completely at high temperature in the absence of solids. The hot combustion products (1,000-1,100^oC) are reinjected at the center of the gasifier. One-fourth of the gas rises through the upper chamber to assure pyrolysis of the biomass fuel, whereas the remaining three-fourths travels down through the lower chamber containing the char produced from the biomass in the upper chamber. The char is gasified by reacting with the CO_2 and H_2O produced by combustion as in other gasifiers. The high-temperature combustion chamber may permit more thorough destruction of the tars.

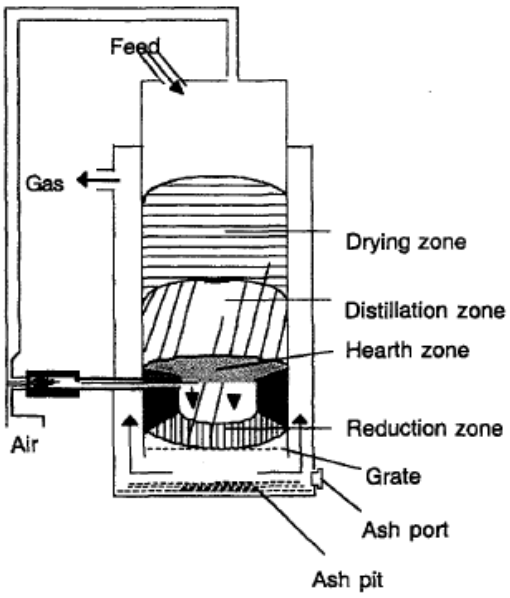

Fig. 2-6 Schematic diagram for the DeLaCotte tar-recycling gasifier (Source: Kaupp A. and Gross J.R., 1981)

Thermal tar cracking

Temperature above 800^oC rapidly cracks the primary pyrolysis oils to olefins and aromatic compounds. These compounds continue to react in the absence of oxygen to make polynuclear aromatic compounds (PNAs) and eventually soot. While high temperatures (above 800^oC) can destroy tars rapidly, these same high temperatures also promote reaction with char, which in turn rapidly quenches the gas to 800^oC. Therefore, the time available for tar

cracking in a bed of hot charcoal is very short. For this reason, a bed of hot char may not be very effective in tar cracking.

2.4.4 Susanto and Beenackers' gasifier

Herri Susanto and Antonie A.C.M. Beenackers [12] have developed a moving-bed gasifier with internal recycle of pyrolysis gas in year 1994 which had similar manner as DeLaCotte tar-recycling Gasifier. For the system process in principle, the feedstock enters at the top of the gasifier, while the producer gas and the solid residue leave at the bottom. The gasifying air is introduced in the centre of the bed, and the recycle gas containing pyrolysis products is sucked from the top of the bed by an internal venturi-type injector and mixed with the gasifying air. This mixture is burnt in a special combustor in the middle of the bed. Figure 2-7 shows the principle of the gasification process in this modified co-current moving bed gasifier.

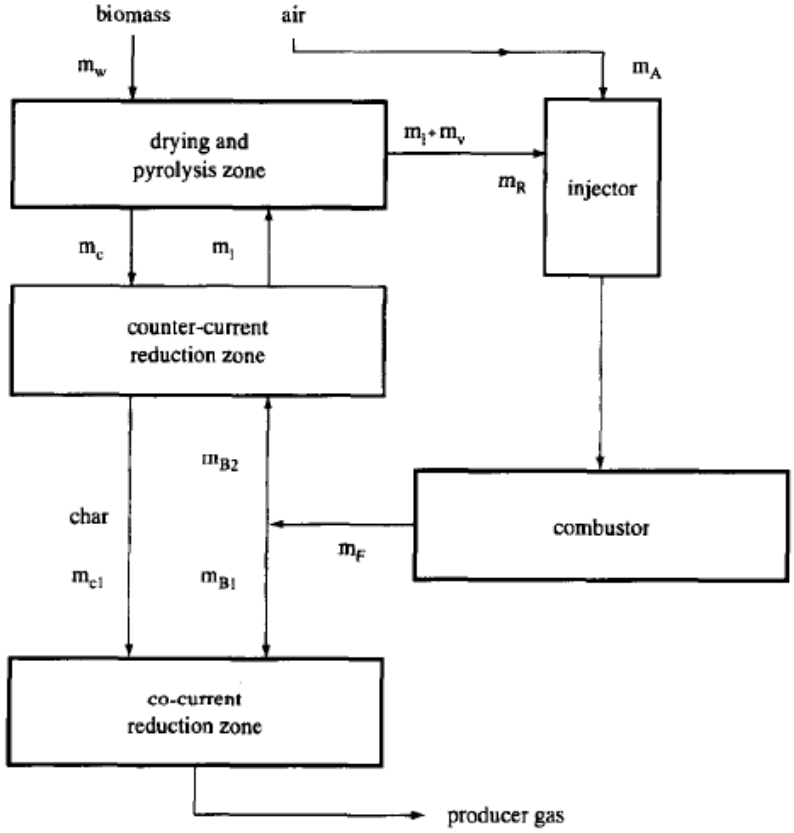

Fig. 2-7 Principle process of Susanto and Beenackers' gasifier with internal recycle and separate combustion of pyrolysis gas (Source: H. Susanto and A.A.C.M. Beenacker, 1996)

The feedstock m_w first undergoes drying and decomposition in the pyrolysis zone to produce char m_c and volatiles m_v (see Fig. 2-7). The volatiles are sucked off upwards together with some gas m_I from the countercurrent reduction zone. In the venturi injector, the recycle gas m_R consisting of m_v and m_I is mixed with the gasifying air m_A and injected into the combustor.

The flue gas m_F from the combustor is split into two streams: the downdraft blast m_{a1} into the co-current reduction zone and the updraft blast m_{a2} into the counter-current reduction zone. The ratio m and m_{a1} depends on the recycle ratio applied, i.e. the ratio of the recycle gas to the gasifying air (v/v at s.t.p.). The updraft blast m_{B2} reacts with char m_c to produce the injected gas m_I.

Part of the char from the pyrolysis zone, mc2, is consumed in the counter-current reduction zone, whereas the remaining char, m_{cl}, moves further down into the co-current reduction zone. This remaining char m_{cl} then reacts with the downdraft blast m_{B1} to produce a clean producer gas.

2.4.5 Three Stages Fluidized-Bed Gasifier

The three stages fluidized-bed gasifier has been developed by the Department of Alternative Energy Development and Efficiency of Thailand and Kasetsart University [13], which focused on the proper method to eliminate tar in producer gas from high ash content biomass (e.g.rice husk). The system consists of 3 mains section: drying, pyrolysis and gasification, respectively.

The pyrolysis section has been simulated from bubbling fluidized-bed furnace, in order to make the extraction of organic matters in the biomass as well as possible, including tar content. After drying process, rice husk from drying zone will be conveyed by screw feeder to the cylindrical room which contains hot sand (700°C). High speed hot gas (at 200–400°C) will be injected at the bottom of the room and makes hot sand fluidized. Heat from hot sand will be transferred to rice husk and organic matter. Tar, volatile and pyroligneous acid will be extracted. Rice husk organic structure will be transformed into carbon and move into the next zone with extracted organic matter.

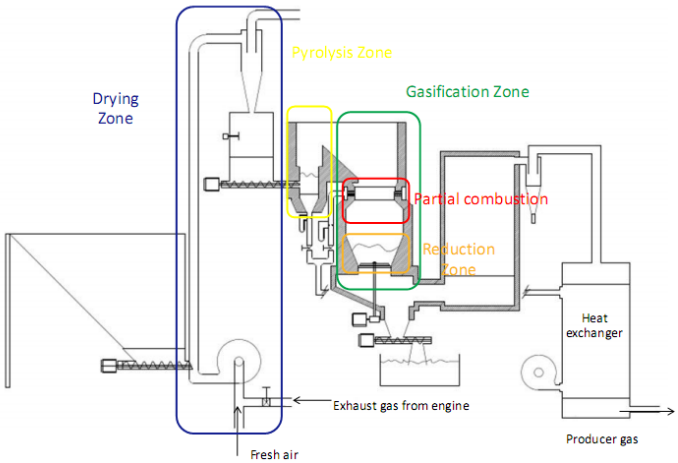

Fig. 2-8 Schematic layout of the three stages gasifier (Source: DEDE, 2011)

In gasification section, 25-30% of a stoichiometric air will be injected into this zone and reacts with carbon and organic matter from pyrolysis zone at the throat of the reactor. In this zone, organic matters from pyrolysis zone and some part of carbon are combusted and transform into carbon dioxide and steam. Extracted tar from pyrolysis zone will be combusted absolutely in this zone before it will be evaporated into gaseous phase. In addition, carbon dioxide

will react with steam in a short time (within 2-3 seconds), and become combustible gas (CO,H_2 and CH_4). As a result, the producer gas contains less than 25 mg/m^3 of tar which can be used for gas engine properly.

Table 2-1 Comparison for each type of conventional downdraft gasifiers

	Imbert Gasifiers	Stratified Gasifier	Tar-cracking gasifiers		
			DeLaCotte tar-recycling gasifier	Susanto and Beenackers' gasifier	Three Stages Fluidized-Bed Gasifier
System merits	- Contain of nozzle and constriction hearth - Air gasifiers can be operated by forcing (pressurized) or drawing (suction) pass through nozzles (tuyeres) - Decrease tar by insulation improving - Using top damper to control reacted air and explosion	- System top damper is neglect (open-top) - Air and fuel will be fed into the gasifier on the top side	- Contain of two solid-fuel chambers and one gas combustion chamber - Using flow of combustion air in an ejector for pyrolysis products movement into gasification zone	- System operation familiar to DeLaCotte type - Combustor is contained centrally in the lower section	- Each main reaction zone is absolutely separated - Biomass is dried in drying zone by using heat from engine exhaust gas - Pyrolysis zone was simulated from bubbling fluidized-bed furnace for more efficient in organic matter extraction
Available biomass properties	- Low moisture content fuel (less than 20%) - Uniformly blocky fuel (wood, corncob, charcoal)	- Low moisture content fuel (less than 20%) - Uniformly blocky fuel (wood, corncob, charcoal)	- Low moisture content fuel (less than 20%) - Uniformly blocky fuel (wood, corncob, charcoal)	- Using wood chips with a 7-9 wt% (db) moisture content	- Small biomass (rice husk, sawdust) with 15% or lower moisture content
Producer gas properties	H_2 7.24% CH_4 5.65% CO 19.53%	(Not Applicable)	(Not Applicable)	Heating value: 4.50 MJ/m^3	CH_4 2.71% H_2 8.10% CO 15.23% Tar 21.00 mg/m^3 Heating value: 4.04 MJ/m^3
System existing capacity	10-400 $kW_{thermal}$	(Not Applicable)	(Not Applicable)	50 kg/h of fuel input	80-400 $kW_{electricity}$
System advantages	- Easy in construction, operation and maintenance - System presents self-adjustment char	- Fuel can be fed more easily through open top - Uniform passage air and fuel keep local temperature in proper.	- Producer gas achieves in low tar content.	- Little number in heat loss - Very low tar content in the producer gas (48 mg/m^3) - Particularly	- Generate low tar content producer gas (21 mg/m^3) - Prevent ash melting efficiently

	Imbert Gasifiers	Stratified Gasifier	Tar-cracking gasifiers		
			DeLaCotte tar-recycling gasifier	Susanto and Beenackers' gasifier	Three Stages Fluidized-Bed Gasifier
	bed maintaining. - High turndown ratio	- Easier for conceptually and mathematically comprehend - System can be scaled-up - Cylindrical construction permits continuous flow without bridging and channeling		effective for gasifying biomass having a low ash melting point such as rice husk and municipal waste-derived fuel	
System disadvantages	- Hearth constriction ring has the limit in biomass fuel shape - System scaling-up (existing capacity increasing) is unavailable	- Inert char and ash from the char gasification zone at the bottom increase high pressure drop of producer gas - Complicate in excess air permission - Not be widely commercialized	- Producer gas consists lower heating value compares with the ordinary gasifier.	- Complication in system construction and operation	- Complication in system construction and operation - Biomass feedstock is only homogeneous and uniform - System is under demonstration.

From the summarized information of each gasification technology, it can be found that the ordinary type of gasifier (i.e. Imbert's gasifier) is given the merits in easy construction and operation, however, some of organic substance such as tar and dust is attached with the gas and causes of problem in system adhering, especially, if the fuel gas will be used for internal combustion engine. Accordingly, modified gasification systems have been developed. Modern gasifier can efficiently generate fuel gas with low tar content. Nonetheless, it can be investigated that the heating value of fuel gas produced from the modified gasifiers usually present lower heating value compare with the traditional type of gasifier. When extracted tar passes through the combustion zone, energy content in tar is combusted and converted into heat energy for other zones inside gasifier. Hence, it can be concluded that the modified gasifier can be given in cleaner producer gas that is proper for using in an internal combustion engine. However, it requires much amount of fuel gas due to calorific value of producer gas obtained from modified gasifier that lower than fuel gas generated from traditional gasifier.

2.5 Literature reviewing on biomass gasification researches

T.H. Jayah et.al. [14] have conducted for computer simulation of a 70 kW_{th} downdraft wood gasifier for tea drying. The simulation program consists of two sub-models of pyrolysis and gasification model zones, respectively. The pyrolysis sub-model has been used to determine the maximum temperature and the composition of the gas entering the gasification zone (reduction zone), and the gasification sub-model has been calibrated using data gathered from the experiments. In addition, it was found that a wood chip size 3-5 cm with a moisture content below 15% (d.b.) should be used in the gasifier. Feed material with a fixed carbon content of higher than 30% and heat losses of more than 15% should be avoided.

Due to the results, the significant parameters were concluded as;

1) The 15% moisture content woodchip can be led for 56% of producer gas conversion efficiency at the 22 cm gasification zone length, whereas the conversion efficiency is decreased to 53% if using 30% of moisture content woodchip.
2) Inlet air temperature: it was found that if increase the ambient air temperature (by preheating) to 400 and 600 K, the producer gas conversion efficiency are 56 and 56.5% at 50 kg/h air flow rate, respectively.
3) System heat loss: an average heat loss in experiment was 12.8% approximately which resulted in the producer gas conversion efficiency 56%. Moreover, it can be also found that heat loss has the greatest effect on the conversion efficiency, which decreases by approximately 11% for every 5% increase in heat loss.
4) Throat angle: the conversion efficiency will decrease whereas throat angle increase. The experimental result was shown that at throat angle 61^{o}, the conversion efficiency will be 56% at the gasification zone length 22 cm.

Venselaar [15] has compared the design characteristics of a number of gasifiers that were commercially available during the Second World War. A distinction is made between “no throat” “single throat” and “double throat” (Imbert type) designs. Venselaar concluded that the three types differ mainly in maximum allowable hearth load, giving values of the maximum surface area of the narrowest constriction (B_{max}) of 0.03, 0.11 and 0.4, respectively for “no throat” “single throat” and “double throat” (Imbert type) gasifiers. Further conclusions from this comparison are that:

- Nozzle air inlet velocities should be around 30-35 m/s
- Throat inclination (throat angle) should be around 45^{o}-60^{o}
- Hearth diameter at air inlet height should be 10 cm larger than “throat” diameter in case of a “single throat” design, an about 20 cm larger than the diameter of the narrowest constriction in case of “double throat” design.
- Height of the reduction zone should be more than 20 cm (the average height of reduction zone for the gasifiers reviewed was 32 cm).
- Height of the air inlet nozzle plane should be 10 cm above the narrowest constriction.

Gunther Stahl [16] has explained that a suitable producer gas for internal combustion engines should consist of about 20-28 vol. % CO, 12-18 vol. % H_2 and 1-5 vol. % gaseous C_mH_n while the rest is nitrogen. The hydrogen content accelerates the combustion process in the internal combustion engine while CO and CH_4 contribute to a high knock resistance.

A. Cuoci et.al. [17] have studied for the mathematical modelling of gasification and combustion of solid fuel and wastes. The result of model shown that if 1 cm of cellulose particle with air at stoichiometry ratio 0.33 were taken place, when air and solid flow rates increase the gasification process is incomplete, fuel particles leave the unit at high temperature and ashes still contain unconverted material. The model characterizes the solid and gaseous streams including a large detail of unconverted tar components and becomes a useful toll for the design of gasifier units.

Jieheng Guo [18] has studied for the pyrolysis of wood powder and gasification of wood-derived char, which had an objective to provide practical data and a theoretical perspective about the chemical kinetics and the transport phenomena in pyrolysis and gasification of biomass from both an experimental and a modeling perspective of Lignocel wood-derived char.

J.J. RAMÍREZ, J.D. MARTÍNEZ and S.L. PETRO [19 have conducted for the pilot scale of a fluidized-bed gasifier for rice husk. The experimental apparatus made up of a reaction chamber of 0.3 m of internal diameter and 3 m of overall height, was designed from researchers' theoretical and experimental information. Finally, the prototype generated approximately 70 kW of useful energetic power.

M.J.Prins et.al. [20] have studied for the wood-based gasification via torrefaction process. One kilogram of wood was used, which the torrefaction reactor's conditions were conducted by 250^{o}C at 30 minutes and 300^{o}C at 10 minutes. The schemes of gasification process used for the experiment consisted of 1) Circulating Fluidized-bed (CFB) wood gasification 2) CFB gasification with torrefied wood and 3) Entrained flow (EF) gasification with torrefied wood. The results were shown that the using CFB gasification with torrefied wood presented for lower system's overall efficiency compared with using normal fuelwood as a fuel source. Especially, high torrefaction temperature causes of a large amount of energy contained in the volatiles and, which were not used in the process. In addition, the evaluated overall efficiency by using the EF gasification with the 250^{o}C torrified wood presented as 75% approximately, while using the 300^{o}C torrified wood with the same reactor resulted a little bit higher efficiency (78%). Furthermore, a system exergy was also evaluated in this research. It was found that more exergy was conserved in as chemical exergy in the product gas (68.6%).

W. Arjharn et.al.(2012) [21] have studied for ten different types of biomass served as fuel to generate electricity using a pilot-scale downdraft biomass gasification power plant. It was found that temperature profiles depended on syngas flow rate and type of biomass feedstock and can be divided into three groups. An increase in syngas flow rate from 105 to 211 m^3/h (across all biomass types) was found to have little effect on gas composition, causing calorific values peaking between 4.2 and 5.6 MJ/Nm^3. Maximum electrical power output of each tested biomass feedstocks was observed at the highest syngas flow rate, ranging from 47 to 63 kW with specific biomass consumption below 2.0 kg/ kWh. Among them, gasification efficiency exceeding 70% was achieved from Eucalyptus and corncob, and Giant Leucaena. Engine-generator set efficiency and electrical efficiency ranged from 11.0 to 25.8% and from 6.3 to 18.6%, respectively. Overall, biomasses varying widely in their properties showed a strong potential for electricity generation using downdraft gasification technology.

J. Chuchottaworn (2012) [22] has studied for the heat production from *Pennisetum Purpureum cv. Pakchong1 Grass* through gasification process. The produced Napier Pakchong1 Grass pellet samples are analyzed for physical properties of moisture content, ash, volatile matter, fixed carbon and heating value. The results show that Napier

Pakchong1 grass pellets yield a gross calorific value (HHV) of 18.31 MJ/kg. The produced grass pellets are then fed into a downdraft gasification reactor at variable air/biomass equivalent ratio (ER) of 0.2, 0.3 and 0.4. At steady-state operation, the producer gas from each case of ER is collected and analyzed for their composition from gasification by gas chromatography. As a result, the equivalent ratio 0.4 issued height heating value of gas per fuel weight is 4.91 MJ/kg pellet.

K. Pianthong (2012) [23] studied for biomass gasification using in ceramic furnace and found that venturi type of producer gas burner presented in most proper for ceramic production process. At the operation pressure 0.5 MPa, biomass producer gas profile played the same result as LPG using in ceramic production.

2.6 Calculation of the significant parameters of gasification

2.6.1 Mass balance in gasifier

In order to compute for the mass balance in the gasifier system, main combustible contents in producer gas as carbon monoxide (CO), hydrogen (H_2) and methane (CH_4) can be used. The CO_2, H_2O and N_2 proportions in the fuel gas will depend on the fuel chemical composition and the amount of air in the reaction. According to this, the following global reaction of the gasification process is raised [24].

$$\begin{aligned} x_1(3.05C + 5.83H + 2.29O + 0.24N) \quad &\rightarrow \quad x_7(\alpha CO + \beta H_2 + \gamma CH_4 + x_3 H_2O \\ +x_2(O_2 + 3.76N_2) + aH_2O + bH_2O \quad &\qquad +x_4 CO_2 + x_5 N_2) + x_6 C \end{aligned} \tag{2.9}$$

where $x_1, x_2, ..., x_7$ = biomass and gasification air reaction coefficients

α, β, γ = % volumetric of the concentrations of the energetic compounds in the producer gas

a, b = water mole in biomass and air, respectively

2.6.2 Equivalence ratio

The equivalence ratio of the gasification process is one of the most important parameters for the adjustment of the operating conditions. The value can be defined as [25]:

$$\xi = \frac{(R_{A/C})_r}{(R_{A/C})_s} \tag{2.10}$$

where ξ = equivalence ratio

$(R_{A/C})_r$ = air-fuel real relation

$(R_{A/C})_s$ = air-fuel stoichiometric relation

2.6.3 Energy balance in gasifier

The energy balance of the gasification process can be simply established by following equation [26]:

$$E_{biomass} + E_a = E_g + E_{loss} \tag{2.11}$$

In which: $E_{biomass}$ = energy in the input biomass
E_a = energy in the reaction air
E_g = energy in the producer gas
E_{loss} = energy loss from the system

Energy in the input biomass can be calculated by:

$$E_{biomass} = \frac{\dot{m}_{biomass} \cdot LHV_{biomass}}{3{,}600} \quad (2.12)$$

Where: $\dot{m}_{biomass}$ = mass flow rate of input biomass (kg/h)
$LHV_{biomass}$ = low heating value of input biomass (kJ/kg)

2.6.4 Gasifier efficiency

If the gas is used for direct burning, the gasification efficiency is sometimes defined as [7]:

$$\eta_{th} = \frac{(H_g \times Q_g) + (Q_g \times \rho_g \times C_p \times \Delta T)}{H_s \times M_s} \times 100\% \quad (2.13)$$

In which:
η_{th} = gasification efficiency (%) (thermal)
ρ_g = density of the gas (kg/m^3)
C_p = specific heat of the gas (kJ/kg-K)
ΔT = temperature difference between the gas at the burner inlet and fuel entering the gasifier (K)

2.6.5 Significant equations of thermochemical processes inside the downdraft gasifier

1) Biomass drying

The mechanism of moisture transfer to biomass includes diffusion through the fluid film around the solid particles and diffusion through the pores to internal adsorption sites. The actual process of the physical adsorption is practically instantaneous, and equilibrium can be assumed to exist between the surface and the fluid envelope (A.K.Sharma, 2010) [27]. As moist biomass particles came into contact with air having low humidity level, the particles tends to lose moisture to the surrounding air until equilibrium is attained.

The local thermal equilibrium between the gaseous and solid media is assumed in each control volume, which makes it implicit that heat transfer between the solid and gases is much faster than the mass transfer. Thus, mass transfer determines the rate of moisture removal from the biomass particles to the gases/air flowing around them. The analytical solution for one-dimension mass diffusion in a sphere particle of biomass is used.

Diffusion Equation [28]

$$\frac{X_{in} - X_{eqb}}{X_{out} - X_{eqb}} = \frac{8}{\pi^2}\left(e^{-(\pi/2)^2 \beta} + \frac{1}{9}e^{-9(\pi/2)^2 \beta} + \ldots\right) \quad (2.14)$$

where $\beta = \frac{4D_{dif}t_{res}}{d_p^2}$ and $t_{res} = \frac{M_{b,CV}}{\dot{m}_b}$

Simpson relationship [29]

$$X_{eqb} = \frac{1800}{W} \times \left(\frac{Kh}{1-Kh} + \frac{K_1 Kh + 2K_1 K_2 K^2 h^2}{1 + K_1 Kh + 2K_1 K_2 K^2 h^2} \right) \quad (2.15)$$

where $W = 349 + 1.29(T-273) + 0.0135(T-273)^2$ (2.15a)

$K = 0.805 + 0.000736(T-273) - 0.00000273(T-273)^2$ (2.15b)

$K_1 = 6.27 + 0.00938(T-273) - 0.000303(T-273)^2$ (2.15c)

$K_2 = 1.91 + 0.0407(T-273) - 0.000293(T-273)^2$ (2.15d)

Relative humidity ratio

$$h = \frac{\omega_{air}}{\omega_{air,sat}} = \frac{\omega_{air}}{p_{v,sat} mw_w / p_a mw_a} \quad (2.16)$$

Antoine equation[30]

$$\log_{10}(p_{v,sat}) = A - \left(\frac{B}{T+C} \right) \quad (2.17)$$

Table 2-2 Coefficients for Antoine equation for saturation vapour pressure

Temperature range (K)	*A*	*B*	*C*
255.8-373	4.6543	1435.264	-64.848
379-573	3.55959	643.748	-198.043

2) Pyrolysis

In downdraft gasifier, the pyrolysis process can be modelled at slow heating rate to predict pyrolytic yields (viz., volatile composition and char) and devolatilization rate as a function of temperature and residence time [27]. The biomass particles shrink on pyrolysis giving char and ash. Following assumptions are invoked:

- Char and biomass particles are non porous.
- Char yields from cellulose, hemicellulose and lignin considered to be pure carbon.
- Char yield in the gasifier in insensitive to pyrolysis temperatures encountered in the pyrolysis zone.
- The complex constituents of volatiles are assumed to be decomposed into CO, H_2, CO_2, H_2O, tar (heavy hydrocarbons) and light hydrocarbons (mixture of methane and ethylene).

Rate of devolatilization [32]

$$\frac{dM_{vol}}{dt} = -k_{pyr} M_{vol} = -7.0 \times 10^7 \exp(-1560/T) M_{DB} Y_{vol} \quad (2.18)$$

$$\Delta \dot{m}_{vol,i} = \left(\frac{dM_{vol}}{dt} \right)_i = (\Delta t_{res})_i \left(\frac{dm_{vol}}{dt} \right)_i \quad (2.19)$$

Char yield [33]

$$Y_{char,ash-free} = Y_{cl} Y_{char} + Y_{hc} f_{char} + Y_{lg} \gamma_{char} \quad (2.20)$$

$$Y_{vol} = 1 - Y_{char,ash-free} \quad (2.21)$$

Empirical mass ratios

$$Y_{CO/CO2} = \exp\left[-1.8447896 + \frac{7730.317}{T} + \frac{5019898}{T^2}\right] \quad (2.22)$$

$$Y_{H_2O/CO2} = 1 \quad (2.23)$$

$$Y_{ME/CO2} = 5\times10^{-16} T^{5.06} \quad (2.24)$$

Heat of pyrolysis

$$\Delta h^0_{pyr} = \left(h^0_f\right)_{DB} - Y_{char}\left(h^0_f\right)_{char} - Y_{vol}\sum_{k=1}^{k=6} Y_k \left(h^0_f\right)_k \quad (2.25)$$

3) Oxidation (combustion)

The pyrolysis products get oxidized in short supply of oxygen in the oxidation zone (near air tuyers) of a gasifier. Owing to the widely varying reaction equilibrium constants and the reaction time scales, some of the reactions might not be attaining equilibrium in the oxidation zone, and hence the solution of full equilibrium equations to compute oxidation process in the gasifier would both be erroneous and numerically difficult. Therefore, a heuristic approach is adopted.

Table 2-3 Chemical reactions in oxidation zone [34]

Reac. No.	Oxidation reactions	Rate expressions	A_j	E_j/Ru	
R1	$H_2 + 0.5O_2 \rightarrow H_2O$	$k_{H_2} = A_{H2}T^{1.5}\exp(-E_{H2}/R_uT)[O_2][H_2]^{1.5}$	1.63 x 10^9	3,420	(2.26)
R2	$CO + 0.5O_2 \rightarrow CO_2$	$k_{CO} = A_{CO}\exp(-E_{CO}/R_uT)[CO][O_2]^{0.25}$	1.3 x 10^8	15,106	(2.27)
R3	$C_{1.16}H_4 + 1.58O_2 \rightarrow 1.16CO + 2H_2O$	$k_{CH_4} = A_{CH4}\exp(-E_{CH4}/R_uT)[O_2]^{0.8}[CH_4]^{0.7}$	1.585 x 10^9	24,157	(2.28)
R4	$C_6H_{6.2} + 4.45O_2 \rightarrow 6CO + 3.1H_2O$	$k_{tar} = A_{tar}TP_A^{0.3}\exp(-E_{tar}/R_uT)[O_2]^1[HC]^{0.5}$	2.07 x 10^4	41,646	(2.29)
R5	$C + 0.5O_2 \rightarrow CO$	$k_{char} = A_{char}\exp(-E_{char}/R_uT)[O_2]^1$	0.554	10,824	(2.30)

4) Reduction

Reduction of the oxidation zone products are primarily dominated by heterogeneous reactions of solid-char and homogeneous reactions of gas-gas in complete absence of oxidants. These reduction reactions are inherently slower than the oxidation reactions by several orders of magnitude, thus, equilibrium may not be established in the reduction region. At moderately high temperature (<800^{o}C), the equilibrium products may deviate from reality, thus, kinetic or non-equilibrium models are suitable and accurate.

Table 2-4 Chemical reactions in reduction zone

Reac. No.	Oxidation reactions	Rate expressions	A_j[35]	E_j[36]	
R6	$C + CO_2 \rightarrow 2CO$	$r_1 = A_1 \exp(-E_1 / R_u T)\left(P_{CO_2} - \frac{P_{CO}}{K_{eq,1}}\right)$	3.616 x 10^4	77.39	(2.31)
R7	$C + H_2O \rightarrow CO + H_2$	$r_2 = A_2 \exp(-E_2 / R_u T)\left(P_{H_2O} - \frac{P_{CO}P_{H_2}}{K_{eq,2}}\right)$	1.517 x 10^7	121.62	(2.32)
R8	$C + 2H_2 \rightarrow CH_4$	$r_3 = A_3 \exp(-E_3 / R_u T)\left(P_{H_2}^2 - \frac{P_{CH_4}}{K_{eq,3}}\right)$	4.189	19.21	(2.33)
R9	$CH_4 + H_2O \rightarrow CO + 3H_2$	$r_4 = A_4 \exp(-E_4 / R_u T)\left(P_{CH_4}P_{H_2O} - \frac{P_{CO}P_{H_2}^3}{K_{eq,4}}\right)$	73.01	36.15	(2.34)

2.6.6 Fluid flow equation of the downdraft biomass gasifier

The concerning equations to the fluid flow inside the downdraft biomass gasifier contain of air inflow from the open top and through the air tuyers, and the pressure drop through the gasifier bed as a function of flow rate[27]. The pressure drop can be computed from the Darcy-Weisbach equation. The pressure drop through the gasifier bed has been obtained using Ergun correlation [37] for complete flow regime. Pressure drop through concentric annulus is modelled from modified Darcy-Weisbach friction factor in terms of effective Reynold number and effective (annulus) diameter.

1) Gasifier's tuyer

$$\Delta P_{tuy} = \left(P_{atm} - P_{in,tuyer}\right) + \left(P_{in,tuyer} - P_{exit,tuyer}\right) = \frac{\rho V_m^2}{2} + \left(f\frac{L}{D} + K_{dev}\right)\frac{\rho V_m^2}{2} \quad (2.35)$$

$$= \left(1 + f\frac{L}{D} + K_{dev}\right)\frac{\rho V_m^2}{2}$$

2) Pressure drop parameter[38]

$$K_{dev} = \exp\left(0.3 - 2.9\times10^{-3} / \left(\frac{L_{dev}}{\mathrm{Re}\cdot D}\right) - 1.43\times10^{-6} / \left(\frac{L_{dev}}{\mathrm{Re}\cdot D}\right)^2\right) \quad (2.36)$$

$$\frac{L_{dev}}{D} \cong 0.06\,\mathrm{Re}\ ;\ \text{for Re} < 2300$$

$$\frac{L_{dev}}{D} \cong 4.4\,\mathrm{Re}^{1/6}\ ;\ \text{for Re} > 4000$$

3) Porous bed: Ergun equation

$$\Delta P_i = \frac{150\left(1-\varepsilon_{b,i}\right)^2 \mu(T_i)l_i}{\rho(T_i)\varepsilon_{b,i}^3 d_{p,i}^2 A_T}\left(\dot{m}_f\right)_i + \frac{1.75\left(1-\varepsilon_{b,i}\right)l_i}{\rho(T_i)\varepsilon_{b,i}^3 d_{p,i}^2 A_T^2}\left(\dot{m}_f\right)_i^2 \quad (2.37)$$

where ε_b means bed's porosity.

$$\varepsilon_b = 0.5 - 0.2\left(1 - d_p / d_b\right) \quad (2.37a)$$

4) Concentric annulus[39]

$$\Delta P_{an} = \left(K_{dev} + f_{mfd} \frac{dL_1}{D_{eff}} \right) \frac{\dot{m}_{pg}^2}{2\rho_{pg} A_{an}^2} \tag{2.38}$$

$$\mathrm{Re}_{eff} = \frac{\mathrm{Re}_{Dh}}{\xi}; \quad D_{eff} = \frac{D_h}{\xi} \tag{2.38a}$$

$$\xi = \frac{(1-\hat{r})^2 (1-\hat{r}^2)}{(1-\hat{r}^4) + (1-\hat{r}^2)^2 / \ln(\hat{r})} \quad \text{where } \hat{r} = r_o / r_i \tag{2.38b}$$

2.6.7 Heat transfer

For heat transfer analysis, fuel bed is assumed to be isotropic; solid and gases are considered to be in local thermal equilibrium. These assumptions are justified for fixed bed gasifiers operating under steady state conditions, since residence time of solids in the control volume is two or three order magnitude higher than that of gases. The formulation of energy interaction for the heat inflows and outflows due to advection of fluid and solids, heat loss through insulated wall, internal thermal interaction between adjacent control volumes and the quantity of heat generated or consumed, are described [27].

1) Energy equation

$$\left[\sum_{solid} \left(\dot{m}_i C_{p,i} \right)_{in} + \sum_{gases} \left(\dot{m}_i C_{p,i} \right)_{in} \right] T_{in} + \dot{Q}_{vap} + \dot{Q}_{pyr} + \dot{Q}_{oxid} + \dot{Q}_{red} + \dot{Q}_{red} + \sum_{jk} \dot{Q}_{dif,jk} = \left[\sum_{solid} \left(\dot{m}_i C_{p,i} \right)_{out} + \sum_{gases} \left(\dot{m}_i C_{p,i} \right)_{out} \right] T_{out} \tag{2.39}$$

2) Effective thermal conductivity[40]

$$k_{eff} = \frac{2k_s k_f C_1 (\ln C_2 + C_1)}{k_g (\ln C_2 + C_1) - k_s C_1} + \frac{k_s d_{ct}^2}{d_p^2} + 4\sigma\Omega d_p T^3 \tag{2.40}$$

and $$\Omega = \varepsilon_b / 1 + \frac{\varepsilon_b (1-\varepsilon_{rad})}{2\varepsilon_{rad} (1-\varepsilon_b)} \tag{2.41}$$

3) Thermal resistance for ith *zone*[41]

$$\dot{Q}_{dif,jk} = \frac{\Delta T_{jk}}{R_{si}} \tag{2.42}$$

where $R_{si} = R_{t(i,bed)} + R_{t(i,isn)} + R_{t(i,o)}$ (2.42a)

and jk = up, down, side

2.6.8 Properties of biomass producer gas

Specific properties of biomass producer gas generated from biomass gasification process such as thermal conductivity, viscosity and specific heat can be determined by the following equations.

1) Thermal conductivity[42]

$$k_b = Sg_b (0.1941 + 0.4064 Y_w) + 0.1864 + 0.002 (T - T_A) \tag{2.43}$$

$$k_{char} = 1.4 \times 10^{-6} T^2 - 6.4 \times 10^{-4} T + 0.211 \tag{2.44}$$

$$k_k = A_k + B_k T + C_k T^2 + D_k T^3 \tag{2.45}$$

$$k_{mixture} = \frac{\sum_{k=1}^{k} \chi_k k_k \left(MW_k\right)^{0.333}}{\sum_{k=1}^{k} \chi_k \left(MW_k\right)^{0.333}} \tag{2.46}$$

2) Specific heat

$$C_{p,DB} = 0.1031 + 0.003867T \tag{2.47}$$

$$C_{p,b} = \left[C_{p,DB} + 4.19Y_W\right]/\left(1 + Y_W\right) + \left(0.02355T - 1.32Y_W - 6.191\right)Y_W \tag{2.48}$$

$$C_{p,char} = 1.39 + 0.00036T \tag{2.49}$$

$$C_{p,k} = a_k + b_k T + c_k T^2 + d_k T^3 + e_k T^4 \tag{2.50}$$

$$C_{p,mixture} = \sum_{k=1}^{k} Y_k C_{p,k} \tag{2.51}$$

3) Viscosity [43]

$$\mu_k\left(T\right) = \mu_k\left(T_a\right)\left(T/T_a\right)^n \tag{2.52}$$

$$\mu_{H_2O} = 7\times10^{-12}T^2 + 5.1\times10^{-8}T - 6.04\times10^{-6} \tag{2.53}$$

$$\mu_{tar} = -1.3404\times10^{-11}T^2 + 5.1\times10^{-8}T - 2.2588\times10^{-6} \tag{2.54}$$

$$\mu_{mixture}\left(T\right) = \sum_{k=1}^{k} \frac{\chi_k \mu_k}{\sum_{l=1}^{l} \chi_k \varphi_{kl}} \tag{2.55}$$

Where $$\varphi_{kl} = \frac{\left[1 + \left(\mu_k/\mu_l\right)^{0.5}\left(MW_l/MW_k\right)^{0.25}\right]^2}{2.828\left[1 + \left(MW_k/MW_l\right)\right]^{0.5}} \tag{2.56}$$

2.7 Producer gas treatment systems

The objectives of gas cleanup should be based on the degree of contamination, the size, distribution, and nature of the contaminants, as well as the degree of cleanliness required by the equipment. Both solid and liquid contaminants are present in producer gas. The solids are char, ash and soot, and they cover a wide range of sizes. The liquid is initially a fine mist or fog composed of droplets smaller than 1 m, but the droplets agglomerate to increase in size as the gas cool[11] .

In this research, utilized gas treatment devices contain of:

1) Cyclone separator
2) Tar extraction unit
3) Fabric filter

2.7.1 Cyclone separator

Hot gas cyclone separators are well suited to remove solid particles larger than 10 μ m as a prefilter for the gas cooler and fine particle removal. The cyclone separator imparts a rotary motion to the gases and thereby enhances the settling rate to many times that induced by gravity alone. It is essentially a gravitational separator that has been

enhanced by a centrifugal force component. The cyclone separator grade efficiency curve, Fig. 2-9, applies to all cyclone separators, as well as to inertial and gravitational collectors.

Cyclone performance is rated in terms of particle cut diameter or cut size. The cut size, d_{p50}, is the particle size, which is captured 50%.

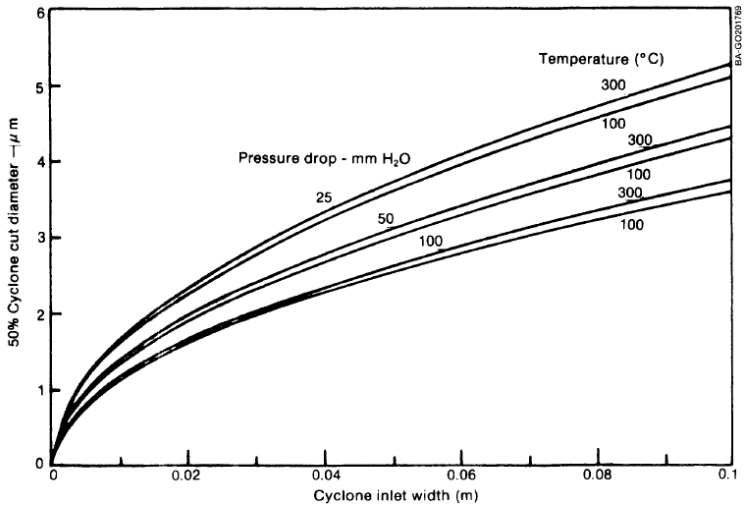

Fig. 2-9 Cyclone cut size versus inlet width (m)

The relationship between particle cut diameters for this type separator is given by Eq. 2.57, where d_p is the particle diameter and the numerical subscript denotes the collection efficiency of that size particle.

The particle size that can be separated with 50% efficiency is predicted for general cyclones and for the high-efficiency cyclone proportions[44].

$$d_{pc} = \sqrt{\frac{9\mu_G b}{\left[2\pi \cdot N_e \cdot V_i \cdot \left(\rho_p - \rho_G\right)\right]}} \tag{2.57}$$

The cyclone's pressure drop is computed by:

$$\Delta p = \frac{(0.065)(\rho_G)(V_i^2)A_d}{D_e^2} \tag{2.58}$$

2.7.2 Condenser (Tar extraction unit)

Tar content in producer gas is generated by various reasons such as moisture content in the fuel or during the gasification reaction. Tar occurs mostly as a mist or fog composed of fine droplets. Tar mist continually agglomerates into larger droplets and tend to saturate and coat solid particles. Therefore, one method is to make tar mist condense before it flows with producer gas to other devices.

A tar extraction condensing unit is simulated from a shell and tube counter-flow heat exchanger. Cold water flows through the tubes in the heat exchanger, whereas producer gas flows in the shell outside the water tubes that makes the producer gas temperature decrease rapidly. At the same time, the tar content in gas is condensed and then falls down to the lower side, while low-tar content producer gas flows out of the condenser. In order to design the

extraction condensing unit, the log mean temperature difference (LMTD) is the most appropriate method [41], as described in Eq. (2.59) and (2.60).

$$Q_{H.E.} = UA_s \Delta T_{lm} \quad (2.59)$$

where

$$\Delta T_{lm} = \frac{\{(T_{h,in} - T_{c,in}) - (T_{h,out} - T_{c,out})\}}{\ln\left(\frac{T_{h,in} - T_{c,in}}{T_{h,out} - T_{c,out}}\right)} \quad (2.60)$$

2.7.3 Fabric filter

A fabric filter must be selected to be part of a gas treatment system, in order to eliminate remaining tar and dust particles after producer gas passes through the cyclone and tar extraction unit.

2.8 Overview of incineration technology

Incineration is a waste treatment process that involves the combustion of organic substances contained in waste materials[45]. Incineration and other high temperature waste treatment systems are described as "thermal treatment". Incineration of waste materials converts the waste into ash, flue gas, and heat. The ash is mostly formed by the inorganic constituents of the waste, and may take the form of solid lumps or particulates carried by the flue gas. The flue gases must be cleaned of gaseous and particulate pollutants before they are dispersed into the atmosphere. In some cases, the heat generated by incineration can be used to generate electric power.

In fact, incinerators reduce the solid mass of the original waste by 80–85% and the volume by 95-96 %, depending on composition and degree of recovery of materials such as metals from the ash for recycling.

In this research, high-moisture materials (biomedical waste and cremation) will be directly emphasized which the main ideas will focus only incinerators and emission treatments (without energy or power generation).

2.9 Classification of incinerators

There are basically three types of incinerators that are available for the incineration of biomedical waste, which namely[46]:

1) Multiple-chamber (retort and in-line)
2) Controlled-air
3) Rotary kiln

In the past, the most prevalent type of incinerator used for the disposal of biomedical waste has been the multiple-chamber unit. However, since the middle of 1970, preference has shifted to the controlled-air design. In addition, the rotary kiln type has also been used in recent years to incinerate biomedical waste in some hospitals in the United State of America.

Regardless of the type of incinerator, it must provide sufficient temperature, turbulence and retention time to ensure complete destruction of the biomedical waste.

2.9.1 Multiple-chamber incinerator

The multiple-chamber incinerator has a minimum of three chambers, passes, or zones. The primary chamber is equipped with a solid hearth (either hot or cold type) complete with a lip (or trough) about 5.0 cm deep to contain fluids. A hot hearth is constructed of conducting refractory and offers significant heat conductivity and a more complete burn. Open grate hearths cannot contain fluids and are therefore not suitable for use in biomedical waste incinerators.

The retort incinerator is characterized by 90-degree directional turns of the gas flow laterally and vertically. The combustion gases may be directed under the solid hearth on which wastes are disposed of, or to the secondary chamber. The flow of hot gases under the solid hearth is advantageous and desirable because it allow for heat transfer to the solid hearth which will aid in combustion in the primary chamber, and helps to ensure sterilization of the resulting ash.

The in-line incinerator is usually larger and combustion gas flow is directed through 90-degree turns in the vertical plane only. Unlike the retort unit, the in-line incinerator is usually equipped with a grate, which renders it unsuitable for wastes with a high fluid content. However, the in-line incinerator can be equipped with a separate hot hearth to accommodate biomedical waste incineration.

Multiple-chamber incinerators have been widely used for the destruction of pathological waste. The basic unit is capable of operating at a high combustion temperature and appropriate controls can be provided to contain fats and other liquids until burnout is achieved. It can also be operated on an intermittent basis, which makes it particularly amenable to the incineration of anatomical and infectious wastes which are seldom generated in large quantities by a single facility.

Multiple-chamber incinerators operate in the excess air mode with an overall excess air range of 150-400%. Combustion air is normally provided by natural draft and admitted through manually-operated ports. Barometric dampers are used to control the draft and thus the quantity of air induced into the incinerator.

An important consideration in the operation of multiple-chamber incinerators is that the waste should be charged across the hearth in a single layer to provide for maximum exposure of surface area to the burner flame. This is best accomplished by the frequent charging of small amounts of waste to the incinerator.

When multiple-chamber incinerators were in widespread use, the composition of pathological waste designated for incineration was not highly variable. The waste had a higher heating value in the order of 2,320 kJ/kg and required appreciable quantities of auxiliary fuel to sustain combustion in the incineration process. Under these conditions, steady heat input of the burners throughout the total duration of the burn cycle was necessary for complete destruction of the waste.

The physical and thermal characteristics of resent biomedical waste have become much more complex, thereby placing severe limitations on the use of multiple-chamber incinerators. The design is still suitable for burning pathological waste (e.g. animal carcasses) that has a slow heat release rate and relatively constant oxygen demand. However, most biomedical waste generated at present has a much higher heat release rate and greater oxygen demand fluctuation during incineration, due to its higher plastics content.

As a result, the use of a damper to control the air required for the incineration of biomedical waste is not efficient due to its slow response. This leads to incomplete combustion causing excessive emissions and opacity problems. In addition, the need for a steady heat input from the burners to maintain the temperature of the large volume of excess air has, from an energy cost viewpoint, placed the multiple-chamber incinerators in a non-competitive position compared with other incinerator designs requiring less excess air.

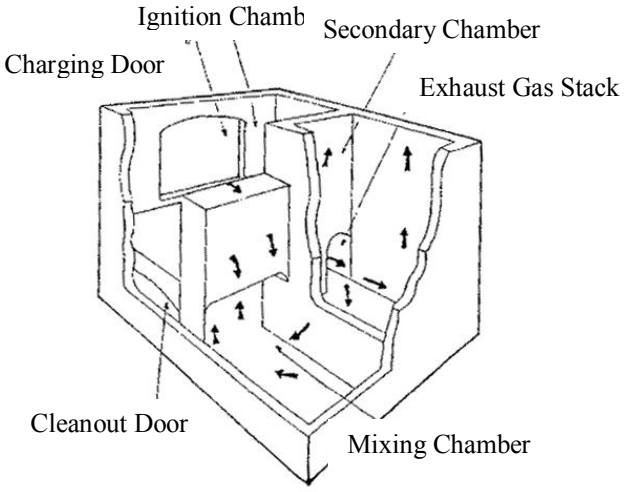

Fig. 2-10 Retort type multiple-chamber pathological waste incinerator

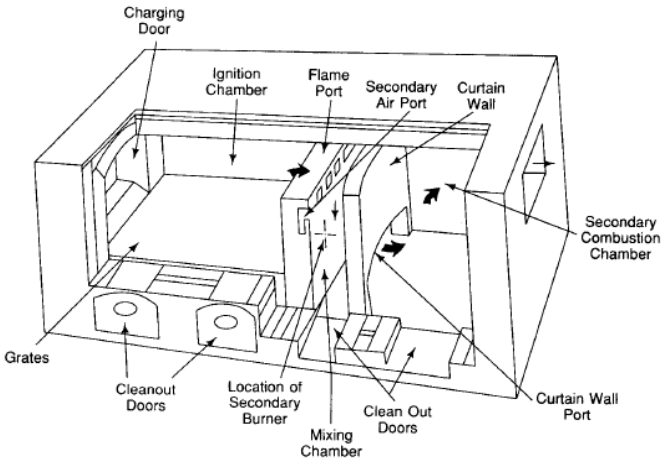

Fig. 2-11 In-line type multiple-chamber incinerators (source: Handbook of Environmental Engineering Calculations, McGraw-Hill, 2007) [45]

2.9.2 Controlled-air incinerators

The controlled-air incinerators, also referred to as the modular incinerator, makes use a two-stage combustion process. It usually consists of a primary chamber, followed by a secondary combustion chamber. The mode of

operation of the primary chamber is used to classify controlled-air incinerators as either excess-air or starved-air (sub-stoichiometric) units. The differences in these two modes of operation are:

1) Starved-air incinerator
   - Provides less than the theoretical (stoichiometric) quantity of air in the primary chamber (typically 30-80% of stoichiometric requirements).
   - Pyrolysis gases are formed in the primary chamber.
   - Provides excess air in the secondary or afterburner section to complete combustion (total excess air in the afterburner section varies between 40-250%)

2) Excess-air incinerator
   - Provides air in the primary chamber in excess of that required for combustion (typically 60-200% excess air).
   - No pyrolysis gases leave the primary chamber.
   - Promotes almost complete combustion in the primary chamber (in the order of 90-95%)
   - Gas-phase combustion is completed in the secondary chamber with additional air as required.

Of the two types of controlled-air incinerators, the starved-air unit appears to be more widely used. The success of the starved-air design has, in larger part, been due to its ability to reduce the entrainment of particulate matter in the flue gas. This is attributed to the minimum disturbance of the fuel bed and a slower rate of volatilization, which reduces fly ash formation and generates a lower uplift velocity.

The temperature in the primary chamber is usually maintained in the range of 400-870^{o}C, whereas the secondary chamber may operate at a temperature as high as 1,100^{o}C. Retention time for the gas phase in the secondary chamber is in the order of 0.5 to over 1.0 second.

The major difference between the controlled-air and multiple-chamber incinerators relates to the amount of combustion air supplied and the manner in which this is introduced into the unit. In a controlled-air incinerator, the rate of combustion air supplied to each chamber is controlled by temperature. Automatic fan damper positioning is normally used to control the air flow and, therefore, temperature in each chamber. The controlled-air concept is particularly attractive when incinerating waste materials that exhibit a wide variation in composition, such as non-anatomical biomedical waste. The controlled-air incinerator is better than the multiple-chamber in that it provides higher combustion efficiency, faster response to temperature fluctuations, and easier operating control.

2.9.3 Rotary kiln incinerator

The key component of the rotary kiln incinerator is a refractory lined cylindrical shell, mounted at a slight incline from the horizontal plane and usually followed by an afterburner section to ensure complete combustion.

Feeding system for the rotary kiln include a ram feed mechanism and a charging auger. The ram feed mechanism for waste charging can be designed to provide manual feed or a hopper and guillotine-door arrangement. The charging auger is usually arranged to receive the waste from an overhead hopper. The compaction of waste by the auger at the feed point of the kiln occurs as a result of the reduction in casing diameter and minimizes the potential for burnback into the waste. For additional burnback protection, a water spray fire-protection system can also be included in the design.

The length to diameter (L/D) ratio for rotary kilns ranges from 2:1 to 10:1, and rotational speeds range from 0.3 to 1.5 metres per minute at the kiln periphery. Speed of the rotation can be varied to maintain adequate solids retention time in the kiln to ensure good burnout of the waste. Residence time vary from a few seconds for gases, to a few hours for solid. Typical operating temperatures for rotary kiln incinerators are in the range of 800-1,200^{o}C. Since the rotary kilns are normally totally refractory-lined and have no exposed metallic parts, they can be operated at high incineration temperatures with minimal corrosion effects.

Rotary kilns have been successfully applied to various industrial operations, including pulp and paper bisulphite mills and cements plants. The technology is well suited for the incineration of a wide variety of liquids and solids, and this particularly amenable to the destruction of wastes that are difficult to thermally degrade, since temperature in excess of 1,400^{o}C can be achieved. In addition, rotary kilns can accommodate the direct charging of bulk containers without preparation. Although the use of rotary kilns in the destruction of biomedical waste is relatively new, they do offer potential application in this area.

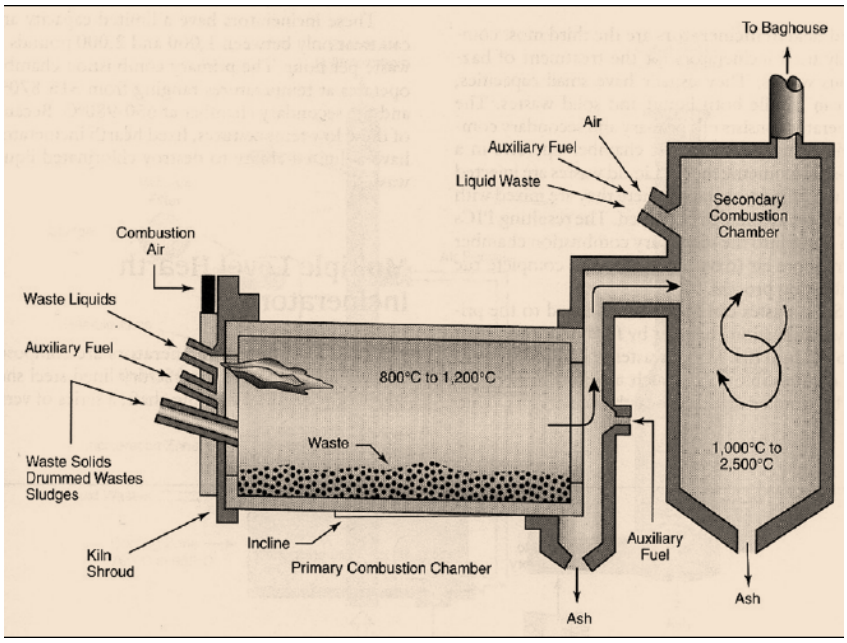

Fig. 2-12 Diagram of a Rotary Kiln with a Secondary Combustion Chamber [47]

Nonetheless, there are some disadvantages in the use of rotary kiln technology for waste incineration, such as relatively high particulate loadings in the exhaust gases due to high turbulence, and low thermal efficiency resulting from air leakage or tramp air via the kiln end seals.

2.10 Combustion process calculations in the incinerator

2.10.1 Heat balance

As the heat of combustion is released, the temperature of the air supplied for combustion combined with the gaseous products of combustion rises. The temperature achievable when only the stoichiometric or ideal air is

supplied is above that which the refractory materials used to form combustion chambers can withstand without slagging and rapid deterioration. From this standpoint alone, at least 50% and up to 150% excess air must be provided in the combustion process, resulting in "total air" of 150% to 250% of ideal air which must be supplied is determined by the desired final temperature, usually in the range from 982.22°C (1,800°F) to 1,204.44°C (2,200°F), and can be calculated by performing a heat balance between the heat released and the quantity of gases generated by the combustion process, taking into account the specific heats of the gases generated throughout the temperature range between supply and exhaust of the gases[48].

Heat balance can be computed by following equation:

$$Q = \int WC_p dT \qquad (2.61)$$

or

$$Q = WC_p \Delta T \qquad (2.61a)$$

where Q = heat transferred, Btu/h or calories/h
W = mass flow rate of gas, lb/h or mol/h
C_p = specific heat of gas, Btu/lb-°F or cal/mol-K
ΔT = temperature difference

2.10.2 Specific heat and enthalpy

Heat balance calculations can be made by using the mean specific heat of each component of the products of combustion over the range of temperatures; alternatively, the enthalpy of the gases at the temperatures involved may be used.

The specific heats of the products of combustion vary with temperature. However, the overall specific heat over the range of temperatures is quite difficult to calculate because the variation with temperature is not linear relationship. Furthermore, specific heat for some gas can be calculated by following equations[49]:

$C_p \; of \; CO_2; \; C_p = 10.34 + 0.00274T - 19{,}550/T^2$ cal/mol-K

$C_p \; of \; O_2 \; ; \; C_p = 8.27 + 0.00258T - 187{,}700/T^2$ cal/mol-K

$C_p \; of \; N_2 \; ; \; C_p = 6.50 + 0.00100T$ cal/mol-K

2.10.3 Temperature calculation

The heat released by combustion (Q) raises the temperature of the flow stream (W) of the products of combustion. The temperature rise (ΔT) of the products is dependent on the specific heat (C_p) of the mixture of gases. Consequently, Eq. 2.61a can be used to calculate for heat released:

$$Q = WC_p \Delta T \qquad (2.62)$$

where Q = heat released, Btu/h or calories/h
W = flow rate, lb/h or mol/h
C_p = specific heat, Btu/lb-°F or cal/mol-K
ΔT = temperature difference between gas entering and leaving the heat exchanger zone

2.10.4 Adiabatic flame temperature

An adiabatic flame temperature (or theoretical flame temperature) means the temperature the combustion products theoretically reach if no energy is lost to the outside environment. It can be defined for two types: one for constant-pressure combustion and one for constant-volume. If a fuel-air mixture burns adiabatically at constant pressure, the standardized enthalpy of the reactants at the initial state (298 K, 1 atm) equals the standardized enthalpy of the products at the final state (T_{ad}, 1 atm).

$$H_{reac}\ (T_i,\ P) \quad = \quad H_{prod}\ (T_{ad},\ P) \tag{2.63}$$

Equation 2.63 can be also written in term of a standardized enthalpy, which is the sum of enthalpy that takes into account the energy associated with chemical bonds (or lack thereof), the enthalpy of formation (h_f), and a sensible enthalpy change (Δh_s).

$$\bar{h}_i(T) \quad = \quad \bar{h}^0_{f,i}\left(T_{ref}\right) + \Delta\bar{h}_{s,i}(T) \tag{2.64}$$

or

$$\bar{h}_i \quad = \quad \bar{h}^0_{f,i} + \int_{298}^{Tad} \bar{c}_{p,i}\, dT \tag{2.65}$$

On the other hand, the constant-volume adiabatic flame temperature, which usually required in an ideal Otto-cycle analysis. The first law of thermodynamics requires

$$U_{reac}\ (T_{init},\ P_{init}) \quad = \quad U_{prod}\ (T_{ad},\ P_f) \tag{2.66}$$

where U is the standardized internal energy of the mixture.

2.10.5 Stoichiometry and combustion equivalent ratio

The stoichiometric quantity of oxidizer is just that amount needed to completely burn a quantity of fuel. If more than a stoichiometric quantity of oxidizer is supplied, the mixture is said to be fuel lean; while supplying less than the stoichiometric oxidizer results in a fuel-rich, or rich mixture. The stoichiometric oxidizer-(or air-) fuel ratio (mass) is determined by writing atom balances, assuming that thefuel reacts to form an ideal set of products. For a hydrocarbon fuel given by C_xH_y, the stoichiometric relation can be expressed as

$$C_xH_y \quad + \quad a(O_2 + 3.76N_2) \quad \rightarrow \quad xCO_2 + (y/2)\ H_2O + 3.76\ aN_2 \tag{2.67}$$

where $a = x + (y/4)$

Accordingly, the stoichiometric air-fuel ratio can be found as

$$(A/F)_{stoic} = \left(\frac{m_{air}}{m_{fuel}}\right)_{stoic} = \frac{4.76a}{1}\frac{MW_{air}}{MW_{fuel}} \tag{2.68}$$

where MW_{air} and MW_{fuel} are the molecular weights of the air and fuel, respectively.

The equivalent ratio (Φ) is commonly used to indicate quantitatively whether a fuel-oxidizer mixture is rich, lean, or stoichiometric [50]. The equivalent ratio is defined as

$$\Phi = \frac{(A/F)_{stoic}}{(A/F)} = \frac{(F/A)}{(F/A)_{stoic}} \quad (2.69)$$

From the definition, it can be seen that for fuel-rich mixtures ($\Phi > 1$), and for fuel-lean mixtures ($\Phi < 1$). For a stoichiometric mixture, Φ equals unity. Other parameters frequently used to define relative stoichiometry are percent stoichiometric air, which relates to the equivalent ratio as

$$\%\ stoichiometric\ air = \frac{100\%}{\Phi} \quad (2.70)$$

and percent excess air, or

$$\%\ excess\ air = \frac{(1-\Phi)}{\Phi} \times 100\% \quad (2.71)$$

2.11 Concepts of high-moisture material incineration process

Because the constituent of high-moisture material such as human corpse or municipal waste is mainly moisture (approximately 62% by weight), an auxiliary fuel is necessary to perform high temperature that the moisture can be evaporated efficiently, and dry combustible substance achieves flash point. According to the actual corpse combustion process, there is much complicate sub-reaction with a great deal of product occurred. The thermal destruction of corpse (or other solid fuel) is accomplished in four phases, as shown in Table 2-5 [51].

Table 2-5 Combustion mechanisms of solid material

Phase	Mechanisms
I	Moisture is driven off as the material is heated past the vaporization temperature of water. Drying is usually complete by the time the material has reached 150°C
II	This phase is the volatilization of vapors and gases which occurs as the temperature of the waste continues to rise. Vapors and gases diffuse out as their respective volatilization temperatures are attained.
III	The third phase in the burn-down of solids is the in-place oxidation of the burnable solids left after the vapors and gases have been volatilized.
IV	The fourth phase in the process involves the final burn-down of char and the consolidation and cooling of the inert residues, known as bottom ash.

2.12 Combustion residence time

An essential criterion in the design of combustion systems, especially the design to burn a difficult-burned waste, is the time provided for the combustion process to be completed while the gases are maintained, calculated at the typically mandated at proper combustion temperature. This time is called “retention time” and “residence time”, and is typically measured from the location where the last overfire air ports are placed[45].

Residence time is determined by the velocity of gases and the distance they travel through the combustion chamber. By multiplying the velocity and distance by the cross-section of the chamber that the volume flow rate of the gases and the volume of the chamber are obtained. Residence time is thus determined by the equation:

$$t_{res} = \text{(chamber length) / (gas velocity)} \quad (2.72)$$

or $$t_{res} = \text{(chamber volume) / (gas volume flow rate)} \quad (2.73)$$

2.13 Characteristics of turbulent nonpremixed flame

Turbulent nonpremixed flame have been employed in the majority of practical combustion systems, principally because of the ease with which such flames can be controlled[52]. Because of the many applications of nonpremixed combustion, there are many types of nonpremixed flame.

Turbulent nonpremixed jet flames visually have brushy of fuzzy edges, similar to premixed flame; however the nonpremixed hydrocarbon flames generally are more luminous than premixed counterparts, since some soot is usually present within the flame.

Flame length

Common definition of flame length include visual determinations by a trained observer, averaging a number of individual instantaneous visible flame lengths from photographic records, measuring the axial location of the average peak center line temperature, or etc.

About factors affecting flame length, four primary factors determine flame length.

- Relative important of initial jet momentum flux and buoyant forces acting on the flame, Fr_f.
- Stoichiometry, f_s.
- Ratio of nozzle fluid to ambient gas density, ρ_e / ρ_∞.
- Initial jet diameter, d_j.

The first of these factors, the relative importance of initial momentum and buoyancy, can be characterized by a flame Froude number, Fr_f. A flame Froude number was defined to establish momentum-controlled and buoyancy controlled regimes for laminar jet flames. For turbulent jet flame, the following definition of the flame Froude number is useful [53].

$$Fr_f = \frac{v_e f_s^{3/2}}{\left(\frac{\rho_e}{\rho_\infty}\right)^{1/4}\left[\frac{\Delta T_f}{T_\infty} g d_j\right]^{1/2}} \quad (2.74)$$

where ΔT_f is the characteristic temperature rise resulting from combustion.

The density ratio (ρ_e / ρ_∞) and initial jet diameter (d_j) can be combined as a single parameter, frequently referred to as the **momentum diameter**, d_j^*, and defined as

$$d_j^* = d_j (\rho_e / \rho_\infty)^{1/2} \quad (2.75)$$

The flame Froude number appears as the abscissa, and the remaining three factors are used to define a dimensionless flame length.

$$L^* = \frac{L_f f_s}{d_j (\rho_e / \rho_\infty)^{1/2}} \quad (2.76)$$

or $$L^* = \frac{L_f f_s}{d_j^*} \quad (2.77)$$

Delichatsios developed the following correlation for the dimensionless flame length L^* as

$$L^* = \frac{13.5 Fr_f^{2/5}}{\left(1 + 0.07 Fr_f^2\right)^{1/5}} \ . \quad (2.78)$$

2.14 Theory and calculation of gas burner

A burner usually plays an important role for the combustion process inside the incinerator, in order to blend proportionally air and fuel, and then, the mixture will be ignited and distributing heat to the combustion chamber [2-58].

The burner's type can be defined by the characteristic and structure of flame, which consists of 1) non-aerated flame, 2) partial aerated flame and 3) fully aerated flame.

1) Aerated flame

An aerated flame is that of the Bunsen burner with the air hole open, where primary air is entrained into the gas stream prior to combustion at the top of the burner tube. All aerated flames are generally considered to consist of three distinct regions or zones:

a) Preheat zone: In the preheat zone, unburnt gases are taken from ambient temperature to a temperature (about 700 to 1,000 K) where combustion is initiated. Heat for this is supplied by radiation and conduction against the direction of flow from further downstream. Carbonaceous fuels may pyrolyse in the preheat zone, thereby affecting the nature of the fuel. The preheat zone thickness is about 1 mm in atmospheric pressure flames.

b) Reaction zone: Combustion actually takes place in the reaction zone or flame, which is a region of intense chemical activity just 0.1 mm thick at atmospheric pressure. It is clearly visible in hydrocarbon flames as a turquoise-blue inner cone. In this region, temperature increases to over 2,000 K and the gas expands rapidly such that gas velocity increases to about seven times that of the unburnt mixture.

c) The burnt gases: The reactive chemical fragments formed in the reaction zone give rise to stable combustion products such as water vapour, carbon monoxide and carbon dioxide; additionally, depending on whether the flame is partially or fully aerated, excess fuel or oxygen will remain. In a partially aerated hydrocarbon flame, the unused fuel continues to react with secondary oxygen diffusing into the hot gases, thereby forming a well-defined violet outer mantle which extends downstream from the reaction zone. In a fully aerated flame, no further oxygen is required, so no outer mantle exists, although there is usually a visible afterglow extending downstream from the reaction zone.

2) Non-aerated flame

If a Bunsen burner is operated with the air hole closed, then no primary air can be entrained and neat gas issues from the burner tube. Combustion takes place as oxygen from the surrounding atmosphere diffuses into the emerging gas stream. The resultant flame is not as well structured spatially as an aerated flame, there being no easily defined regions. Unlike aerated flames, chemical reaction is not confined to a well defined reaction zone. However, mathematical treatments usually find it convenient to locate a reaction zone as an infinitesimally thin region where the fuel/oxygen ratio is stoichiometric, such that inside the enclosed volume the mixture is fuel-rich, while outside that volume the mixture is fuel-lean.

2.14.1 Calculation for partially-aerated burner

Due to the disadvantage of the non-aerated burner that causes of poor flame stability when gasfuel is used, a partially-aerated burner has been modified and taken place for various application, including incinerator's burner. Figure 2-13 shows the schematically the basic design of a typical aerated burner. Gas emerges from an injector nozzle consisting of one or more small holes. On leaving the injector, the gas entrains primary air by a momentum-sharing process between the emerging gas and ambient air. The gas/air mixture enters a mixing tube, which may be shaped in the form of a tapered venturi or may have parallel sides. As its name suggests, the mixing tube is designed to ensure thorough mixing of gas and air, such that a constant air/gas ratio is maintained throughout the burner head. Accordingly, three of main burner's components are considered, which are the injector, air entrainment and mixing tube.

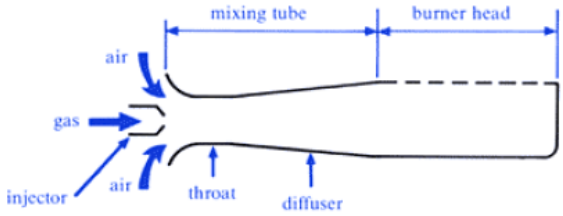

Fig. 2-13 General layout of an atmospheric injection aerated burner

1) Injector

The size and shape of an injector orifice control the gas flow rate and hence heat input for a given gas composition and supply pressure. The siting of the injector with respect to the mixing tube affects air entrainment, so the injector must be positioned with a high degree of precision during manufacture of a burner or assembly of an appliance. This section covers various fundamental and practical aspects of injector design.

The injector (or orifice) calculation is based on the Bernoulli's equation of the incompressible viscous flow.

$$\frac{p}{\rho}+\frac{v^2}{2g}-f(losses) \quad = \quad \text{constant} \tag{2.79}$$

where: p is the gas pressure (N/m^2),

ρ is the gas density (kg/m^3),

v is the gas velocity (m/s),

g is the acceleration due to gravity (9.81 m/s^2),

z is head (m). For a gas, head (z) can be ignored.

Using compressible flow theory, flow though a nozzle of area A is:

$$\dot{m} = A_0 \sqrt{2\left(\frac{\gamma}{\gamma-1}\right) p_0 \rho_0 \left[\left(\frac{p_1}{p_0}\right)^{\frac{2}{\gamma}} - \left(\frac{p_1}{p_0}\right)^{\gamma+1/\gamma}\right]} \tag{2.80}$$

where: p_0 is the pressure of the gas upstream of the nozzle (N/m^2)

ρ_0 is the density of the gas upstream of the nozzle (kg/m^3)

γ is the specific heat ratio $\left(c_p / c_v\right)$

A_0 is the area of the nozzle (m^2)

The actual flow rate through the orifice can be determined as:

$$Q = C_d Q_i = C_d A_0 \sqrt{2g(\Delta h)} \tag{2.81}$$

where: C_d is the coefficient of discharge for the orifice

Q_i is the ideal flow rate

Δh is the head loss (m)

By combining Eq. 2.80 and 2.81 and rearrange, the new compressible flow equation is obtained:

$$\dot{m} = C_d \rho_0 A_0 \sqrt{2\left(\frac{\gamma}{\gamma-1}\right)\frac{p_0}{\rho_0} r^{2/\gamma}\left(1 - r^{(\gamma-1)/\gamma}\right)} \tag{2.82}$$

or $$Q = C_d A_0 \sqrt{2\left(\frac{\gamma}{\gamma-1}\right)\frac{p_0}{\rho_0} r^{2/\gamma}\left(1 - r^{(\gamma-1)/\gamma}\right)} \tag{2.83}$$

Equation 2.83 can be simplified into the empirical equation as Eq.2.84 and 2.85

$$Q = 0.0467 C_d A_0 \left(\frac{p}{s}\right)^{1/2} \tag{2.84}$$

or $$Q = 0.036 C_d d_0^2 \left(\frac{p}{s}\right)^{1/2} \tag{2.85}$$

where Q is the gas volume flow rate (m^3/hr)

A_0 is the area of orifice (mm^2)

p is a gas pressure before the orifice (mbar)

s is the specific gravity of the gas

2) Air entrainment

The basic air entrainment mechanism may be described by reference to Fig. 2-13. The gas stream emerges as a free jet from the orifice at a rate dependent on gas pressure, orifice dimensions and gas composition. Momentum transfer occurs between the jet and the surrounding air, resulting in entrainment and expansion into the entrance of the

mixing tube. It is normally assumed that, owing to turbulence, mixing is virtually complete at the throat, at which point, depending on the precise geometry, the static pressure of the gas/air stream maybe reduced to almost that of the surrounding atmosphere. Further downstream, the static pressure must increase sufficiently to overcome resistances to flow within the burner and at the flame ports. A pressure increase can only be induced by a decrease in momentum and velocity, and this can only arise from a gradual expansion within the mixing tube. It is normally achieved by a suitably shaped diffuser section in the burner. The gas/air mixture then flows into the burner head prior to discharge from the flame ports.

In deriving equations for air entrainment, a number of simplifying assumptions are made:

a) Flow is turbulent in the mixing tube such that there are no radial components of velocity, temperature or composition.
b) Air is entrained perpendicular to the axis of the mixing tube, and therefore contributes no axial momentum.
c) Flow is incompressible, i.e. density is not dependent on pressure.
d) The pressure distribution at the burner head is uniform.
e) The combustion chamber is at atmospheric pressure, i.e. the effects of flue pull or fan pressure are ignored.
f) Buoyancy of the unburnt gas/air mixture is neglected.

Momentum and energy balance

The principle behind the derivation is the application of a momentum balance to the mixing process and energy balances to the pressure increase behind the burner ports and to the discharges from the injector and from the burner ports. For the physical properties of the burner assembly, p, A and C_d representing pressure, area and discharge coefficient, are used with subscripts o, j, t and p for ambient, injector outlet, throat and diffuser exit respectively. For gas and air, ρ and V represent density and volume flow rate, while subscripts g, a and m, are used for gas, air and the mixture [54].

Neglecting stream contraction, a force-momentum balance for the mixing process between the injector outlet and the throat gives:

$$(p_t - p_o)A_t = \frac{\rho_g V_g^2}{A_j} - \frac{\rho_m V_m^2}{A_t} \quad (2.86)$$

An energy balance between the throat and the diffuser outlet (i.e. just upstream of the burner ports) gives:

$$(p_p - p_t) = \frac{\rho_m V_m^2}{2A_t^2}(1 - C_L) \quad (2.87)$$

where C_L is a friction loss coefficient for the throat and diffuser, expressed as a fraction of the kinetic head in the throat of the mixing tube.

An energy balance discharge from the injector can be represented as:

$$(p_i - p_o) = \frac{\rho_g V_g^2}{2A_i^2 C_{dj}^2} \quad (2.88)$$

Injector/throat area ratio

Francis [55] introduces dimensionless pressure efficiency η, defined as the ratio of the static pressure behind the burner ports to the dynamic pressure of the gas jet issuing from the injector, i.e.

$$\eta = \frac{p_p - p_o}{\left(\frac{\rho_o V_g^2}{2A_t^2}\right)} \tag{2.89}$$

which, on combining with Eq. 2.88, gives:

$$\eta = \frac{p_p - p_o}{C_{dj}^2 (p_i - p_o)} \tag{2.90}$$

In order to simplify the algebra, two parameters will be defined:

$$\theta = \frac{A_j}{A_t} \quad ; \qquad \lambda = \left(\frac{\rho_m V_m^2}{\rho_g V_g^2}\right)(1 + C_L)$$

Therefore, Eq. 2.90 can be written in the form:

$$\eta = 2\theta - \lambda\theta^2 \tag{2.91}$$

Optimum, performance for aerated burners is given by the maximum value of η, i.e. the greatest static pressure behind the burner ports for a particular gas rate from a given injector.

$$\frac{d\eta}{d\theta} = 2 - 2\lambda\theta \tag{2.92}$$

and

$$\frac{d^2\eta}{d\theta^2} = -2\lambda \tag{2.93}$$

Therefore, η is a maximum when $\lambda\theta$ =1, i.e. when

$$\frac{A_j}{A_t} = \frac{\rho_g V_g^2}{\rho_m V_m^2 (1 + C_L)} \tag{2.94}$$

If R is the entrained air to gas volume ratio, then V_a=RV_g and V_m=V_g(1+R). Substitution into Eq. 2.94 gives:

$$\frac{A_j}{A_t} = \frac{\rho_g}{\rho_m (1 + R^2)(1 + C_L)} \tag{2.95}$$

From mass balance, a mixture density is obtained

$$\rho_m = \frac{\rho_g V_g + \rho_a V_a}{V_m} = \frac{\rho_g (\sigma + R)}{\sigma (1 + R)} \tag{2.96}$$

where σ is the relative density of the gas. Substituting this expression into Eq. 2.95 gives:

$$\frac{A_j}{A_t} = \frac{\sigma}{(\sigma + R)(1 + R)(1 + C_L)} \tag{2.97}$$

This equation relates the optimum injector/throat area ratio to properties of the gas and gas/air mixture.

Entrainment (air/gas) ratio

From Eq. 2.97, a quadratic equation is arranged as:

$$(\sigma + R)(1 + R) = \frac{\sigma}{1 + C_L} \cdot \frac{A_t}{A_j} \tag{2.98}$$

$$R^2 + R(1 + \sigma) + \sigma\left(1 - \frac{A_t}{A_j(1 + C_L)}\right) = 0 \tag{2.99}$$

$$R = \frac{-(1 + \sigma) \pm \sqrt{(1 - \sigma)^2 + \frac{4\sigma A_t}{A_j(1 + C_L)}}}{2} \tag{2.100}$$

Since $(1 - \sigma)^2$ is small compared with $\frac{4\sigma A_t}{A_j(1 + C_L)}$.

The solution can be approximated by:

$$R = \frac{-(1 + \sigma)}{2} + \sqrt{\frac{\sigma A_t}{A_j(1 + C_L)}} \tag{2.101}$$

In addition, the R value can be determined by the stoichiometry volume flow rate of gas and air mixture.

Chapter 3
Calculation and Design for the Experimental Apparatuses

3.1 Design on downdraft biomass gasification system

Due to the required biomass producer gas that can perform smooth and uniform experimental conduction, tar content in the producer gas should be eliminated as much as possible, by the most appropriate gasifier type with optimal operation condition. Accordingly, an Imbert downdraft gasifier type was selected for the experiment.

The Imbert gasifier type mainly contains of nozzle (or tuyere) and constricted hearth. The nozzles are installed radically that permit air to be drawn into the biomass as they move down to be gasified. Typically, there are an odd number of nozzles so that the hot gases from one nozzle do not impinge on the opposite tuyere. This gasifier type also requires a low-moisture (less than 20%) and uniformly blocky fuel in order to allow easy gravity feeding through the constricted hearth.

In order to choose the proper dimensions of any gasifier, a superficial velocity (V_S) is an important factor that can be calculated where the gas passes through the narrowest part of the gasification zone. Furthermore, the related term to the superficial velocity is the hearth load (B_H), which expresses in gas volume per hearth area. For the Imbert gasifier type, the maximum hearth load $(B_{H\max})$ is 0.9 Nm^3/cm^2-h, while this value corresponds to the superficial velocity at 2.5 m/s.

If the diameter of gasifier and diameter of the narrowest part (hearth zone) are defined as D_r and D_H, respectively, the relation of both parameters can be used to estimate other design parameters such as number of nozzles, height of reduction zone, height range between tuyere plain and hearth zone.

The volumetric flow rate of producer gas generation can be estimated by conducting of nitrogen neutral between biomass fuel and producer gas, assuming the highest calorific value of producer gas is given when the injected air equivalent ratio is equal to 0.2.

The producer gas generated from wood has a composition, as shown in Table 3-1.

Table 3-1 Composition of producer gas generated from wood

No.	Gas compositions	% of volumetric concentration (% v/v)
1	H_2	7.24
2	CH_4	5.65
3	CO	19.53
4	O_2	7.97
5	CO_2	9.00
6	N_2	50.61
	Total	**100.00**

Source: Department of Alternative Energy Development and Efficiency, Ministry of Energy of Thailand [56]

Design criterion for prototype gasifier is the maximum fuel input rate equals 15 kg per hour. Then, approximated volumetric gas generation rate is 18.22 m^3 per hour. Consequently, the proper hearth zone diameter that calculated volumetric gas flow rate (18.22 m^3 per hour) can be achieved the maximum hearth load ($B_{H\max}$ = 0.9 Nm^3/cm^2) is 6 cm (60 mm).

The relationship of gasifier diameter and hearth zone diameter ratio (d_r/d_h) can be employed to determine the height between tuyere plain and hearth zone (h). It is found that at hearth diameter (d_h = 60 mm), the proper gasifier diameter (d_r) is 268 mm. Then, the height between tuyere plane and hearth zone becomes 80 mm. At a same time, other parameters such as amount of tuyere, tuyere inner diameter, diameter between tuyere and reduction zone height.

Table 3-2 Determined parameters for gasifier design

Gasifier Diameter (d_r)	Hearth Zone Diameter (d_h)	Diameter Between Tuyere ($d_{r'}$)	Tuyere Inner Diameter (d_m)	Amount of Tuyere	Height between Hearth Zone and Tuyere plain (h)	Height of Reduction Zone (h_R)
268	51	150	7.5	5	80	100

Unit: millimeter

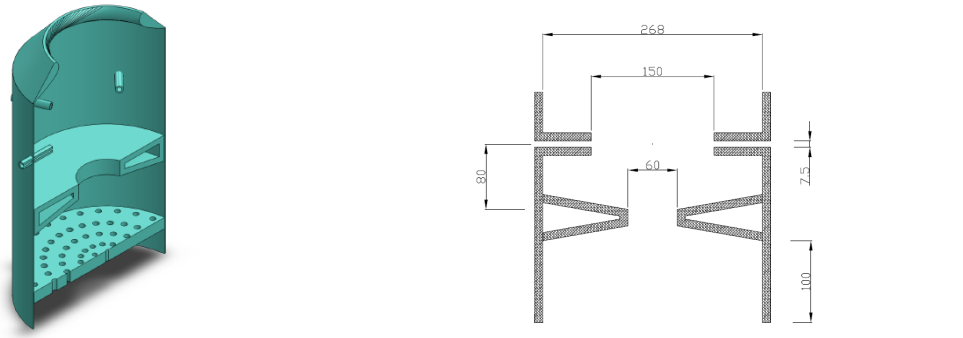

a) 3-Dimensions drawing b) Dimensions of combustion and reduction zone

Fig. 3-1 Drawing of gasifier prototype

3.2 Calculation and design on double-chambered incinerator prototype

Main criteria to design for proper incinerator in this research are that the incinerator prototype must contain of two combustion chambers. The main chamber (primary chamber) is used to combust sample high-moisture material by heat from producer gas combustion, and the secondary chamber (post combustion) is used to eliminate dust particle and combustion gas product from the primary chamber before release to the atmosphere.

The adequate volume of primary combustion chamber was determined by the estimation of combustion gas product (producer gas and sample material) residence time inside incinerator. The proper volume of the primary chamber was determined by Eq. 3.1 [57].

$$V_{chamber} = \frac{Q_{net}}{(Q_R)_V} \quad \text{m}^3 \qquad (3.1)$$

and

$$Q_{net} = \{(m_{fuel} \times HHV_{fuel}) + (m_{gas} \times HHV_{gas})\} - Q_{loss} \quad \text{MJ} \qquad (3.2)$$

Where Q_{net} means net heat generation inside the incinerator, $(Q_R)_V$ is the heat release from the incinerator (MJ/m^3-hr), and Q_{loss} is the total heat loss from incinerator.

Due to the constituent of biomass producer gas, as shown in Table 3-1, it can examine an air fuel ratio (*A/F*) from combustion of biomass producer gas at stoichiometric condition. Main combustible gases consist of hydrogen (H_2), carbon monoxide (CO) and methane (CH_4). Likewise, some of oxygen constituent in the fuel gas can support the gas combustion, or this means that it needs less amount of outside air for theoretical combustion.

From the theoretical combustion calculation of biomass gas, it can be found that the amount of oxygen needed to burn 9 m^3 of biomass producer gas is equal to 1.50 m^3. Thus, an amount of air needed for fuel gas theoretical combustion becomes 7.16 m^3, or it equivalents to 0.80 A/F ratio. At a same time, stoichiometric gas product after combustion is equal to 15 m^3.

A weight of high-moisture material used for the experiment is 5 kg. Moisture content inside the material is approximately 62% by weight of total weight, and the empirical formula of dry material is $C_5H_{10}O_3$. Hence, an amount of air needed for theoretical meat combustion is 7 kg-air per kg of dry material. In addition, an excess air must be introduced into material combustion process, in order to prevent starve air condition. Floyd (2007) [45] recommended the amount of excess air should be approximately 150% of theoretical combustion air, thus, the excess air condition for experiment was equal to 25.38 kg-air.

To calculate the net heat generation inside the primary chamber, heating value of biomass producer gas and high-moisture material are necessary. The high heating value of biomass producer gas is 5.68 MJ/m^3, by referring to the constituent shown in Table 3-1. For the high heating value of high-moisture material, DuLong formula is used for calculation [58],

$$HHV = \frac{(35.5C + 114.8H + 9.5S - 14.5O)}{100} \times (1{,}000 \text{ J/kJ}) \quad \text{kJ/kg} \qquad (3.3)$$

where C, H, S and O are the percent of each component in the fuel.

From DuLong formula, it can be determined that the meat's high heating value is 6.65 MJ/kg. Likewise, heat loss from the primary chamber is assumed by 5% of total heat generation from fuel combustion, and the heat release from the incinerator, $(Q_R)_V$, is 763 MJ/m^{3}hr [59]. Therefore, an adequate primary chamber's volume is equal to 0.105 m^3.

For the secondary chamber, fluid flow in this chamber contains of combustion gas releasing from primary chamber, with the combustion gas obtained from the secondary burner. From the calculation of theoretical

combustion in primary chamber, total volume flow rate of gas product releasing to the secondary chamber was equal to 0.03 m^3/s.

The significant parameter for the secondary chamber design is a residence time (or retention time), which means the time provided for the combustion process to be completed while the gases are maintained. The relation of residence time and volume of secondary chamber is explained in Eq. 3.4.

$$t_{res} = \frac{V_{chamber}}{\dot{Q}_{gas}} \tag{3.4}$$

C.C.Lee and G.L.Huffman (1986) [60] presented the proper residence time in an incinerator should be 1 second, thus, the adequate volume of the secondary chamber is equal to 0.03 m^3.

Thavornund [61] has studied for an energy saving crematory and discovered that the shape of crematory's secondary chamber must be rectangular with U-shape of gas path, to contribute efficient dust particle precipitation.

The arrangement injected air nozzle arrays has been installed by following study of Bubpamala (2007) [62] that proposed the incline arrangement of two opposite air nozzle arrays which the angle 330 degree and 120 degree of left and right air-nozzle from front incinerator wall, can achieve more effective in terms of mixing, mass flow and gas residence time distribution.

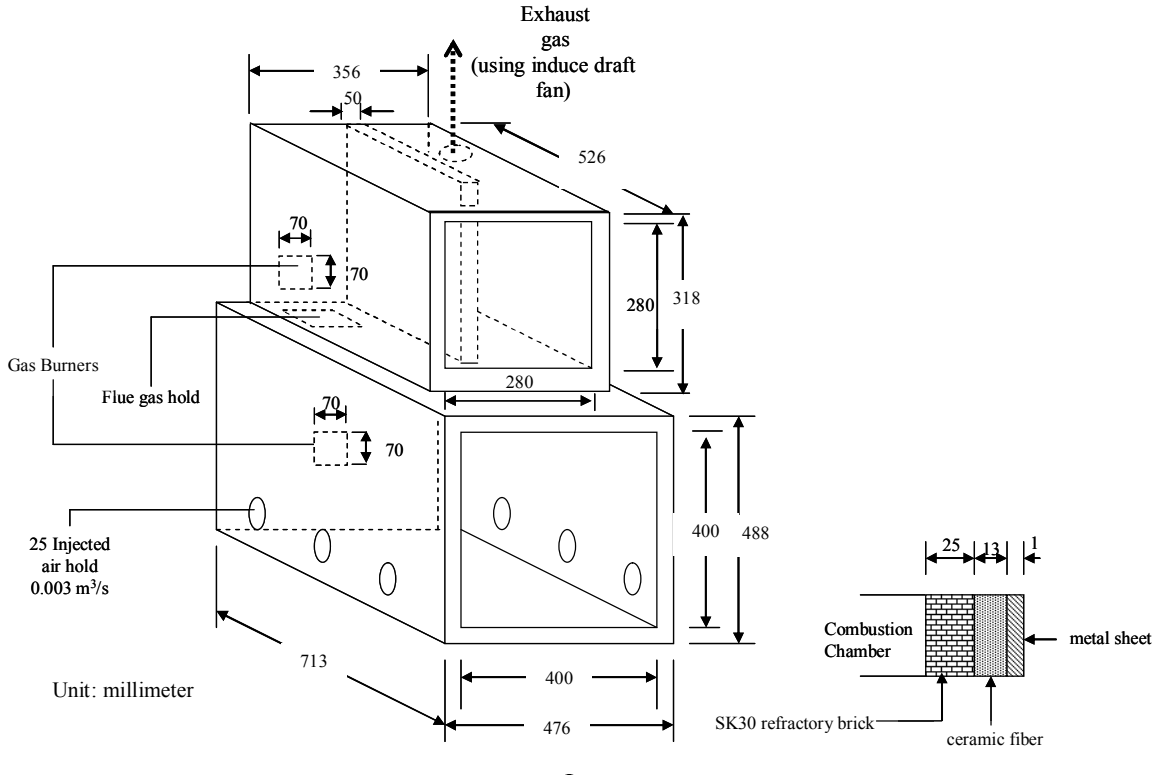

Fig. 3-2 Drawing of designed double-chambered incinerator prototype

3.3 Calculation and design on biomass producer gas burner

In this research, two producer gas burners have been designed for mixing producer gas with primary air, then the fuel mixture will be mixed again with the secondary air at the proper ratio before ignition and distributing heat to the sample high-moisture material (or flue gas at the secondary chamber). Each gas burner contains 3 main parts: the orifice, mixing room and throat.

3.3.1 Burner's orifice

An orifice is used to increase the velocity of producer gas before mixing with primary air, then the potential energy of a high pressure gas supply is mixed into the kinetic energy of an emerging gas jet. The size of the orifice related to the mass flow rate of producer gas is expressed by a combination between the compressible equation and actual volume flow rate at the orifice channel, as described in Eq. 2.84 and 2.85 in Chapter 2.

$$Q = 0.0467 C_d A_0 \left(\frac{p}{s} \right)^{1/2} \tag{2.84}$$

or

$$Q = 0.036 C_d d_0^2 \left(\frac{p}{s} \right)^{1/2} \tag{2.85}$$

Following data are substituted into the volumetric flow rate equation to examine the proper orifice's diameter;

Producer gas flow rate from gasifier	9 m^3/h.
Gas supply pressure	0.88 mbar (88.26 Pa)
Specific gravity of biomass gas	1.10

Accordingly, the result of calculated orifice diameter (d_0) by using above information is equal to 17.22 mm.

H.R.N. Jones has proposed the relationship between the angle of approach and coefficient of discharge (C_d) that should be 33^o and 0.93, respectively. Moreover, in order to maximize (C_d), the length of the orifice channel should be between 1.5 and 2 times the orifice diameter [(54)].

3.3.2 Mixing room

After a producer gas passes through the burner's orifice, the primary air will blend with the fuel gas. The momentum transfer occurs between the jet and the surrounding air, resulting in entrainment and expansion into the entrance of the mixing room. An entrainment ratio, r, is determined by the relation between volume flow rate for air and biomass producer gas. Therefore:

$$r = \text{Volume flow rate of producer gas / Volume flow rate of air} \tag{3.5}$$

Due to the system's design criteria, the volume flow rate of biomass gas is approximately 9 m^3, whereas the volume flow rate of air needed for gas combustion is 7.16 m^3. The entrainment ratio, therefore, is 1.26.

The mixture flow rate at the optimum aeration can be calculated by

$$\dot{Q}_m = \frac{\dot{Q}_{gas}(1+r)}{3{,}600} \quad \text{m}^3/\text{s} \quad (3.6)$$

At the entrainment ratio 1.26 and 9 m^3 of fuel gas volumetric flow rate, it can be found that the calculated mixing flow rate becomes 5.65×10^{-3} m^3/s.

3.3.3 Burner throat

A burner's throat is a final important part of a gas burner. The diameter of the burner's throat theoretically relates to the entrainment ratio and diameter of orifice. Thus, its diameter can be determined by substituting the entrainment ratio into Prigg's formula.

$$d_t = \left(\frac{r}{\sqrt{SG_{gas}}} + 1\right) d_0 \quad \text{mm} \quad (3.7)$$

From Eq. 3.7, the calculation result of the burner's throat diameter (d_t) is 37.90 mm.

The length of the throat can be estimated by the correlation between the throat diameter and air/gas ratio. In case the air/gas ratio calculated is 91% of the theoretical air/gas ratio, the throat length becomes 2.5 times the size of the throat diameter. Hence, the length of burner's throat becomes 160 mm.

All calculated dimensions of gas burner are shown in Fig. 3-3.

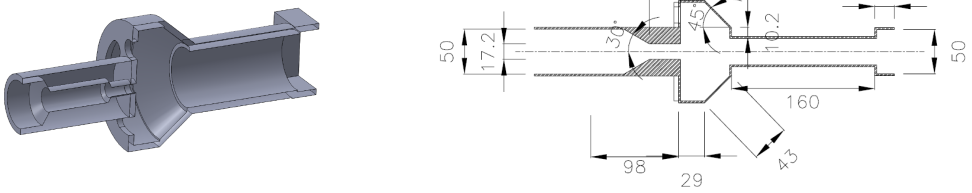

Unit: millimeter

Fig. 3-3 Dimension of designed gas burner

3.4 Design of the producer gas treatment systems

Before using producer gas as a fuel in the incinerator, it is necessary to remove tar and dust content in the producer gas in order to avoid adherence in the pipeline and gas burner. Therefore, a gas treatment system has been designed. The system mainly consists of a cyclone and tar extraction unit (condenser).

3.4.1 Cyclone

The cyclone is the first treatment system that was selected to extract heavy dust particles and flying ash content in producer gas. From the gasifier calculation, the outlet volumetric flow rate of producer gas is 18 m^3 per hour. Thus, the inlet velocity of a cyclone can be computed by Eq. 3.8, assuming the inlet diameter is 5 cm.

$$\vec{V}_{inlet} = \frac{1}{3{,}600}\left(\frac{4\dot{Q}_{gas}}{\pi d_{inlet}^2}\right) \quad \text{m/s} \qquad (3.8)$$

Hence, the inlet velocity is 2.58 m/s.

After obtain the inlet velocity of gas, dimensions of the high efficiency cyclone can be computed. Figure 3-4 shows the relationship between significant cyclone dimensions with the diameter.

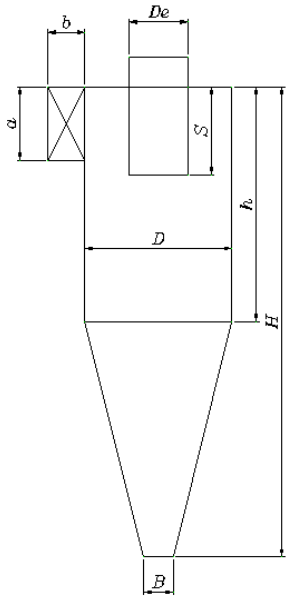

a	Height of gas inlet
b	Width of gas inlet
S	Length of gas outlet
D_e	Diameter of gas outlet
h	Height of the cylinder
H	Total height of cyclone
B	Diameter of dust outlet

Fig. 3-4 Significant dimension for high efficiency cyclone design

Following relationships are used to find cyclone's dimensions:

a	=	*0.5D*
b	=	*0.25D*
S	=	*0.625D*
De	=	*0.5D*
h	=	*2D*
H	=	*4D*
B	=	*0.25D*

Consequently, the proper cyclone parameters are determined, as shown in Fig. 3-5.

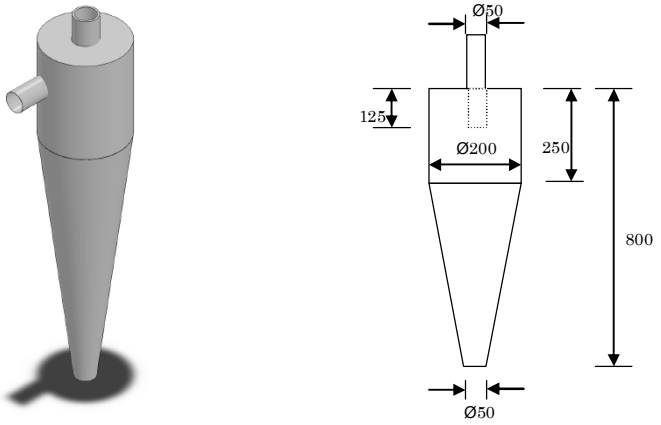

Unit: millimeter

Fig. 3-5 Designed producer gas's cyclone

3.4.2 Condenser (Tar extraction unit)

Tar extraction unit becomes one of an important part of gas cleaning system, in order to extract tar and dust content in biomass gas that cannot be separated by using cyclone. Design criteria of the tar extraction unit in this research refer to the log mean temperature difference (LMTD) method, by using Eq. 2.59 and 2.60 from Chapter 2.

$$Q_{H.E.} = UA_s\Delta T_{lm} \quad \text{Watt} \tag{2.59}$$

where

$$\Delta T_{lm} = \frac{\left\{\left(T_{h,in}-T_{c,in}\right)-\left(T_{h,out}-T_{c,out}\right)\right\}}{\ln\left(\frac{T_{h,in}-T_{c,in}}{T_{h,out}-T_{c,out}}\right)} \tag{2.60}$$

From calculation, the amount of total water tubes are 12 tubes, which has 25 cm diameter and 400 cm length.

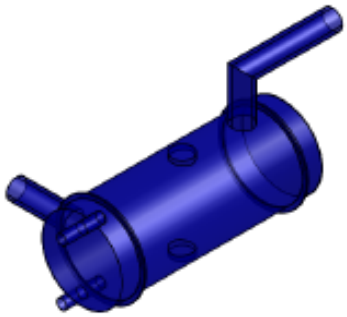

Fig. 3-6 Three dimension drawing of tar extraction unit

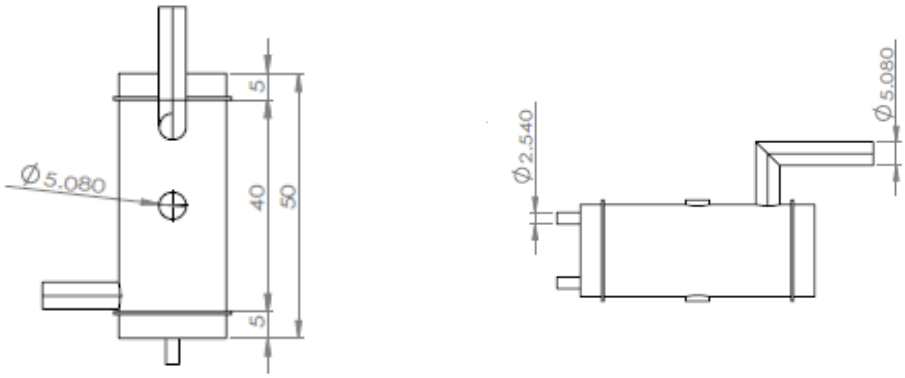

Fig. 3-7 Schematic drawing of the tar extraction unit used in this research

Chapter 4
Apparatuses Preparation and Experiment Conduction

4.1 Biomass fuels

Four kinds of biomass fuel, which are macadamia shell, coffee bean pulp, rice husk and wood charcoal, has been selected to be raw feedstock of biomass gasifier. Criteria of fuel selection consisted of the kinds of biomass must be collected in Thailand, and the fuels must be agricultural wastes.

a) Coffee bean pulp

b) Macadamia shell

c) Wood charcoal

d) Rice husk

Fig. 4-1 Selected biomass fuel

The analysis results (proximate and ultimate analysis) with the heating values of fuels are shown in Table 4-1.

Table 4-1 Proximate and ultimate analysis of selected biomasses

Biomass	Proximate analysis (% by weight)				Ultimate analysis (% by weight)						Gross Calorific Value (MJ/kg)
	Moisture	Ash	Volatile matter	Fixed carbon	Ash	C	H	N	S	O	
Coffee bean pulp	11.29	0.38	73.94	14.39	0.43	50.28	5.46	0.15	0.05	43.62	17.91
Macadamia shell	10.14	0.40	69.86	19.59	0.45	53.11	6.15	0.35	0.05	39.89	21.10
Rice husk	7.71	22.98	59.03	15.70	15.50	38.50	5.70	0.50	0.00	39.80	15.30
Wood charcoal	-	1.04	39.50	59.46	3.40	80.30	3.10	0.20	0.00	11.30	31.02

4.2 High-moisture material sampling

Main property of the sampling material is necessary to determine the stoichiometric air for complete combustion reaction. Therefore, the chemical composition of animal anatomical waste data was taken and referred for the calculation and incinerator design. The dry combustible empirical formula of the whole dead animal is $C_5H_{10}O_3$. Table 4-2 describes the ultimate analysis result of the high-moisture material.

Table 4-2 Ultimate analysis for high-moisture material

Constituent	Ultimate Analysis	
	As charged (% by weight)	Ash and moisture free combustible (% by weight)
Carbon	14.7	50.80
Hydrogen	2.7	9.35
Oxygen	11.5	39.85
Water	62.1	-
Nitrogen	Trace	-
Mineral (ash)	9.0	-

According to above property, it can be determined that the stoichiometric air needed for meat's combustion is 7 kg-dry air per kg-meat. Because any meats are classified as solid fuel, excess air condition must be performed to meat combustion. An amount of excess air should be 100-150%[46].

For high-moisture material used to be burnt in the designed incinerator, five kilograms of fresh chicken meat was selected as a sample material. The meat's weight was measured before starting experiment. Likewise, unburnt material after combustion (i.e. ash), will be measured again after finish every experiment.

4.3 Experiment measurements

4.3.1 Gas and air volumetric flow rate

The results of volumetric flow rate of biomass producer gas and air play and important role to determine the amount of these fluids for the important evaluation such as energy and mass balance. Accordingly, Venturi flow meter was selected to be measured the volume flow rate.

In order to use Venturi flow meter, following equations need to be concerned [63].

$$Q_1 = A_1 V_1 \tag{4.1}$$

$$V_1 = \sqrt{\frac{2\Delta P}{\rho_{gas}\left[\left(\frac{A_1}{A_2}\right)^2 - 1\right]}} \tag{4.2}$$

$$\Delta P = \rho_{water} g \Delta h \tag{4.3}$$

Where: Q_1 = volume flow rate of biomass gas/air(m^3/s)

V_1 = velocity of biomass gas/ air (m/s)

A_1, A_2 = cross section area of the venture throat (m^2)

ΔP = pressure difference causes changing of flow rate (Pa)

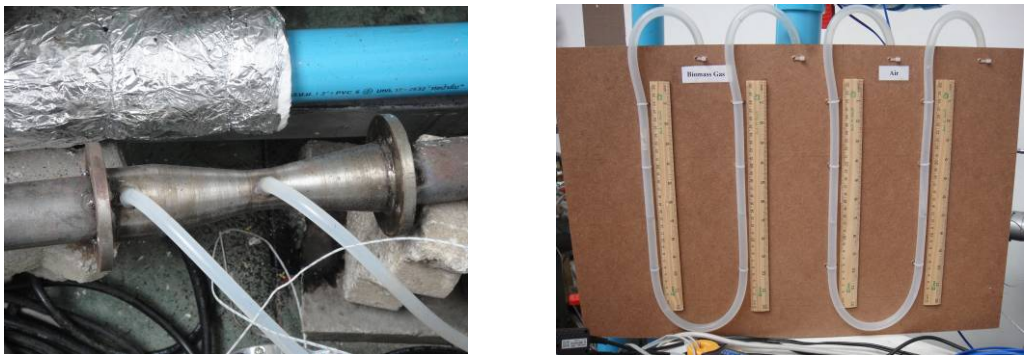

Fig. 4-2 Photography of Venturi flow meters and manometers used in the experiment

4.3.2 Temperature measurement

K-type of thermocouple is used for temperature measurement in both gasifier and incinerator. There were totally 30 positions installed for temperature measuring. All temperature positions were connected to the data logger (HIOKI 8422-50) for temperature record.

4.3.3 Electricity consumption

An electricity power consumption of electricity devices (gas blower, injected air blower and induced draft fan) is investigated by using power meters (HIOKI-3169-01). These power consumption values will be used to calculate the energy balance of all system, respectively.

Arrangements of thermocouples, data loggers and power meters are described in Fig. 4-3.

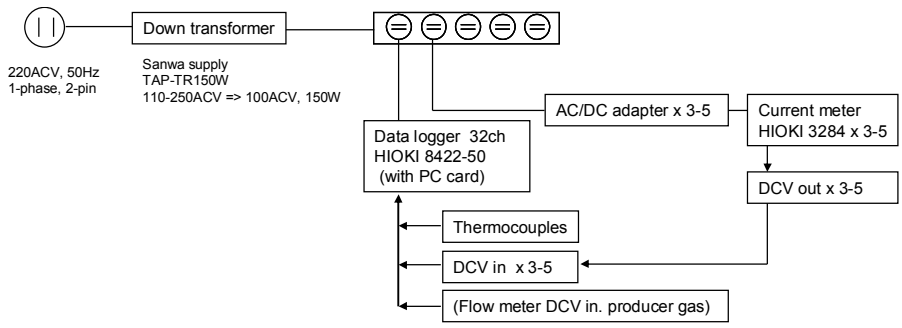

Fig. 4-3 Schematic diagram of the data loggers and power meters arrangement

Fig. 4-4 Data loggers and power meters set up

4.3.4 Exhaust gas property

A gas analyzer (TESTO 330) was used to measure the property of combustion exhaust gas such as CO_2, CO, O_2, excess air, and temperature. Especially, the amount of excess air released from the stack will be able to determine the amount of combustion air needed, by using Eq. 4.4 [50].

$$\% \text{ excess air} = \frac{(1-\Phi)}{\Phi} \times 100 \ \% \tag{4.4}$$

4.3.5 Opacity of exhaust gas

The opacity of flue gas measurement using Ringelmann's chart (BS. 2742: 1969) [64] was selected for adequate method to measure the rate of emission releasing from high-moisture material and producer gas combustion.

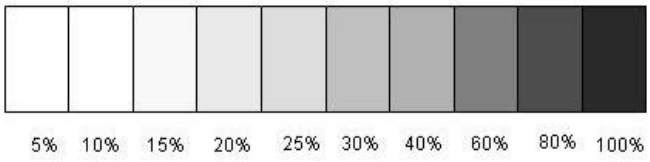

Fig.4-5 Ringelmann's chart

In these experiment conductions, an observer has observed the opacity of flue gas released from incinerator's stack, and then, compared with value shown in Ringelmann's chart. The observation was carried out every minute until finishing experiment.

4.4 Experimental apparatuses set up

4.4.1 Prototype of high-moisture material incinerator

A prototype of high-moisture material double-chambered incinerator used in this research was constructed. The material used to build the combustion chamber was a refractory brick (SK30 refractory brick, 25-mm.). Beside the refractory layer, a ceramic fiber insulator, which has 12.5 mm thickness, was composed. Finally, a 1.5 mm.-thickness metal sheet was covered the insulator.

Fig.4-6 Prototype of high-moisture material's double-chambered incinerator

4.4.2 Producer gas tube and flow control

After system design and construct, all experimental apparatuses were composed together. A steel tube was used to convey the producer gas from gasifier to the incinerator via gas cleaning system. Before obtaining proper producer gas for ignite at the incinerator, incombustible gas should be exhausted. Consequently, a steel ball valve was also installed to control producer gas direction, including flow rate of gas during experiment.

To control the amount of air injected to the incinerator, a centrifugal fan with inverter were also set up. Same as induced draft fan that was installed at the flue gas stack to sustain both of gas flow and residence time in both primary and secondary chamber. The schematic diagram of system installation is shown in Fig. 4-7.

The experiment were set up and conducted at the Renewable Energy and Energy Conservation, Faculty of Engineering of Chiang Mai University, Thailand.

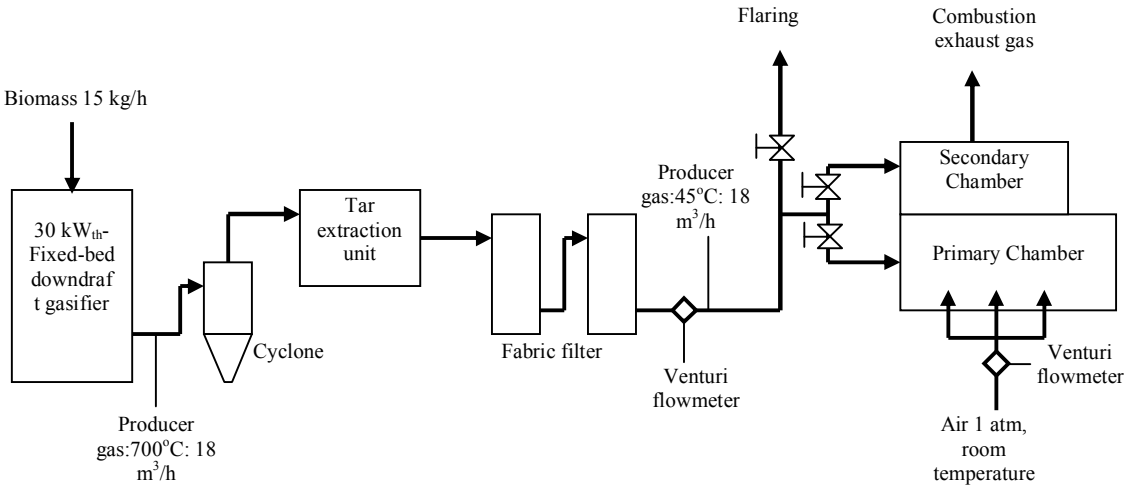

Fig. 4-7 Schematic diagram of experimental apparatuses

4.4.3 Electrical devices

Electrical devices, such as producer gas blower, exhaust fan, injected air controlled blower, were connected to the power meters, as described earlier. After finishing the experiment, all recorded data were transferred to a personal computer, and evaluated, respectively.

4.5 Conduction for the experiment

Due to the type of biomass gasifier that presents fixed-bed downdraft type, it is important to conduct for the bed (reduction zone or char zone), in order to origin the significant reaction for producer gas generation. From the investigation, the best gas quality will be generated when the temperature of reduction zone is higher than 800°C because carbon dioxide will decompose into carbon monoxide, and carbon dioxide completely changes into carbon monoxide if temperature is higher than 900°C [(65)].

Accordingly, 4 kg of wood charcoal were ignited until the temperature reaches 400°C, and then, scorched charcoal will be introduced into the gasifier. By using the draft flow influence from gas blower, air will be drafted into the gasifier, and increases the combustion rate of charcoal, as shown in Fig. 4-7. When the temperature of the gasifier's char bed achieving 850°C, selected biomass fuel was instantaneously fed into the gasifier, and biomass producer gas can be obtained.

After biomass producer gas will be ready to be used, by ignition testing at the flaring stack, fuel gas was injected to the gas burner and started combustion. In case both of primary and secondary chamber were conducted simultaneously, the secondary burner firstly start ignition, and temperature achieved maximum point before igniting the primary burner, in order to destroy toxic gas released from high-moisture material combustion.

Fig. 4-8 Gasifier's reduction zone

Fig. 4-9 Introduction of biomass fuel into the gasifier

Fig. 4-10 Ignition of biomass producer gas at the primary burner

4.6 Biomass producer gas sampling

After producer gas was already generated, some of fuel gas sample was imbibed into a sampling bag and analyzed by using Gas Chromatography (GC). The sampling method referred to API method that using both solid and liquid trapping, by passing biomass producer gas through unabsorbed solution and adsorbent (silica gel, activated carbon), in order to separate dust and organic matter from fuel gas. Figure 4-11 shows the photography of gas sampling method.

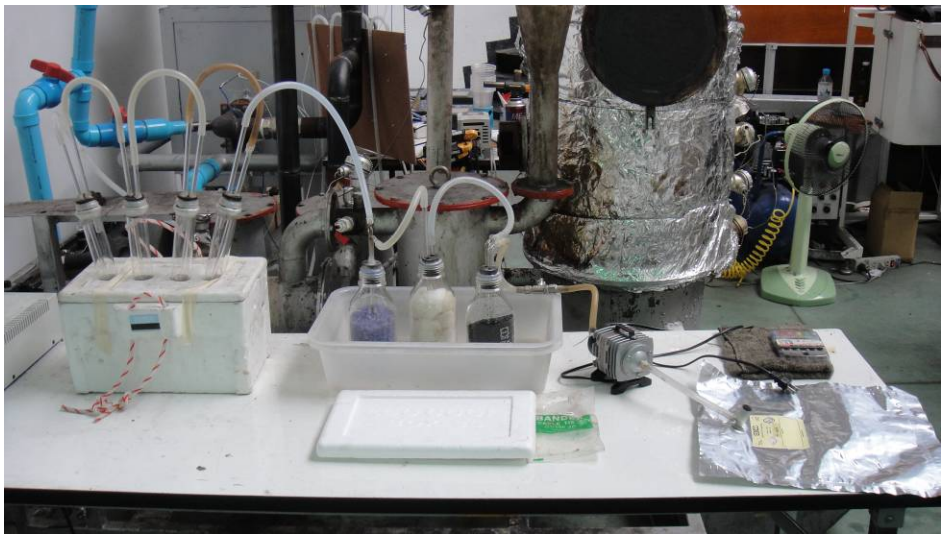

Fig. 4-11 Biomass producer gas sampling

Chapter 5
Evaluations on Experimental Results and Discussions

5.1 Biomass producer gas analysis

After biomass producer gas was generated from the gasifier, some of gas will be sampled and analyzed by using Gas Chromatography. Following table explains the result of producer gases analysis.

Table 5-1 Biomass producer gas analysis results

Biomass	Gas content (% by volume)					
	H_2	O_2	N_2	CO	CH_4	CO_2
Macadamia shells	11.2	8.1	46.2	17.7	3.0	13.8
Coffee bean pulp	14.9	6.2	39.7	22.5	2.9	13.8
Rice husk	14.7	9.6	39.7	8.9	2.5	24.6
Wood charcoal	7.2	8.0	50.6	19.6	5.7	9.0

From above information, it is found that biomass gas generated from coffee bean pulp contains richest ratio of CO and H_2. Rice husk producer gas, on the other hand, consists for high H_2 but has low quantity of CO, because biomass gas generated from rice husk was produces at low gasifier's reduction zone temperature (char bed) that is lower than 900^{o}C. Thus, CO_2 cannot be disintegrated and become CO, which can be investigated from high constituent of CO_2 in above table. Likewise, the gas produced by using wood charcoal presents concentration in methane (CH_4) and CO. However, the constituent of H_2 results the lowest, compares with H_2 content in other fuel gas.

Table 5-2 Heating value of biomass producer gas

Biomass	Heating Value (MJ/m^3)
Macadamia shells	4.60
Coffee bean pulp	5.58
Rice husk	4.04
Wood charcoal	5.68

Table 5-2 describes the heating value of each biomass producer gas. The highest heating value occurs from wood charcoal gas. Whereas, the gas generated from rice husk presents lowest heating value. These results explain the rich content of CH_4, which release highest heating value compares with CO and H_2, in charcoal gas, by the reaction of H_2

with carbon (C) and becomes CH_4 as described in Eq. 5.1. Furthermore, high constituent of CO also promotes the heating value of producer gas, which can be found by the decrease of CO_2 amount from gas analysis.

$$C + 2H_2 \rightarrow CH_4 \quad (5.1)$$

About the heating value of rice husk producer gas, it is discovered that it has low constituent of combustible gas such as CO and CH_4. Hence, it results for low energy content in the gas.

In addition, it can be investigated that the fuel that contains high calorific value does not usually result for high gas heating value. For example, the heating value of macadamia shell is higher than the heating value of coffee bean pulp. Nevertheless, heating value of gas generated from coffee bean pulp results in higher value compares with macadamia shell gas. This phenomenon can be excused that carbon content in macadamia shell's char does not react and transform to fuel gas, which can be found there is much amount of remaining carbon in the macadamia ash.

5.2 Combustion temperature of biomass producer gas at any equivalence ratio

An adequate amount of air usually plays an important role for fuel gas combustion. Especially, the temperature of secondary chamber that must be achieved the highest point to prevent the exhausting of toxic gas. Thus, it is necessary to determine the parameter of air and fuel proportion. An equivalent ratio (E.R., Φ) is used to judged the quantity of air needed to blend with fuel gas.

Theoretically, E.R. has a relation with the amount of excess air, as shown in Eq. 5.2. The amount of excess air can be measured by using gas analyzer, and then, the E.R. will be computed. In addition, when the starve air condition was set, the amount of CO content in exhaust gas was measured and converted into E.R. value. E.R. number for the starve air condition is higher than 1.0.

$$\%\ excess\ air = \frac{(1-\Phi)}{\Phi} \times 100\% \quad (5.2)$$

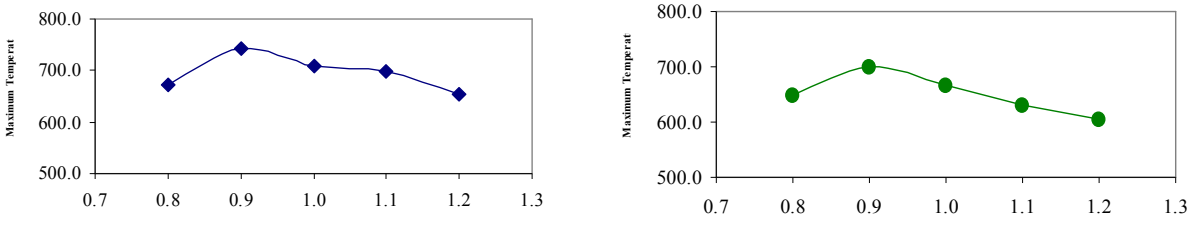

a) Coffee bean pulp b) Macadamia shell

Fig. 5-1 Maximum temperature occurring when adjust any equivalence ratio

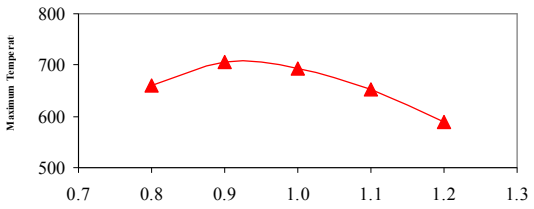

c) Rice husk

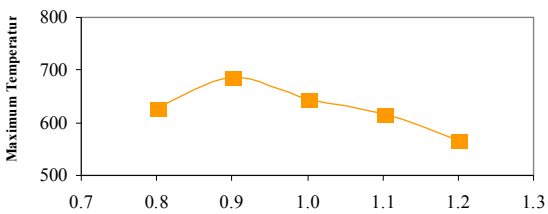

d) Wood charcoal

Fig. 5-1 Maximum temperature occurring when adjust any equivalence ratio (continued)

Figure 5-1 shows the maximum temperature occurring from biomass producer gas combustion when adjusting E.R. from 0.8 to 1.2. It is found that the temperature of all producer gas achieve highest when E.R. is equal to 0.9, or means 11% of excess air. When increase the equivalent ratio or it means decrease air quantity for combustion, the highest temperature occurred was decrease. On the other hand, if there is much excess air amount or decreasing in equivalent ratio, the temperature also decreases. These phenomena explain the essential effect of air fed to burner. From these temperature tendency graphs, it is found that combustion of coffee bean pulp can achieve highest temperature, which is approximately 750^{o}C. In contrary, the combustion of producer gas produced by charcoal is not good. Although, it seems the gas produced from the highest calorific value can achieve highest temperature. Another reason is that the flame length of charcoal gas is shorter than other fuel, thus, heat distribution from flame throughout chamber was not good.

5.3 Flame shape and theoretical flame length calculation

Shapes of flame at any E.R. adjustment were also investigated during the experiment. The photographs of flame are shown in Fig. 5-2. If E.R. value is equal to 0.6 or 66% of excess air condition, the flame occurs short length that is not enough to impinge onto high-moisture material. When increase E.R. to be 0.8, as shown in Fig. 5-2 (b), flame length became longer, and high temperature contour shows at the center of flame.

If increasing E.R. to be 0.9, which is the most proper condition, the flame shape becomes longer and there is wider in flame diameter. When setting the equivalent ratio to be 1.2 or perform a starve condition at burner, it is found that producer gas combustion temperature become low, as shown in Fig. 5-2 (d). Furthermore, it is investigated that the flame vortex direction will blow away from the material position. Hence, it can be explained that because when decrease amount of air feeding to burner to hand in starve air combustion, the mixing velocity of fuel will decrease and cause of reducing in flame speed. Thus, this result also supports the demerit of starve air condition that will be adjusted for incineration.

a) E.R.: 0.6

b) E.R.: 0.8

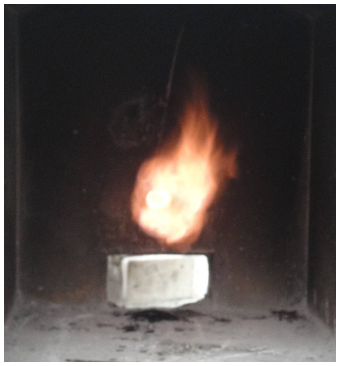

c) E.R.: 0.9

d) E.R.: 1.2

Fig. 5-2 Shape of flame when adjust any equivalence ratio

The theoretical flame length estimation was also carried out, by referring to the Delichatsios correlation. Figure 5-3 shows the estimation results of flame length by adjusting various E.R. number. The theoretical flame length becomes shortest if E.R. is set as 0.8, which is approximately 18-19 cm. However, the estimated flame length of gas generated from rice husk presents in longer length compares to other kinds of gas. When changing E.R. to be 0.9, the flame length increases to be 20 cm, which is close to the actual flame length. Likewise, it is discovered the flame length does not become longer if E.R. is set as more than 1.0 or starve air providing to the experiments. These estimation results can be described by according to the theory of premixed turbulent flame length that relates to initial jet momentum flux and buoyancy force acting on flame. These phenomena are in agreement with the study of Bahadori et al. [66] if neglecting the flame's blowout effect, increasing amount of fuel by increase jet velocity of gas fuel results in constant flame length after achieving any maximum length.

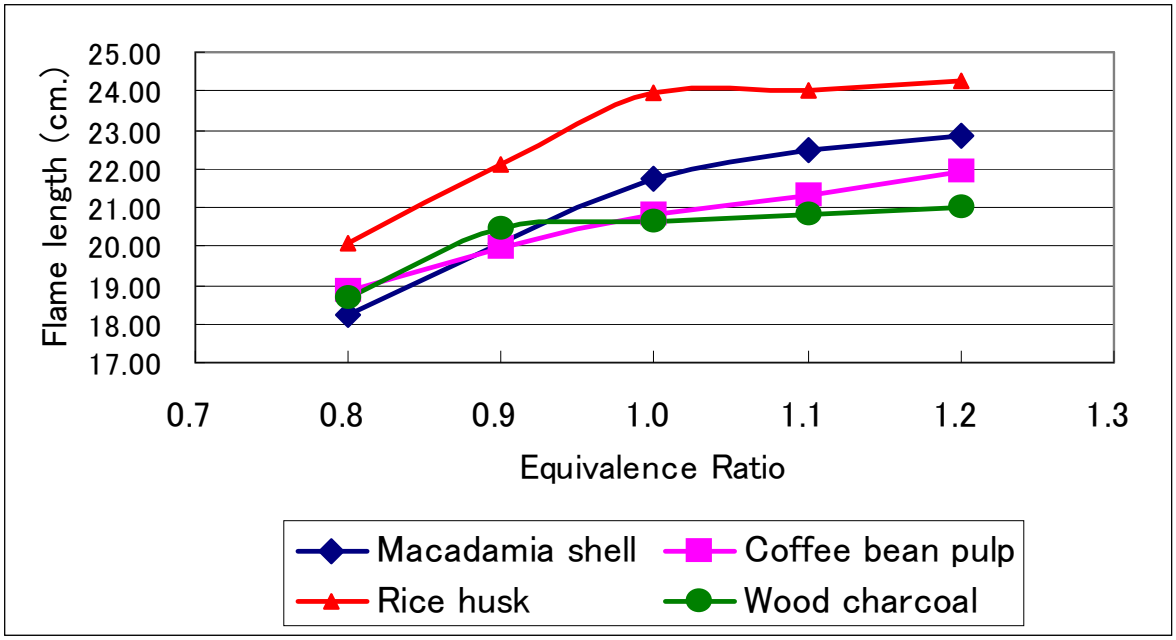

Fig. 5-3 Estimation results of producer gas flame length at any equivalence ratio

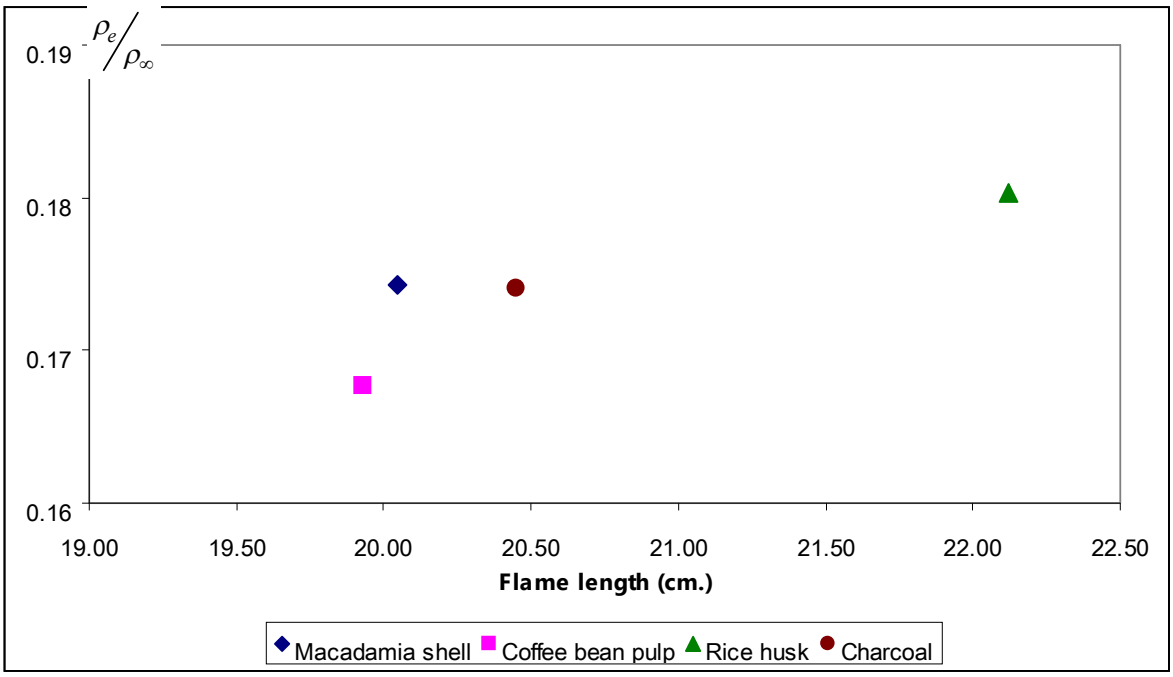

Fig. 5-4 Relationship between flame length with ratio of fuel gas and air density (ρ_e / ρ_∞)

Besides the jet momentum flux and buoyancy force, the ratio of fuel gas and ambient gas (air) density also affect to the flame length. This regime supports the accuracy of rice husk's fuel gas that has longer length than other gases, because the density of rice husk gas is lower than other gases' density. Thus, the ratio, ρ_e / ρ_∞, of gas generated from rice husk become highest and results in longest length of flame.

Although the theoretical estimation of flame length occurring from producer gas combustion present in good results that appropriate for impingement with high-moisture material. However, the actual flame length obtained from experiments present in different result. For example, it can be found that the actual flame is shorter than the estimation. The main possible reason that supports this phenomenon is the continuity and quality of biomass producer gas. Lean constituent of combustible gas sometimes generates non-uniform combustion and performs worse heat distribution, as explained in the temperature tendencies in Fig. 5-2.

5.4 Temperature accuracies inside the double-chambered incinerator prototype

After the adequate conditions of fuel-air mixing at the gas burner were determined, experiments with high-moisture material combustion will be conducted. Then, conductions of experiments with high-moisture material (5 kg fresh chicken meat) were classified into 3 criteria, up to an amount of excess air fed into the primary chamber, which were 100%, 150% and 230% excess air, respectively.

Generally, an operation of double-chambered incinerator starts by ignition of secondary chamber and heats up for temperature until achieving maximum point, and then, the primary chamber, which high-moisture refuse is input, is operated. These operations are recommended for any incineration concerning to high moisture content with hazardous waste such as municipal garbage or human cremation, to efficiently prevent toxic substance and unpleasant smell releasing to ambient [(4)].

Accordingly, a procedure of experiment conduction was begun by ignition of secondary burner with the proper condition (E.R. 0.9). After that, sample meat was contained into the primary chamber, and then, producer gas was influences to the primary burner and started combustion. At a same time, an auxiliary combustion air was fed into the primary chamber. The temperature accuracies of both primary and secondary chamber are described in Fig. 5-5.

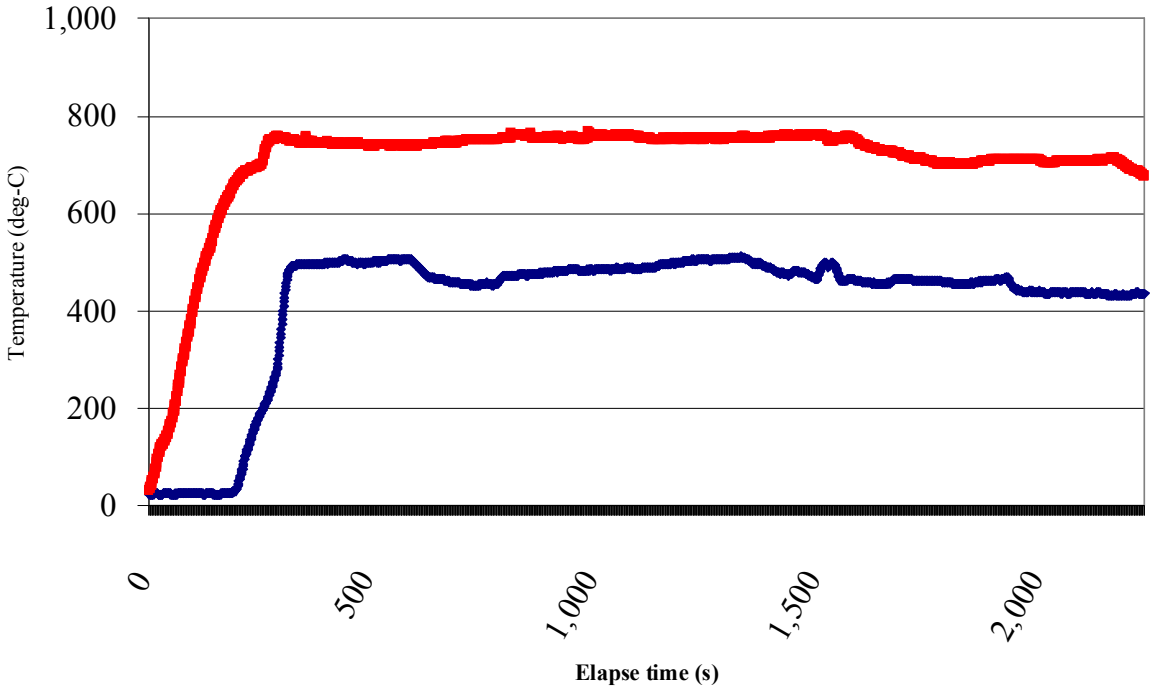

a) 100% excess air condition

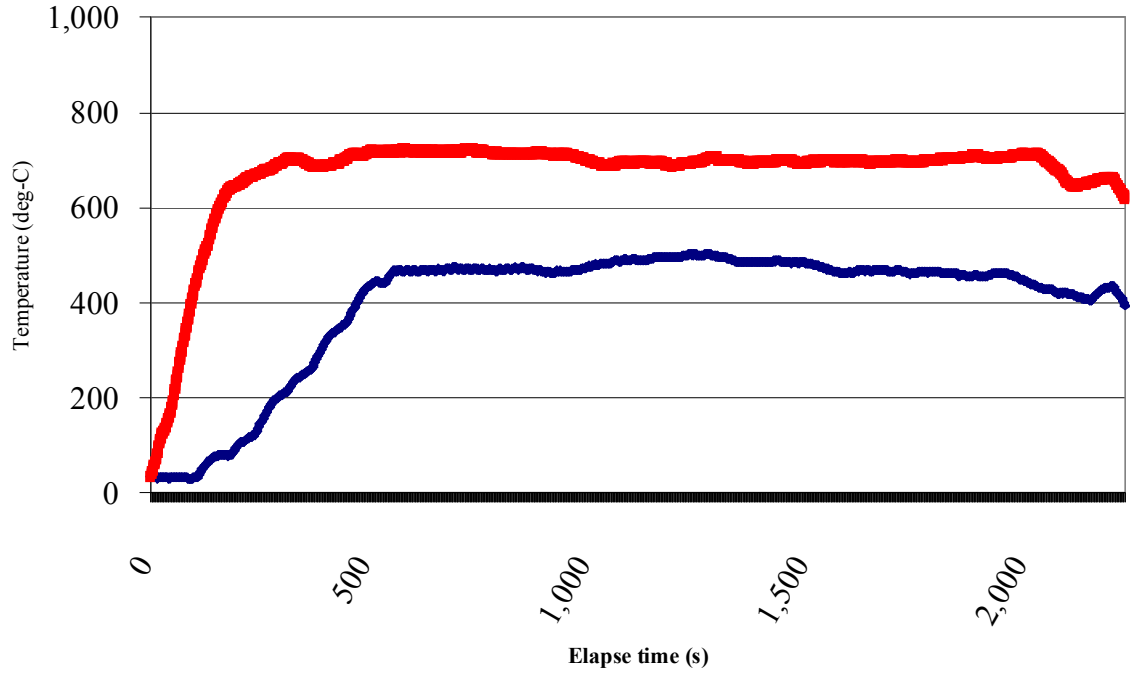

b) 150% excess air condition

Fig. 5-5 Temperature accuracies of primary and secondary chamber when adjust any excess air condition

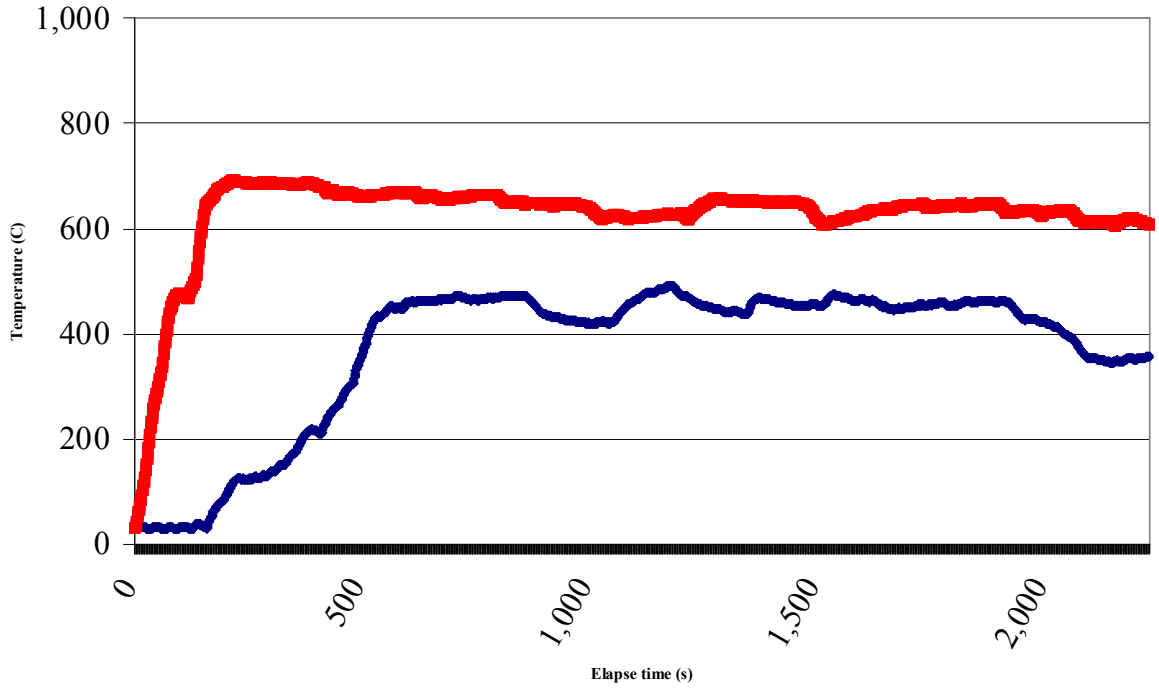

c) 230% excess air condition

Fig. 5-5 Temperature accuracies of primary and secondary chamber when adjust any excess air condition (continued)

When the primary burner was ignited and the primary chamber's excess air was set at 100%, it was found that the temperature inside primary chamber was increased within a short time until it reached a maximum of 500°C, which took approximately 350 seconds until achieved maximum temperature point. During the experimental conduction, the average temperature did not change drastically, and stayed around 450-500°C. For the temperature of the secondary chamber, the maximum temperature increased rapidly until it achieved 750°C, and also became steady throughout the experiment.

If the excess air fed to the primary chamber was changed to 150%, it was observed that it took a little bit of time for the primary chamber's temperature to achieve its maximum point, compared to the 100% excess air condition adjustment. Meanwhile, the temperature of the secondary chamber also presented a lower maximum point compared to 100% excess air condition, which was 700°C on average.

It was found that the primary chamber's temperature needed a longer time for it to increase and to achieve its maximum point if the amount of excess air was 230% of stoichiometric condition. In addition, the maximum temperature became lower than 500°C, and the temperature fluctuated throughout the experiment conduction time. Concerning the secondary chamber, the temperature achieved its maximum point at 650°C on average, which presented the lowest maximum temperature of those excess air conditions. These experimental results describe the influence of excess air to the temperature of combustion chambers. Much amount of excess air fed for sample meat

combustion does not exactly present an advantage to maximum temperature maintaining, including combustion efficiency of high-moisture material.

Besides the influence of excess air, one of significant variable that affects directly to temperature and combustion efficiency is evaporated water from high-moisture material. M. Saito et al. [67] studied for combustion characteristics of waste material containing high moisture and proposed that the ignition of water containing material occurred before the water was evaporated completely, and the vaporization of water and combustion of volatile matter were proceeding simultaneously in the volatile matter combustion regime. Moreover, the mentioned research presented the retention period of volatile matter combustion increased with increasing of water content. With these informations, it can be concluded that during combustion of organic matter (volatile) of sample meat, the evaporation of water content inside sample meat took place. Hence, evaporated water always disturbed the temperature and makes the ignition of other meat's part delay.

5.5 Results on pollution investigation

Due to the specific combustion property of biomass gas derived from gasification process that difference from petroleum fuel, such as heating value and fuel uniform, it is important to investigate emission releasing if the producer gas is used to incinerate high-moisture refuse. The result of pollution investigation also plays an important role for system operation that can prevent emission released as much as possible. A measurement of exhaust gas opacity was carried out to observe for emission releasing in this research, by using Ringelmann opacity chart. The results of emission investigation are show in Fig. 5-6. If there was only sample meat combustion in the primary chamber (without secondary chamber operation), it can be found that gas opacity was increase rapidly until achieving maximum at 60%, and became steady of rate throughout the experiment time. When both of the primary and secondary chamber were operated, at the excess air condition 100%, the maximum gas opacity was 10% throughout the experiment. If the excess air was set at 150%, it was found the average opacity of gas became 15% and sometimes increased to 20%. Finally, if the excess air was increased to 230%, the observed opacity showed 20% on average, while the maximum was 25%.

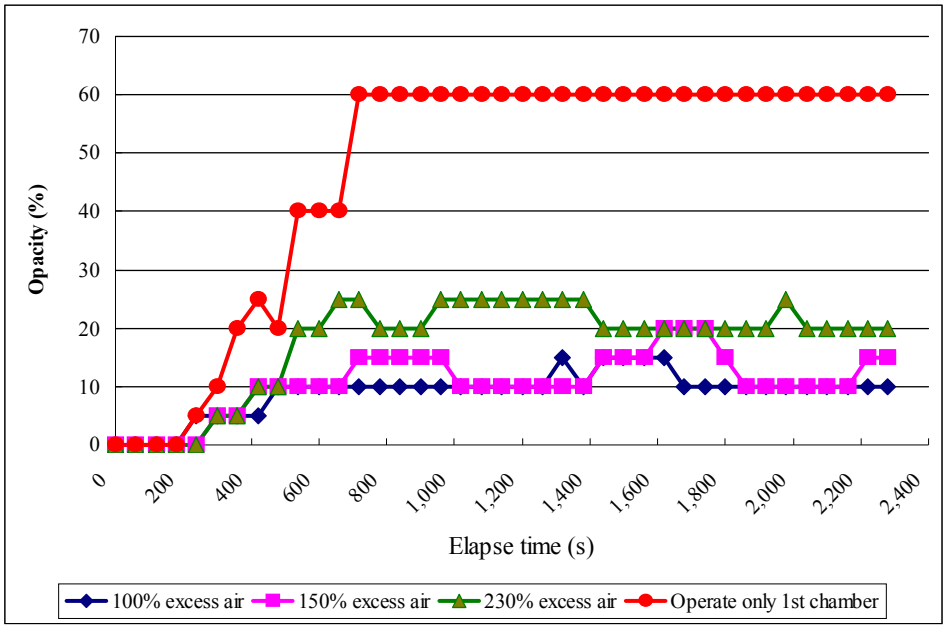

Fig. 5-6 Exhaust gas opacity

There are a few reasons to explain the increasing of gas opacity when increasing the excess air condition. First, much amount of excess air fed into the chamber is not only disturbing temperature and heat distribution, but it caused of turbulent flow inside the primary chamber, and then, some of unburnt substance that extract during combustion process (i.e. dust and soot) was flown by this turbulent flow stream and drafted again into the secondary chamber. Moreover, low temperature of secondary chamber caused by excess air cannot burn unburnt matter. Then, this matter was exhausted to ambient and resulted in high number of opacity. Second, there was some of vapor volatile matter that evaporated during combustion process. When this volatile vapor passed through the stack and exhausted to ambient, low temperature made this matter condensed, and then, the opacity of gas became higher by this reason. Consequently, these experimental results also support the advantage of secondary chamber operation for high-moisture material incineration.

5.6 Energy balance evaluations

An analysis on energy balance of the prototype of double-chambered incinerator refers to the first law of thermodynamics and energy conservation, which total energy input is theoretically equal to the total energy output. Energy input consists of chemical energy from producer gas combustion, energy from sample meat combustion and energy from electricity. For the energy output, it contains of energy losses and energy used.

$$\sum E_{input} = \sum E_{output} \tag{5.3}$$

where $$\sum E_{input} = E_{i,producergas} + E_{i,fuel} + E_{i,elec.} \quad (5.4)$$

and $$\sum E_{output} = E_{used} + E_{o,exhaust} + E_{o,wall} + E_{o,unburnt} + E_{o,unaccounted} \quad (5.5)$$

5.6.1 Energy input

a) Chemical energy in biomass producer gas

Chemical energy content in biomass producer gas is total fuel gas used per one experiment time with the calorific value of fuel.

$$E_{i,producergas} = \dot{Q}_{producergas} \times LHV \quad (5.6)$$

b) Chemical energy in sample high-moisture material

Chemical energy input from the sample high-moisture material was derived from the LHV of the dry combustible substance of the sample material (raw meat).

$$E_{i,fuel} = m_{fuel} \times LHV \quad (5.7)$$

in which $$LHV = HHV - 5.72(9H + M) \quad (5.8)$$

c) Electricity power consumption

The electricity used in the experimental rigs consisted of power used in the gas blower, power used for the air blower, and power used for the draft fan, which were measured by a digital power meter.

5.6.2 Energy output

a) Energy loss in exhaust gas

Energy loss in exhaust gas can be determined from the composition of the measured exhaust gas and the gas mass flow rate.

$$E_{i,exhaust} = \dot{m}_{gas} C_{p,gas} (T_{gas} - T_a) \quad (5.9)$$

b) Energy loss through the incinerator wall

Energy loss through the incinerator wall presents the conduction heat transfer. Thus, Fourier's law is used to calculate the total heat conduction through the incinerator's wall layers.

$$\dot{Q}_{conduct} = -kA\frac{dT}{dx} \quad (5.10)$$

c) Energy loss in unburnt material

Energy loss in unburnt material occurred due to some unburnt material contents lingering in the sample with the remaining material. Therefore, it was necessary to calculate unused energy in the conduction.

$$E_{o,unburnt} = m_{unburnt}\overline{C}_{p,unburnt}(T_h - T_c)_{unburnt} \quad (5.11)$$

where T_h and T_c are hot and cold temperatures of the unburnt material, respectively.

d) Unaccounted losses

Because of the complexity of determining unaccounted losses, such as radiation heat loss and heat contained in the incinerator after finishing experiment, these losses were computed by the difference between the heat input and determinable output. Furthermore, if the secondary chamber was ignited, the energy needed to maintain the maximum temperature for efficient combustion gas elimination was considered an unaccounted loss.

e) Energy used

Energy used in the incinerator consists of energy needed to evaporate moisture content in the sample meat and energy needed to burn the meat's dry combustible matter.

$$E_{used} = \{m_{water}C_{p,water}(T_{boil} - T_{initial})_{water}\} + \{m_{water}h_{fg}\} + \{m_{dry}C_{p,dry}(T_f - T_{initial})_{dry}\} \quad (5.12)$$

f) Incinerator efficiency

An efficiency (or the first law efficiency) of the incinerator is the ratio of the incinerator's energy utilization to the total energy input, which can be calculated by Eq. 5.13.

$$\eta_{incinerator} = (Energy\ used / Energy\ input) \times 100\ \% \quad (5.13)$$

5.6.3 Results on energy balance evaluation and discussions

1) Energy input

For energy input, it can be found that producer gas generated from coffee bean pulp can achieve highest energy input value (approximately 27 MJ), due to its calorific value, whereas the energy generated by rice husk gas presents for poor result.

Energy released from sample meat was computed by referring to the calorific value of dry meat with neglecting the energy in water (low heating value), which total energy in meat is approximately 8.90 MJ.

About the energy input referred to electricity consumption, from the evaluation, it can be investigated that electricity consumed when both primary and secondary chamber are operated is lower than operation only primary chamber condition, because it took a longer time for biomass producer gas to combust sample meat if there was only

primary chamber operation. Different from the primary and secondary chamber operation, the amount of fuel gas was consumed for both two chambers, and then, it became finish early.

2) Energy output: heat loss through exhaust gas

Evaluation on energy output results that the majority of energy loss taking place from loss in exhaust gas, which is approximately 9-12 MJ, or equivalents to 30% of total loss. Figure 5-7 described a relationship between heat loss through the exhaust gas with the incinerator's operation time. It can be found that at the same operation time, energy loss through the exhaust gas of the two chambers operation is higher than only primary chamber operation, because the exhaust gas consisted of high temperature occurred from secondary burner.

However, the operation of single chamber took a longer time. Total loss through exhaust gas by this condition finally results in higher value, therefore. The heat loss became increase before finishing the experiment due to heat content in the combustion chamber. Moreover, moisture content in sample meat was evaporated completely before finishing experiment, thus, temperature of combustion in the chamber was higher and caused of a great deal heat loss.

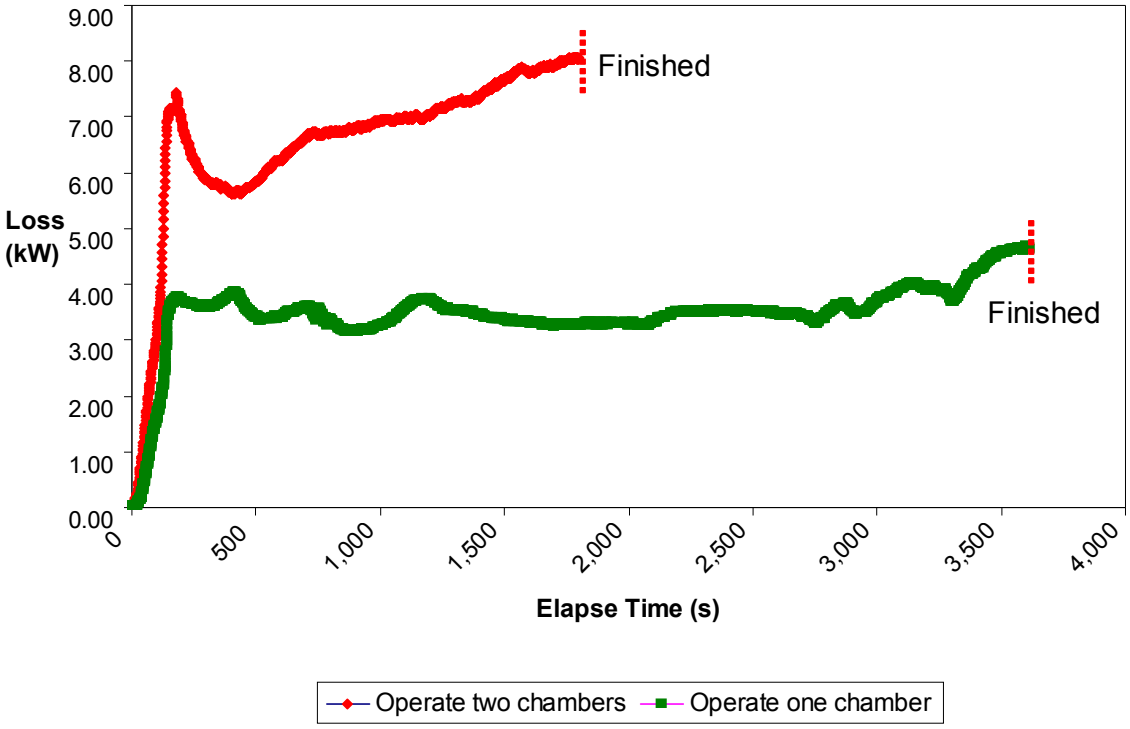

Fig. 5-7 Evaluated energy loss through exhaust gas

3) Energy output: heat loss through incinerator's wall layers

Loss of heat through the incinerator's wall layers shows a similar number compares with loss in exhaust gas. It is conjectured that heat loss for this loss type is 7 MJ by estimate, or equivalents to 22% of the energy output. The position of most heat loss is the incinerator's bottom, in which mainly obtained heat from meat combustion. The average rate of heat loss is approximately 226 Watts at this position. Whereas the average lowest heat loss is the secondary chamber's backside wall under the stack position, which is equal to 15 Watts.

4) Energy output: heat loss in ash and unburnt material

Heat loss in unburnt material was investigated after finishing experiment, according to the total quantity of generated biomass producer gas that was not enough to completely burn sample meat. Hence, heat loss for this issue can be determined base on remaining weight and final temperature of sample meat, or ash.

The evaluations show that if there were two chambers operations, heat loss in ash and unburnt material became higher than that of one chamber operations. This result occurred because sample meat cannot be burnt if producer gas was used in both chambers simultaneously, and it led to much amount of remaining unburnt material at the end of experiment.

Table 5-3 Evaluation results of heat loss through incinerator's wall

Positions	**Heat loss**	
	Watt	**%**
Primary chamber		
Heat loss through left wall	228.25	15.53
Heat loss through right wall	258.12	17.56
Heat loss through backside wall	226.27	15.39
Heat loss through front door	69.12	4.70
Heat loss through bottom side	347.13	23.62
Secondary chamber		
Heat loss through left wall	111.62	7.59
Heat loss through front wall	74.55	5.07
Heat loss through right wall	82.67	5.62
Heat loss through back wall	15.23	1.04
Heat loss through top wall	56.93	3.87
Total	**1,469.89**	**100.00**

5) Energy output: unaccounted losses

As explained beforehand, it is difficult to evaluate exact unaccounted losses. In fact, there are a lot of undeterminable losses during the experiment, such as natural convection and radiation. Amount of these losses was estimated by the difference between the heat input and determinable output. In case of two chambers operations, it is found that the amount of unaccounted losses result higher than one chamber operation, because it is necessary to maintain high temperature in the secondary chamber in order to prevent emission. Therefore, heat used for this reason

was assumed as one of unaccounted loss. It was investigated that the unaccounted loss when two chambers were operated is approximately 8-10 MJ, while the unaccounted loss of one chamber's operation was 4 MJ, by estimation.

6) Useful energy and system's overall efficiency

An energy used in this evaluation is mainly heat used for meat combustion. At first, moisture content in sample meat was evaporated by some amount of gas combustion heat. Next, the other heat is utilized to heat up meat's temperature upon reaching the fire point. Consequently, it can be estimated the heat required for mentioned using. It can be found that the useful energy was equal to 8-12 MJ if there is only one chamber operation. On the other hand, the useful energy decreased to be 4-5 MJ when two chambers were operated. These evaluated results are in agreement with the results of unaccounted losses evaluation. Because some of heat was used in the secondary chamber, sample meat cannot be burnt in much ratio.

After calculate the useful energy, system efficiency can be evaluated by ratio of energy used and total energy input. If there was only primary chamber operation, the efficiency of system was equal to 29.28 % for macadamia shell gas using, and 31.97% for coffee bean pulp gas using. In contrary, the system efficiency when rice husk producer gas presented for worse result, as well as utilization of charcoal gas. Low calorific value of rice husk gas influenced to meat combustion, whereas the deficient of charcoal gas scheme came from short flame length that cannot burn sample meat efficiently, compared with the previous gases.

Table 5-4 Results of energy balance calculation if operate only primary chamber

Parameters	**Producer gases**			
	Macadamia shell	**Coffee bean pulp**	**Rice husk**	**Wood charcoal**
Energy input				
Producer gas (MJ)	22.63	27.36	19.81	27.83
Sample meat (MJ)	8.90	8.90	8.90	8.90
Power consumption (MJ)	0.78	0.74	0.65	0.74
Total energy input	**32.31**	**37.00**	**29.36**	**37.47**
Energy output				
Exhaust gas (MJ)	9.82	12.65	8.87	11.43
Heat loss through wall (MJ)	7.23	7.45	7.16	7.28
Heat loss in ash and unburnt material (MJ)	1.43	1.06	2.25	1.87
Unaccounted loss (MJ)	4.37	4.01	3.11	7.58
Useful energy (MJ)	**9.46**	**11.83**	**7.97**	**9.31**
Incinerator efficiency ($\eta_{incinerator}$), (%)	**29.28 %**	**31.97 %**	**27.15%**	**24.85%**

Table 5-5 Results of energy balance calculation if operate both primary and secondary chambers

Parameters	Producer gases			
	Macadamia shell	**Coffee bean pulp**	**Rice husk**	**Wood charcoal**
Energy input				
Producer gas (MJ)	22.08	27.05	19.59	27.55
Sample meat (MJ)	8.90	8.90	8.90	8.90
Power consumption (MJ)	0.38	0.33	0.30	0.34
Total energy input	**31.36**	**36.28**	**28.79**	**36.79**
Energy output				
Exhaust gas (MJ)	8.60	11.43	8.04	9.57
Heat loss through wall (MJ)	7.06	7.31	7.02	7.14
Heat loss in ash and unburnt material (MJ)	2.81	2.63	3.01	2.96
Unaccounted loss (MJ)	8.29	9.67	9.94	12.09
Useful energy (MJ)	**4.60**	**5.24**	**3.79**	**5.03**
Incinerator efficiency $(\eta_{incinerator})$, (%)	**14.67 %**	**14.44 %**	**13.16%**	**13.67%**

If there were two chambers operation, the efficiency decreased. It is discovered the highest efficiency occurred from for macadamia shell gas that was equal to 14.67%, and 14.44% efficiency for coffee bean pulp gas utilization. These evaluations explained that because some of heat from fuel gas combustion must be used in the secondary chamber and assumed as unaccounted loss. Hence, the amount of heat for meat combustion was separated for this reason, and then, it drastically concluded for lower efficiency.

5.7 Chapter's conclusions

In this chapter, the results obtained from experimental conduction were reported, then, the significant parameters have been evaluated. Due to the comparison between heating value of solid biomass and producer gas calorific value, it is found that biomass fuel, which contains high heating value, does not present high heating value when it is converted into fuel gas. The quality of producer gas usually depends on a gasifier's operation, especially, temperature and height of reduction (char) zone.

To achieve maximum producer gas and air blending, excess air is needed to be injected at gas burner at the equivalence ratio 0.9 in order to completely burn fuel gas and prevent escape of unburnt CO. This operation condition finally concludes for highest temperature, as well as long flame length. Moreover, it can be investigated that the most significant variable that influences to the combustion behavior inside the incinerator is an amount of auxiliary air fed

into the primary chamber. According to the literature reviewing, the recommended air for adequate combustion of high moisture solid waste should be 150% of the stoichiometric combustion air needed. Thus, it impliedly means some of uncombusted air will be draft into the secondary chamber, and then, temperature of the secondary chamber will be decreased by this excess air. This phenomenon was found when increasing amount of excess air from 100% to be 150% and 230%. The temperature was decreased, as well as increasing in exhaust gas opacity or emission occurred from high moisture material combustion. In addition, a great deal of excess auxiliary air also affected to the temperature of both combustion chambers. Consequently, additional amount of biomass gas fuel should be introduced in order to keep high temperature. Nonetheless, this operation will lead the system to be deficient because there is redundant fuel fed to the system.

An evaluation on energy balance shows the difference between operation conditions. It can be found that when operate only primary chamber, the overall efficiency achieved maximum at 30% approximately. In contrary, when operate both of primary and secondary chamber, the incinerator efficiency will decrease to be 15% by estimate because some of fuel amount is necessary to maintain high temperature inside the secondary chamber, for eliminating emission occurred from waste combustion. Although it seemingly wastes a lot of energy through this process, however, it presents for an adequate method to reduce toxic gas released to the atmosphere such as nitrogen oxide or dioxin.

Chapter 6
Investigation of actual scale incinerator's combustion characteristics by using CFD analysis

After the necessary data has been obtained from the experiments, it is essential to simulate the mentioned information for high-moisture material combustion characteristics if an actual double-chambered incinerator will be used, and it will for efficient commercial incinerator design result outcome. Consequently, an analysis by using Computational fluid dynamics (CFD) was also implemented in this research.

6.1 Philosophy of Computational Fluid Dynamics Analysis

Computational fluid dynamics (CFD) is a process to calculate fluid dynamics by numerical methods [(68)]. Moreover, it is the art of replacing the governing partial differential equations of fluid flow with numbers, and advancing these numbers in space and/or time to obtain a final numerical description of the complete flow field of interest. This is not an all-inclusive definition of CFD; there are some problems which allow the immediate solution of the flow field without advancing in time or space, and there are some applications which involve integral equations rather than partial differential equations[(69)].

6.2 Literature reviewing for CFD analysis in combustion and incineration schemes

Doungsupa N. [(70)] studied the simulation of combustion in a ceramic fiber kiln using CFD. The ceramic fiber kiln contains eight LPG burners with a 1 m^3 effective volume, whereas the CFD model solves conservation equations for mass, momentum and energy with the turbulent and non-static running model. The comparison between CFD simulation and actual experiments were that both results showed good agreement for temperatures below 800^oC. In addition, the results also showed that the model with a slowly increasing pressure from 3 to 10 psi and 50% open damper the best condition.

Vorayos N. [(71)] studied computational fluid dynamics to determine the hot air (70^oC) velocity flow field in a 2-dimensional model of tobacco curing barn by appointing the velocity of injected hot air as 2.8 m/s with a turbulent model. The solution showed that the low velocity contour usually took place at the middle of furnace, while the high velocity contour occurred between the low velocity contour and the furnace's wall. In addition, it was also found that if the tobacco furnace has a height and length ratio (H/L) less than 0.3, air distribution cannot reach the back of the furnace, which especially affects the quality of tobacco contained towards the back.

Hwang et al. [(72)] simulated for turbulent model in furnace by using $k-\varepsilon$ model and nonlinear $k-\varepsilon$ model. The results presented that there were not different by using these turbulent model. Lin and Lu (1994) [(73)], on the other hand, conducted for 3 dimensions flow simulation by using Reynolds stress model (RSM) and $k-\varepsilon$ model. It was found that RSM model can observed some flow characteristic better than the $k-\varepsilon$ model.

Donghoon S. et al. [74] used CFD to simulate gas flow inside the furnace chamber that provided 3-dimensional temperature, concentration and velocity vectors. The CFD results were analyzed further in terms of residence time, mixing and thermal decomposition of potential pollutants. It was found that the residence time needed to be carefully determined based on the gas inlet position. The statistical variation requires evaluation of the average and the minimum (or shortest) residence time. Mixing was quantified by defining a local mixedness parameter α with which the effects of secondary air jets were interpreted. Thermal decomposition parameter (β) integrated the temperature and oxygen availability over the residence time, which may be directly related to good combustion.

Bubpamala W. [75] studied human crematory design for energy saving, by simulating commercial crematory as analyzed model and using GAMBIT FLUENT. The results proposed human crematory, which primary combustion chamber located under secondary chamber, has good performance in term of pressure loss and turbulent intensity. In addition, the most proper angle of auxiliary injected air nozzles on left and right wall should be 330^o and 120^o, respectively.

6.3 Related equations used for CFD analysis

6.3.1 Governing equations

Fundamental governing equations used for simulation are Navier-Stokes Equations, which consist of mass conservation and momentum conservation.

$$\frac{\partial \rho}{\partial t} + \nabla \cdot \left(\rho \vec{V}\right) = 0 \tag{6.1}$$

$$\frac{\partial (\rho u)}{\partial t} + \nabla \cdot \left(\rho \vec{V} u\right) = \frac{\partial \left(-P + \tau_{xx}\right)}{\partial x} + \frac{\partial \tau_{yx}}{\partial y} + \frac{\partial \tau_{zx}}{\partial z} + \rho f_x \tag{6.2}$$

$$\frac{\partial (\rho v)}{\partial t} + \nabla \cdot \left(\rho \vec{V} v\right) = \frac{\partial \tau_{xy}}{\partial x} + \frac{\partial \left(-P + \tau_{yy}\right)}{\partial y} + \frac{\partial \tau_{zy}}{\partial z} + \rho f_y \tag{6.3}$$

$$\frac{\partial (\rho w)}{\partial t} + \nabla \cdot \left(\rho \vec{V} w\right) = \frac{\partial \tau_{xz}}{\partial x} + \frac{\partial \tau_{yz}}{\partial y} + \frac{\partial \left(-P + \tau_{zz}\right)}{\partial z} + \rho f \tag{6.4}$$

where;
- ρ fluid's density (kg/m^3)
- $\vec{V}$ flow's velocity vector (m/s) at any position and time, which the component of each direction represents as $\vec{V} = u\hat{i} + v\hat{j} + w\hat{k}$
- P fluid's pressure at any position and time (N/m^2)
- τ_{ij} shear stress (N/m^2)
- t time (s)
- u, v, w fluid's velocity at the x, y and z axis
- f_x, f_y, f_z body force at the x, y and z axis

Isaac Newton has proposed that both of normal and shear stress vary to fluid's velocity gradient (Munson, B.R. et.al., 1998) [76], which is called "Newtonian fluid". Thus, the relationships between fluid's velocity and stress can be expressed as [77]:

$$\tau_{xx} = 2\mu \frac{\partial u}{\partial x} - \frac{2}{3}\mu\left(\nabla \cdot \vec{V}\right) \tag{6.5}$$

$$\tau_{yy} = 2\mu\frac{\partial v}{\partial y} - \frac{2}{3}\mu\left(\nabla\cdot\vec{V}\right) \tag{6.6}$$

$$\tau_{zz} = 2\mu\frac{\partial w}{\partial z} - \frac{2}{3}\mu\left(\nabla\cdot\vec{V}\right) \tag{6.7}$$

$$\tau_{xy} = \tau_{yx} = \mu\left(\frac{\partial u}{\partial y} + \frac{\partial v}{\partial x}\right) \tag{6.8}$$

$$\tau_{xz} = \tau_{zx} = \mu\left(\frac{\partial u}{\partial z} + \frac{\partial w}{\partial x}\right) \tag{6.9}$$

$$\tau_{yz} = \tau_{zy} = \mu\left(\frac{\partial v}{\partial z} + \frac{\partial w}{\partial y}\right) \tag{6.10}$$

In which μ represents fluid's dynamic viscosity of first viscosity.

When the stress values are substituted in the momentum conservation equations, the new Navier-Stokes Equations will be obtained.

$$\frac{\partial(\rho u)}{\partial t} + \nabla\cdot\left(\rho\vec{V}u\right) = -\frac{\partial P}{\partial x} + \frac{\partial}{\partial x}\left[2\mu\frac{\partial u}{\partial x} - \frac{2}{3}\mu\left(\nabla\cdot\vec{V}\right)\right] + \frac{\partial}{\partial y}\left[\mu\left(\frac{\partial u}{\partial y} + \frac{\partial v}{\partial x}\right)\right] + \frac{\partial}{\partial z}\left[\mu\left(\frac{\partial u}{\partial z} + \frac{\partial w}{\partial x}\right)\right] + \rho f_x \tag{6.11}$$

$$\frac{\partial(\rho v)}{\partial t} + \nabla\cdot\left(\rho\vec{V}v\right) = -\frac{\partial P}{\partial y} + \frac{\partial}{\partial x}\left[\mu\left(\frac{\partial u}{\partial y} + \frac{\partial v}{\partial x}\right)\right] + \frac{\partial}{\partial y}\left[2\mu\frac{\partial v}{\partial y} - \frac{2}{3}\mu\left(\nabla\cdot\vec{V}\right)\right] + \frac{\partial}{\partial z}\left[\mu\left(\frac{\partial v}{\partial z} + \frac{\partial w}{\partial y}\right)\right] + \rho f_y \tag{6.12}$$

$$\frac{\partial(\rho w)}{\partial t} + \nabla\cdot\left(\rho\vec{V}w\right) = -\frac{\partial P}{\partial z} + \frac{\partial}{\partial x}\left[\mu\left(\frac{\partial u}{\partial z} + \frac{\partial w}{\partial x}\right)\right] + \frac{\partial}{\partial y}\left[\mu\left(\frac{\partial v}{\partial z} + \frac{\partial w}{\partial x}\right)\right] + \frac{\partial}{\partial z}\left[2\mu\frac{\partial w}{\partial z} - \frac{2}{3}\mu\left(\nabla\cdot\vec{V}\right)\right] + \rho f_z \tag{6.13}$$

If moving the partial viscous stress term to the momentum source term, the Navier-Stokes Equations can be simplified as:

$$\frac{\partial(\rho u)}{\partial t} + \nabla\cdot\left(\rho\vec{V}u\right) = -\frac{\partial P}{\partial x} + \nabla\cdot\left(\mu\nabla u\right) + \rho f_x \tag{6.14}$$

$$\frac{\partial(\rho v)}{\partial t} + \nabla\cdot\left(\rho\vec{V}v\right) = -\frac{\partial P}{\partial y} + \nabla\cdot\left(\mu\nabla v\right) + \rho f_y \tag{6.15}$$

$$\frac{\partial(\rho w)}{\partial t} + \nabla\cdot\left(\rho\vec{V}w\right) = -\frac{\partial P}{\partial w} + \nabla\cdot\left(\mu\nabla w\right) + \rho f_z \tag{6.16}$$

6.3.2 Partial differential equation for heat transfer analysis

A mathematic model of heat transfer can be solved by using the energy conservation law, which is described as Eq. 6.17 [77].

$$\frac{\partial(\rho h_0)}{\partial t}+\nabla\cdot\left(\rho\vec{\nabla}h_0\right) = \nabla\cdot(k\nabla T)+\frac{\partial p}{\partial t}+\left[\frac{\partial(u\tau_{xx})}{\partial x}+\frac{\partial(u\tau_{yx})}{\partial y}+\frac{\partial(u\tau_{zx})}{\partial z}\right] +\left[\frac{\partial(v\tau_{xy})}{\partial x}+\frac{\partial(v\tau_{yy})}{\partial y}+\frac{\partial(v\tau_{zy})}{\partial z}\right]+\left[\frac{\partial(w\tau_{zx})}{\partial x}+\frac{\partial(w\tau_{yz})}{\partial y}+\frac{\partial(w\tau_{zz})}{\partial z}\right]+S_h \quad (6.17)$$

where h_0 means the summary of enthalpy:

$$h_0 = i+\frac{1}{2}\left(u^2+v^2+w^2\right) \quad (6.18)$$

in which i represents an internal energy, and k is a conduction coefficient (W/m-K).

6.3.3 Turbulence equations

The governing equations and heat transfer equation, as described earlier, are usually used to solve general flow problem. Nevertheless, the flow of combustion gas and auxiliary air, including biomass producer gas, usually become turbulent, which represents uncertainty direction, which causes of unsteady condition for each parameter. Consequently, any property of the turbulent flow can be assumed to be 2 parts (Reynolds decomposition), which are the average value that independent to time, and the oscillation value that dependent with the time [78].

By assuming the characteristics of combustion gas and air flow inside the incinerator as steady incompressible viscous flow, a time averaging tensor can be conducted as:

$$\frac{\partial\overline{u_i}}{\partial x_i} = 0 \quad (6.19)$$

and

$$u_j\frac{\partial\overline{u_i}}{\partial x_j} = -\frac{1}{\rho}\frac{\partial\overline{p}}{\partial x_i}+\frac{1}{\rho}\frac{\partial\overline{\sigma_{ji}}}{\partial x_j}-\frac{\partial\overline{u_i'u_j'}}{\partial x_j} \quad (6.20)$$

where $\overline{\sigma_{ji}}$ is a deviatoric part of the viscous stress tensor, which can be determined by:

$$\overline{\sigma_{ji}} = 2\mu\overline{S_{ij}} \quad (6.21)$$

A parameter S_{ij} represents strain tensor that can be calculated by Eq. 6.22.

$$S_{ij} = \frac{1}{2}\left(\frac{\partial u_i}{\partial x_j}+\frac{\partial u_j}{\partial x_i}\right) \quad (6.22)$$

6.3.4 Standard $k-\varepsilon$ model

The remaining non-closed Reynolds-stress tensor has to be modelled. The Favre-averaged standard $k-\varepsilon$ model is applied to close the set of equations, where the eddy-viscosity assumption at high Reynolds Number (Eq. 6.23) is used.

$$\widetilde{u_i''u_j''} = -\nu_t\left(\frac{\partial\widetilde{u_i}}{\partial x_j}+\frac{\partial\widetilde{u_j}}{\partial x_i}\right)-\frac{2}{3}\delta_{ij}\widetilde{k}-\frac{2}{3}\delta_{ij}\nu_t\frac{\partial\widetilde{u_k}}{\partial x_k} \quad (6.23)$$

The turbulent viscosity is defined by:

$$v_t = C_\mu \frac{\widetilde{k}^2}{\widetilde{\varepsilon}} \tag{6.24}$$

The modeled turbulent kinetic energy equation and mechanical dissipation equation explain as Eq.6.25 and 6.26.

$$\overline{\rho}\frac{\partial \widetilde{k}}{\partial t} + \rho\widetilde{u}_k \frac{\partial \widetilde{k}}{\partial x_k} = \frac{\partial}{\partial x_k}\left(\overline{\rho}\frac{v_t}{\sigma_k}\frac{\partial \widetilde{k}}{\partial x_k}\right) - \overline{\rho u_i'' u_j''}\frac{\partial \widetilde{u}_i}{\partial x_j} - \overline{\rho}\widetilde{\varepsilon} \tag{6.25}$$

and

$$\overline{\rho}\frac{\partial \widetilde{\varepsilon}}{\partial t} + \rho\widetilde{u}_k \frac{\partial \widetilde{\varepsilon}}{\partial x_k} = \frac{\partial}{\partial x_k}\left(\overline{\rho}\frac{v_t}{\sigma_k}\frac{\partial \widetilde{\varepsilon}}{\partial x_k}\right) - C_{\varepsilon 1}\overline{\rho}\frac{\widetilde{\varepsilon}}{\widetilde{k}}\widetilde{u}_i'' u_j''\frac{\partial \widetilde{u}_i}{\partial x_j} - C_{\varepsilon 2}\overline{\rho}\frac{\widetilde{\varepsilon}}{\widetilde{k}} \tag{6.26}$$

The mechanical dissipation rate is modelled under the assumption of local isotropy at a high turbulent Reynolds number. There are extra source terms that may be added to the dissipation rate equation to account for buoyancy and volume expansion influences,

$$C_{\varepsilon 3}\frac{\partial \overline{p}}{\partial x_i}\frac{\overline{\rho' u''}}{\overline{\rho}}\frac{1}{\widetilde{\varepsilon}} \text{ and } C_{\varepsilon 4}\overline{\rho}\widetilde{\varepsilon}\frac{\partial \widetilde{u}_k}{\partial x_k}. \tag{6.27}$$

The constants used for standard $k-\varepsilon$ model are described in Table 6-1.

Table 6-1 Constants used in the standard $k-\varepsilon$ model

C_μ	$C_{\varepsilon 1}$	$C_{\varepsilon 2}$	σ_k	σ_ε
0.09	1.44	1.92	1.00	1.30

6.3.5 Finite volume method

In order to calculate and solve the solution by using computational fluid dynamics, a numerical approach is applied. The methodology starts by conduct for the domain of fluid flow with a boundary, and then, flow domain will be divided into small element or mesh (discretisation). Each element will cross together at a grid (or node), which is used to calculate for fluid flow solution. After that, fluid property and boundary condition will be appointed. Algebraic equations are created by substituting fluid flow functions into the fluid's partial differential equation and combine with the mathematical calculation.

A finite volume method (FVM) means a kind of the numerical approach that becomes popular for fluid flow solution solving. This method will arrange the partial differential equation into the algebraic equation at any point on a control volume, and then, boundary conditions will be appointed. Finally, an iteration method is applied to determine the solution.

A general form of partial differential equation used for FVM can be written as,

$$\frac{\partial(\rho\phi)}{\partial t} + div(\rho\phi u) = div(\Gamma grad\phi) + S_\phi \tag{6.28}$$

Transient *Convection* *Diffusion* *Source*

where Γ is a diffusion coefficient of the variable ϕ.

Transport equations for the 2-dimension turbulent flow are shown in Table 6-2,

Table 6-2 Comparison between transport equations of 2-dimension turbulent flow with the ordinary equations

Transport Equations	ϕ	Γ_ϕ	S_ϕ	
Continuity	1	0	0	
X-momentum	$\bar{u}$	u_e	$-\frac{\partial \bar{P}}{\partial x}+\frac{\partial}{\partial x}\left(u_e\frac{\partial \bar{u}}{\partial x}\right)+\frac{\partial}{\partial y}\left(u_e\frac{\partial v}{\partial y}\right)$	(6.29)
Y-momentum	$\bar{v}$	u_e	$-\frac{\partial \bar{P}}{\partial y}+\frac{\partial}{\partial x}\left(u_e\frac{\partial \bar{u}}{\partial y}\right)+\frac{\partial}{\partial y}\left(u_e\frac{\partial v}{\partial y}\right)$	(6.30)
Turbulent kinetic energy	k	$\frac{u_e}{\sigma_k}$	$G-\rho\varepsilon$	(6.31)
Turbulent dissipation	ε	$\frac{u_e}{\sigma_\varepsilon}$	$(C_{\varepsilon 1}G)\frac{\varepsilon}{k}-(C_{\varepsilon 2}\rho\varepsilon)\frac{\varepsilon}{k}$	(6.32)

in which μ_e means an effective viscosity, $(\mu_t+\mu)$,

and $G=\mu_t\left[2\left(\frac{\partial \bar{u}}{\partial x}\right)^2+2\left(\frac{\partial \bar{v}}{\partial y}\right)^2+\left(\frac{\partial \bar{v}}{\partial x}+\frac{\partial \bar{u}}{\partial y}\right)^2\right]$. (6.33)

The partial differential equation (Eq. 6.28) can be changed into the algebraic equation by integration throughout the control volume:

$$\int_{CV}\frac{\partial(\rho\phi)}{\partial t}dV+\int_{CV}div(\rho\phi u)dV=\int_{CV}div(\Gamma grad\phi)dV+\int_{CV}S_\phi dV \tag{6.34}$$

For the steady state $\frac{\partial(\rho\phi)}{\partial t}=0$, the above equation can be rewritten as:

$$\int_{CV}div(\rho\phi u)dV=\int_{CV}div(\Gamma grad\phi)dV+\int_{CV}S_\phi dV \tag{6.35}$$

6.3.6 Diffusion and heat transfer solution

The numerical method can be also used to determine the solution of diffusion and heat transfer. Assuming heat conduction occurring is 2-dimension steady state, conduction heat transfer equation is expressed as:

$$\frac{\partial}{\partial x}\left(\Gamma\frac{\partial\phi}{\partial x}\right)+\frac{\partial}{\partial y}\left(\Gamma\frac{\partial\phi}{\partial y}\right)+S_\phi=0 \tag{6.36}$$

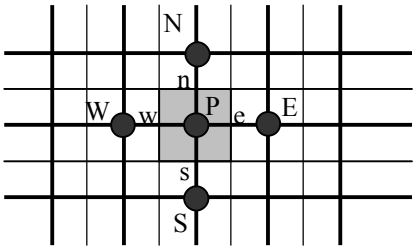

Fig. 6-1 Position of 2-dimension control volume

Integrating an above equation throughout the control volume, the new form of equation becomes:

$$\int_{\Delta V}\frac{\partial}{\partial x}\left(\Gamma\frac{\partial\phi}{\partial x}\right)dxdy+\int_{\Delta V}\frac{\partial}{\partial y}\left(\Gamma\frac{\partial\phi}{\partial y}\right)dxdy+\int_{\Delta V}S_{\phi}dV=0 \tag{6.37}$$

Set $A_e=A_w=1x\Delta y$ and $A_n=A_s=\Delta x1$, the equation becomes:

$$\left[\Gamma_e A_e\left(\frac{\partial\phi}{\partial x}\right)_e-\Gamma_w A_w\left(\frac{\partial\phi}{\partial x}\right)_w\right]+\left[\Gamma_n A_n\left(\frac{\partial\phi}{\partial x}\right)_n-\Gamma_s A_s\left(\frac{\partial\phi}{\partial x}\right)_s\right]=0 \tag{6.38}$$

From above equation, the equations of flux that flows through the control volume are expressed as:

Flux flows through CV surface at west side

$$=\Gamma_w A_w\left.\frac{\partial\phi}{\partial x}\right|_w=\Gamma_w A_w\frac{(\phi_P-\phi_W)}{\delta x_{WP}} \tag{6.38a}$$

Flux flows through CV surface at east side

$$=\Gamma_e A_e\left.\frac{\partial\phi}{\partial x}\right|_e=\Gamma_e A_e\frac{(\phi_E-\phi_P)}{\delta x_{PE}} \tag{6.38b}$$

Flux flows through CV surface at south side

$$=\Gamma_s A_s\left.\frac{\partial\phi}{\partial x}\right|_s=\Gamma_s A_s\frac{(\phi_P-\phi_S)}{\delta x_{SP}} \tag{6.38c}$$

Flux flows through CV surface at north side

$$=\Gamma_n A_n\left.\frac{\partial\phi}{\partial x}\right|_n=\Gamma_n A_n\frac{(\phi_N-\phi_P)}{\delta x_{PN}} \tag{6.38d}$$

where δ means cell volume.

Substituting all of above equations into Eq. 6.37, a new equation form is obtained as:

$$\left[\Gamma_e A_e\frac{(\phi_E-\phi_P)}{\delta x_{PE}}\right]-\left[\Gamma_w A_w\frac{(\phi_P-\phi_W)}{\delta x_{WP}}\right]+\left[\Gamma_n A_n\frac{(\phi_N-\phi_P)}{\delta x_{PN}}\right]-\left[\Gamma_s A_s\frac{(\phi_P-\phi_S)}{\delta x_{SP}}\right]+\bar{S}\Delta V=0 \tag{6.39}$$

Assuming the diffusion of source term inside the control volume is a linear profile, then $\bar{S}\Delta V = S_u + S_p\phi_p$. Therefore Eq. 6.39 can be rewritten as:

$$\left(\frac{\Gamma_w A_w}{\delta x_{WP}} + \frac{\Gamma_e A_e}{\delta x_{PE}} + \frac{\Gamma_s A_s}{\delta x_{SP}} + \frac{\Gamma_n A_n}{\delta x_{PN}} - S_P\right)\phi_P = \left(\frac{\Gamma_w A_w}{\delta x_{WP}}\right)\phi_W + \left(\frac{\Gamma_e A_e}{\delta x_{PE}}\right)\phi_E + \left(\frac{\Gamma_s A_s}{\delta x_{SP}}\right)\phi_S + \left(\frac{\Gamma_n A_n}{\delta x_{PN}}\right)\phi_N + S_u \quad (6.40)$$

Consequently, the ordinary algebraic equation is obtained.

$$a_P\phi_p = a_W\phi_W + a_E\phi_E + a_S\phi_S + a_N\phi_N + S_u \quad (6.41)$$

where;

$$a_W = \frac{\Gamma_W A_W}{\delta x_{WP}} \quad (6.41a)$$

$$a_E = \frac{\Gamma_E A_E}{\delta x_{PE}} \quad (6.41b)$$

$$a_S = \frac{\Gamma_S A_S}{\delta x_{SP}} \quad (6.41c)$$

$$a_N = \frac{\Gamma_N A_N}{\delta x_{PN}} \quad (6.41d)$$

and

$$a_P = a_W + a_E + a_S + a_N - S_P \quad (6.41e)$$

6.3.7 Convection and diffusion problem

An equation of the variable ϕ of the convection and diffusion problem can be written by:

$$\frac{\partial(\rho u\phi)}{\partial x} + \frac{\partial(\rho v\phi)}{\partial y} = \frac{\partial}{\partial x}\left(\Gamma\frac{\partial\phi}{\partial x}\right) + \frac{\partial}{\partial y}\left(\Gamma\frac{\partial\phi}{\partial y}\right) + S_\phi \quad (6.42)$$

Integrating Eq.4.42 throughout the control volume, thus, new equation form is obtained:

$$\int_{\Delta V}\left[\frac{\partial(\rho u\phi)}{\partial x} + \frac{\partial(\rho v\phi)}{\partial y}\right]dV = \int_{\Delta V}\left[\frac{\partial}{\partial x}\left(\Gamma\frac{\partial\phi}{\partial x}\right) + \frac{\partial}{\partial y}\left(\Gamma\frac{\partial\phi}{\partial y}\right) + S_\phi\right]dV \quad (6.43)$$

Considering for each integral term and set the variable $A_e = A_w = 1x\Delta y$ and $A_n = A_s = \Delta x1$, the convection term of x and y axis become:

x-axis:

$$\int_{\Delta V}\left[\frac{\partial}{\partial x}(\rho u\phi)\right]dV = (\rho uA)_e\phi_e - (\rho uA)_w\phi_w = F_e\phi_e - F_w\phi_w \quad (6.44)$$

y-axis:

$$\int_{\Delta V}\left[\frac{\partial}{\partial y}(\rho v\phi)\right]dV = (\rho vA)_n\phi_n - (\rho vA)_s\phi_s = F_n\phi_n - F_s\phi_s \quad (6.45)$$

The diffusion terms are:

$$\int_{\Delta V}\left[\frac{\partial}{\partial x}\left(\Gamma\frac{\partial\phi}{\partial x}\right)\right]dV = \left(\Gamma\frac{\partial\phi}{\partial x}A\right)_e - \left(\Gamma\frac{\partial\phi}{\partial x}A\right)_w = D_e(\phi_E - \phi_P) - D_w(\phi_P - \phi_W) \quad (6.46)$$

$$\int_{\Delta V}\left[\frac{\partial}{\partial y}\left(\Gamma\frac{\partial\phi}{\partial y}\right)\right]dV = \left(\Gamma\frac{\partial\phi}{\partial y}A\right)_n - \left(\Gamma\frac{\partial\phi}{\partial x}A\right)_s = D_n(\phi_N - \phi_P) - D_s(\phi_P - \phi_S) \quad (6.47)$$

The source term is:

$$\int_{CV} S_\phi dV = S_\phi V \tag{6.48}$$

where F and D represent the coefficient of convection and diffusion (ρuA and $\frac{\Gamma A}{\delta}$), respectively.

The value of ϕ can be estimated by using a several scheme such as Central Differencing Scheme, Upwind Differencing Scheme, Hybrid Differencing Scheme or Power-Law Scheme. In this research, the Upwind Differencing Scheme was selected for the most appropriate scheme to solve the mentioned problem.

The Upwind Differencing Scheme [79] has an objective to solve the diffusion and convection problem by assuming the convection value at the interface ϕ_e is occurred by the average between ϕ_E and ϕ_P, and there is no change of the diffusion term. In addition, the convection term can be calculated by assuming that the value of ϕ at the interface is equal to the value ϕ at grid point of the control volume's upstream surface.

$$\phi_e = \phi_P \quad \text{if} \quad F_e > 0 \tag{6.49a}$$

$$\phi_e = \phi_E \quad \text{if} \quad F_e < 0 \tag{6.49b}$$

and

$$\phi_w = \phi_W \quad \text{if} \quad F_w > 0 \tag{6.49c}$$

$$\phi_w = \phi_P \quad \text{if} \quad F_w < 0 \tag{6.49d}$$

Accordingly, the algebraic equation can be written as:

$$a_P\phi_P = a_W\phi_W + a_E\phi_E + a_N\phi_N + a_S\phi_S + S_\phi V \tag{6.50}$$

where

$$a_N = max\,[-Fn,\ 0]$$
$$a_S = max\,[Fs,\ 0]$$
$$a_E = max\,[-Fe,\ 0]$$
$$a_W = max\,[Fw,\ 0]$$

and

$$a_P = a_E + a_W + a_N + a_S + \left(F_n - F_w + F_n - F_s\right) \tag{6.51}$$

where max $[A,B]$ means the maximum value, which is obtained from the comparing between A and B.

6.3.8 Flow field problem

In order to solve for momentum conservation equation, the solution of fluid's flow field will be not in agreement with the solution obtained from mass conservation equation. Accordingly, a Semi-Implicit Method for Pressure-Linked Equation (SIMPLE) method [80] was applied. This algorithm starts the discrete continuity equation and substitute into this the discrete u and v momentum equations containing the pressure terms resulting in a equation for discrete pressures. The pressure field is assumed to be known from the previous iteration. Using the u and v momentum equations are solved for the velocities. At this stage the newly obtained velocities do not satisfy continuity

since the pressure field assumed is only a guess. Corrections to velocities and pressure are proposed to satisfy the discrete continuity equation [81].

Likewise, a staggered grid method is also applied to arrange the velocity grid to be placed at the connection of scalar variable, in order to be in agreement with the continuity equation and also prevent a Checker-board effect that cause of the error in numerical approach [82]. The arrangement of the scalar grid (p), velocity u and v are shown in Fig. 6-2.

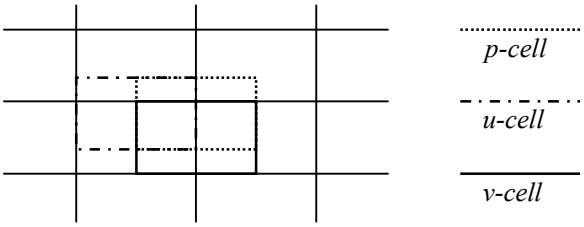

Fig. 6-2 Staggered grid arrangement

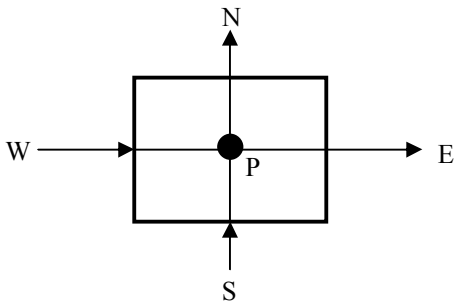

Fig. 6-3 Arrangement of the control volume p-cell

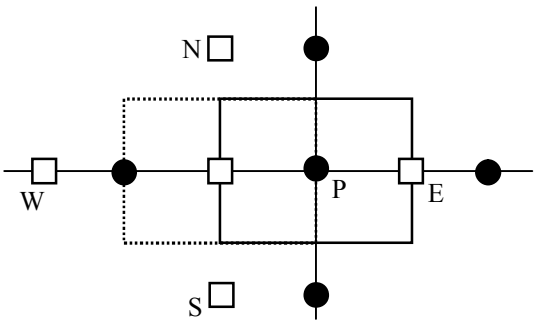

Fig. 6-4 Arrangement of the control volume u-cell

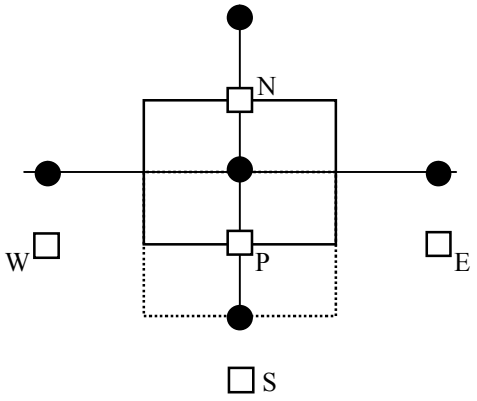

Fig. 6-5 Arrangement of the control volume v-cell

Momentum conservation equations along x and y axis are taken:

$$\frac{\partial}{\partial x}(\rho uu)+\frac{\partial}{\partial y}(\rho vu) = \frac{\partial P}{\partial x}+\frac{\partial}{\partial x}\left(\Gamma\frac{\partial u}{\partial x}\right)+\frac{\partial}{\partial y}\left(\Gamma\frac{\partial v}{\partial x}\right) \tag{6.52}$$

$$\frac{\partial}{\partial x}(\rho uv)+\frac{\partial}{\partial y}(\rho vv) = \frac{\partial P}{\partial y}+\frac{\partial}{\partial x}\left(\Gamma\frac{\partial u}{\partial y}\right)+\frac{\partial}{\partial y}\left(\Gamma\frac{\partial v}{\partial x}\right) \tag{6.53}$$

Integrating Eq. 6.52 and 6.53 throughout the control volume (as shown in Fig.6-4 and 6-5), the discretized equation are obtained:

x-axis: $$a_p u_p = \sum_{nb} a_{nb}u_{nb} + S_u V + \left(P_{I-1,J} - P_{1,J}\right)A \tag{6.54}$$

y-axis: $$a_p v_p = \sum_{nb} a_{nb}v_{nb} + S_v V + \left(P_{I-1,J} - P_{1,J}\right)A \tag{6.55}$$

where $$\sum_{nb} a_{nb}u_{nb} = a_N u_N + a_S u_S + a_E u_E + a_W u_W \tag{6.56}$$

$$\sum_{nb} a_{nb}v_{nb} = a_N v_N + a_S v_S + a_E v_E + a_W v_W \tag{6.57}$$

Mass conservation equation is derived to be a pressure different equation, in order to correct the value of pressure and velocity of fluid flow filed. The procedure starts by assuming the pressure and velocity value.

$$p = p^* + p' \tag{6.58a}$$

$$u = u^* + u' \tag{6.58b}$$

$$v = v^* + v' \tag{6.58c}$$

In which : p, u and v correct pressure and velocity

p*, u* and v* guessed pressure and velocity that is calculated from p^*

p', u' and v' pressure correction and velocity correction

In addition, the velocity u and v can be determined from momentum equation, which has a similar form with Eq. 6.56 and 6.57. The discretized equations of these velocities are presented as:

$$a_w u_w^* = \sum_{nb} a_{nb} u_{nb}^* + S_u V + \left(P_W^* - P_P^*\right) A_w \tag{6.59}$$

$$a_s v_w^* = \sum_{nb} a_{nb} v_{nb}^* + S_u V + \left(P_S^* - P_P^*\right) A_s \tag{6.60}$$

Substituting Eq. 6.58a-6.58c into the discretized equation (Eq. 6.56 and 6.57), and then, minus by Eq. 6.59 and 6.60, the new discretized equation becomes:

$$a_w u_w' = \sum_{nb} a_{nb} u_{nb}' + \left(P_W' - P_P'\right) A_w \tag{6.61}$$

$$a_s v_w' = \sum_{nb} a_{nb} v_{nb}' + \left(P_S' - P_P'\right) A_s \tag{6.62}$$

$\sum_{nb} a_{nb} u_{nb}'$ and $\sum_{nb} a_{nb} v_{nb}'$ can be assumed to be zero [82], when the flow is in agreement with the mass conservation equation. The velocity correction equation of u_w becomes:

$$u_w' = d_w \left(p_W' - p_P'\right) \tag{6.63}$$

where $$d_w = \frac{A_w}{a_w}$$

Thus, $$u_w = u_w^* + d_w \left(p_W' - p_P'\right) \tag{6.64}$$

At a same time, the velocity of east position (u_e) can be also written as:

$$u_e = u_e^* + d_e \left(p_E' - p_P'\right) \tag{6.65}$$

Simultaneously, the velocity correction equation of vs is expressed as:

$$v_s' = d_s \left(p_S' - p_P'\right) \tag{6.66}$$

where $$d_s = \frac{A_s}{a_s}$$

Thus, $$v_s = v_s^* + d_s \left(p_S' - p_P'\right) \tag{6.67}$$

and $$v_n = v_n^* + d_n \left(p_N' - p_P'\right) \tag{6.68}$$

Mass conservation equation (Eq. 6.1) can be written as a differential equation as:

$$\frac{\partial(\rho u)}{\partial x} + \frac{\partial(\rho v)}{\partial y} = 0 \tag{6.69}$$

Integrating above equation throughout the control volume, then,

$$\int_{\Delta V}\left[\frac{\partial(\rho u)}{\partial x}+\frac{\partial(\rho v)}{\partial y}\right]dV = 0 \tag{6.70}$$

$$(\rho uA)_e-(\rho uA)_w+(\rho uA)_n-(\rho uA)_s = 0 \tag{6.71}$$

Consequently, the equation of pressure correction (Eq. 6.72) can be obtained by substituting the velocity value from Eq. 6.64, 6.65, 6.67 and 6.68.

$$a_P p'_P = a_W p'_W + a_E p'_E + a_S p'_S + a_N p'_N + b \tag{6.72}$$

where

$$a_N = \rho d_n A_n$$

$$a_S = \rho d_s A_s$$

$$a_E = \rho d_e A_e$$

$$a_W = \rho d_w A_w$$

$$b = (\rho u^* A)_e - (\rho u^* A)_w + (\rho u^* A)_n - (\rho u^* A)_s$$

Accordingly, the overall process of SIMPLE method can be summarized as:

1) Assuming the value of p^*, u^* and v^*.
2) Calculating for u^* and v^* by using Eq. 6.54 and 6.55.
3) Substituting calculated u^* and v^* into Eq. 6.72.
4) Determining for p' from Eq. 6.72, and then, substituting the calculated p' into Eq. 6.58a, and appointing p^* from p.
5) Calculating for u, v from Eq. 6.64, 6.65, 6.67 and 6.68 by using p' from the previous calculation, and then, using obtained u, v to be new u^* and v^*.
6) Repeating the procedure (2) to (5) until p^*, u^* and v^* become convergence, by observing that the value of the mass source term (*b-term*) converges to zero.

The flow chart of SIMPLE method is shown in Fig. 6-6.

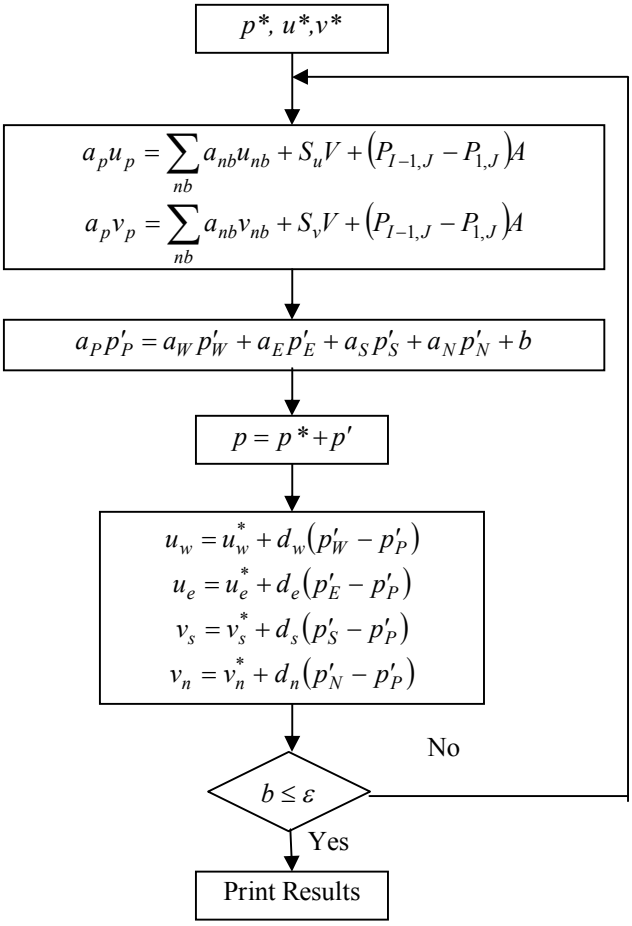

Fig. 6-6 Flow chart of SIMPLE method

6.4 Three-Dimensions model implementations

A model of double-chambered incinerator for simulation was implemented by referring to the commercial scale of double-chambered incinerator used at present. Figure 6-7 shows the layout of implemented incinerator's model. The primary combustion chamber has 338 cm in depth, 100 cm in width and 60 cm in height. The secondary combustion chamber's shape is especially designed as a U-shape for providing maximum efficient of dust precipitation. At the top of the secondary chamber, an exhaust gas stack is implemented. In addition, ten of total auxiliary air nozzles are located at the primary combustion chamber. At the combustion chamber backside, gas burner's models are placed.

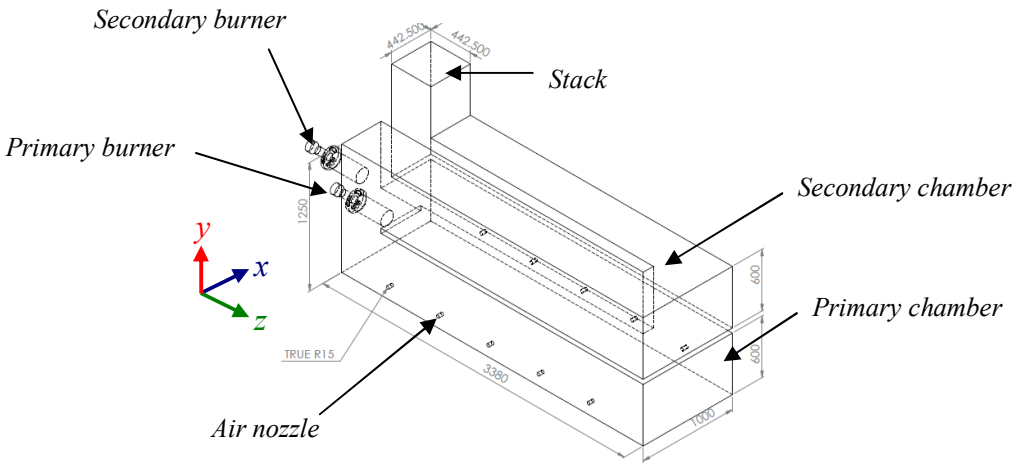

Fig. 6-7 Schematic dimension of the double-chambered incinerator model

In order to simulate the heat distribution and other significant combustion characteristics, the models were classified into 4 types, which named A1 to A4, by the incline angle arrangement of air nozzles and burners. A model A1 represents for the commercial incinerator used at present, in which the angle of burners and air nozzles are equal to zero degree. For the Model A2, the incline angle of air nozzle are modified to be 30 degree along y-axis (α), and 30 degree along z-axis (ϕ), whereas there is no change in burner's incline angle (zero degree).

Table 6-3 Dimension of each double-chambered incinerator model

Conditions	A1 (Commercial type)	A2	A3	A4
		(Modified model)		
Chamber's dimensions (W x H x L) (mm.)	1,000 x 600 x 3,380			
Primary burner incline angle (deg)	0^o	0^o	25^o	25^o
Secondary burner incline angle (deg)	0^o	0^o	0^o	0^o
Auxiliary air incline angle	0^o	$\phi = 30^o$ $\alpha = 30^o$	0^o	$\phi = 30^o$ $\alpha = 30^o$

A model A3 represents for changing in burner's angle from 0 degree to be 25 degree downward, however, the angle of air nozzles are still fixed at zero degree. Finally, model A4, that both of air nozzles and gas burners' incline angle are modified.

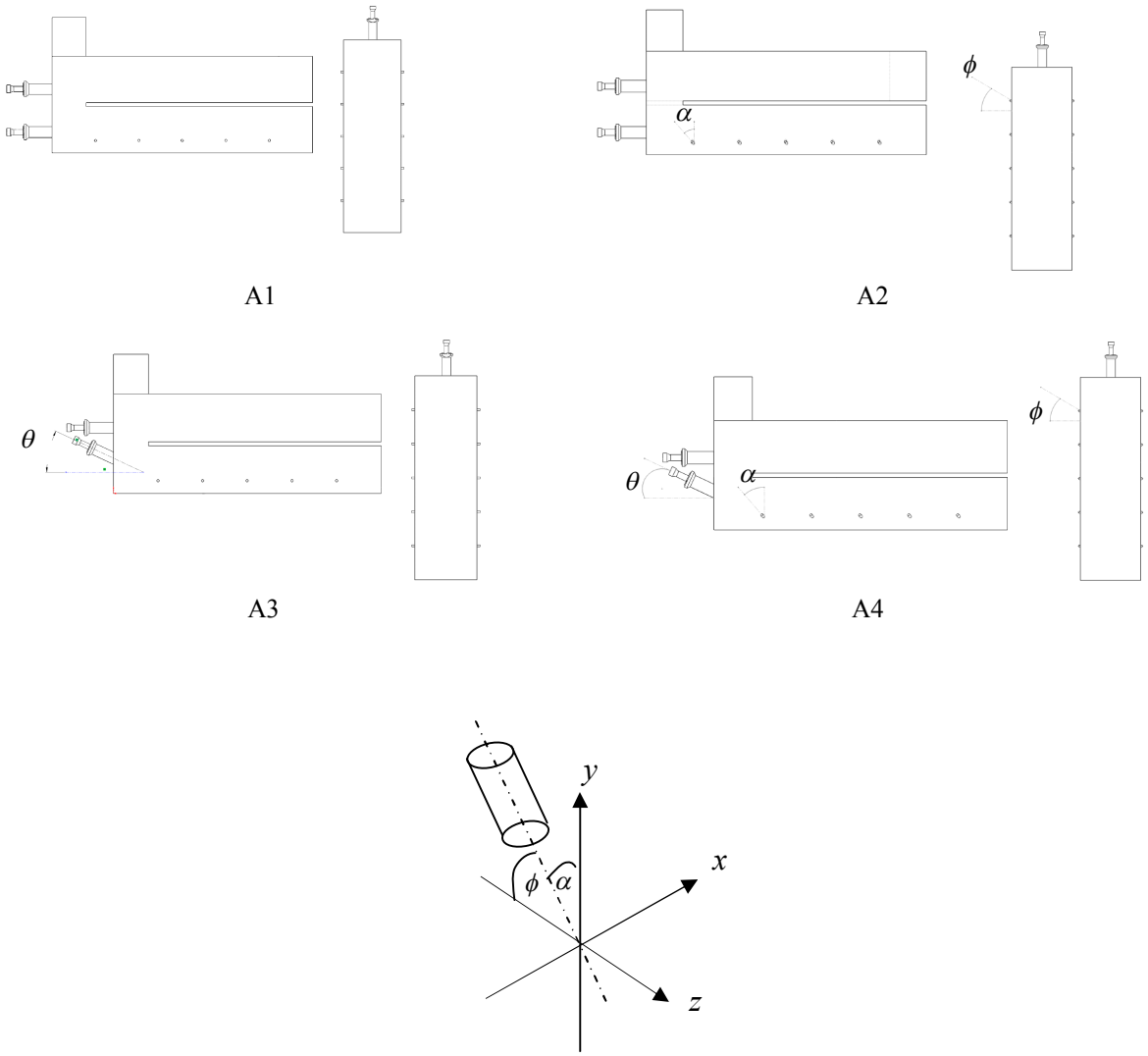

Fig. 6-8 Double-chambered incinerator's model with arrangement of air nozzle and angle

Besides the incinerator's model, the model of high moisture material was also performed, with the dimensions of 50 x 50 x 180 cm, in order for the implemented model to be similar to actual incinerator. All of material models were located at the middle of the incinerator to achieve the flame impingement onto the material.

After finishing models implementation, all models were conducted for meshing by using ANSYS Workbench software. A tetrahedral mesh was applied for incinerator models.

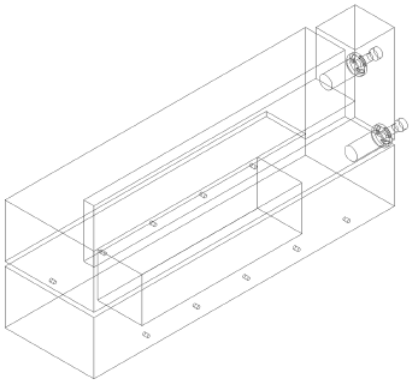

Fig. 6-9 Combusted material model implementation in the incinerator

6.5 Grid sensitivity study

In this research, a study on grid sensitivity was carried out before starting CFD analysis in order to observe the convergence of analysis result. The type of grid was classified into 3 types, which were 1) coarse grid, 2) medium grid and 3) fine grid. The elements of coarse grid, medium grid and fine grid consist of 36,060 152,278 and 365,130 mesh, respectively.

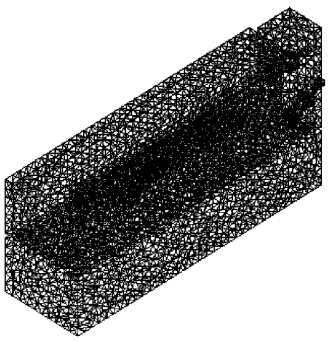

a) Coarse grid

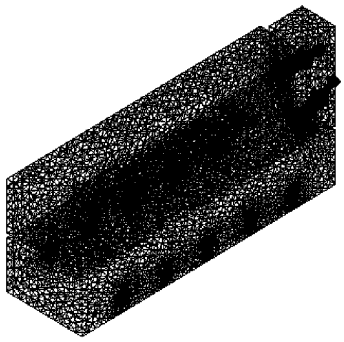

b) Medium grid

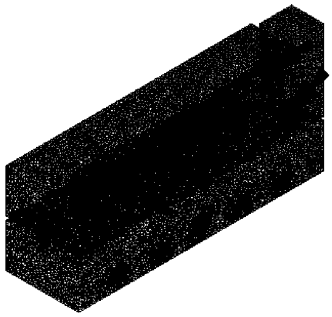

c) Fine grid

Fig. 6-10 Classification of grid type in sensitivity study

Table 6-4 Grid sensitivity study results

Parameters	Coarse grid	Medium grid	Fine grid
Nodes	7,659	30,389	69,667
Elements	36,060	152,278	365,130
Maximum Total Pressure (Pa)	Divergence	359.00	334.22
Maximum Velocity Magnitude (m/s)	Divergence	21.71	21.73
Maximum Temperature (K)	Divergence	1,765.00	1,787.00
Maximum Turbulence kinetic energy (k) (m^2/s^2)	Divergence	9.38	15.68
Maximum Turbulence dissipation rate (epsilon) (m^2/s^3)	Divergence	4,095.48	16,949.62

The results of grid sensitivity study show in Table 6-4. It is discovered that all parameters on coarse grid simulation result in divergence, or the meaning is cannot find the exact solution. Whereas, the result on medium grid and find grid show that mostly values have similar results, for example, pressure, temperature and velocity, except the number of turbulences. The values of both turbulence kinetic energy and dissipation rate of the fine grid scheme result in higher compare to medium grid. These results explain the influence of mesh's element fining to the turbulent schemes. For a large-eddy simulation, the solution of turbulence kinetic energy and dissipation rate with grid dependency show good quality criteria if the intermediate (medium) grid was used, however, the criteria do not depict full convergence although the expected behavior is observed as the grid resolution is increased [83]. Accordingly, the medium grid was used to conduct for simulation in this research.

6.6 Initial conditions of simulation

Initial conditions used for CFD simulation, such as input gas/air velocity or producer gas properties, were calculated by referring to the experimental results. For example, a velocity of biomass producer gas used to combust the high moisture material was estimated as 5 m/s, thus, at the equivalent ratio 0.9, a velocity of air fed to the gas burner was equal to 5.6 m/s. At a same time, it was found that the volume flow rate of air fed to the primary chamber was 0.01 m^3/s, thus, the velocity of air should be 20 m/s per one nozzle. Table 6-5 shows the values of the simulated initial conditions.

Table 6-5 Initial conditions values

Velocity of producer gas at 1st burner	5 m/s
Velocity of producer gas at 2nd burner	5 m/s
Velocity of air injected to 1st burner	5.6 m/s
Velocity of air injected to 2nd burner	5.6 m/s
Velocity of auxiliary air injected to primary chamber	20 m/s
Temperature of producer gas	300 K
Temperature of combustion air	300 K

6.7 Boundary conditions and chemical kinetics of biomass gas combustion

For the boundary condition of the implemented model's wall, it was treated by a constant wall temperature, or this meant there was no loss through the incinerator wall (adiabatic). Hence, the Neumann boundary condition of incinerator's wall can be expressed as:

$$k\frac{\partial T}{\partial x}\bigg|_{wall} = k\frac{\partial T}{\partial y}\bigg|_{wall} = k\frac{\partial T}{\partial z}\bigg|_{wall} = 0$$

In addition, wall was assumed to be stationary with no-slip conditions applied to the wall surface, thus:

$$\vec{V}_x = \vec{V}_y = \vec{V}_z = 0$$

and $$\frac{\partial P}{\partial n} = 0$$ n: normal vector

Chemical kinetic of biomass producer gas combustion

Theoretically, combustion of biomass producer gas occurs from three main flammable gas combustion, which are carbon monoxide (CO), methane (CH_4) and hydrogen (H_2). Accordingly, chemical kinetic of each fuel combustion reaction were performed simultaneously with the standard boundary conditions.

Most of elementary combustion reactions are **bimolecular**; that is, two molecules collide and react to form two different molecules. For an arbitrary bimolecular reaction, this is express as [50];

$$A + B \rightarrow C + D \qquad (6.73)$$

The rate at which the reaction proceeds is directly proportional to the concentrations (kmol/m^3) of the two reactant species, i.e.,

$$\frac{d[A]}{dt} = -k_{bimolec}[A][B] \quad (6.74)$$

The rate coefficient, $k_{bimolec}$, is a function of temperature, but unlike the global rate coefficient, this rate has a theoretical basis. The probability that a collision leads to reaction can be expressed as a product of two factors: an energy factor, $\exp[-E_A/R_uT]$, which expresses the fraction of collisions that occur with an energy above the threshold level necessary for reaction, $\boldsymbol{E_A}$, or **activation energy**.

If the temperature range of interest is not too great, the bimolecular rate coefficient can be expressed by the empirical **Arrhenius form**,

$$k(T) = A\exp(-E_A / R_uT), \quad (6.75)$$

where A is a constant termed the **pre-exponential factor** or the **frequency factor**. R_u represents the universal gas constant (8,314 J/kmol-K) and T is a temperature in Kelvin.

The constants and factors used in the simulation are described in Table 6-6.

Table 6-6 Pre-exponential factors and activation energy values of biomass gas combustion reactions

Reactions	A	E_A
$CH_4 + 2O_2 = CO_2 + 2H_2O$	2.119×10^{11}	2.027×10^{8}
$CO + 0.5O_2 = CO_2$	2.239×10^{12}	1.70×10^{8}
$H_2 + 0.5O_2 = H_2O$	9.87×10^{8}	3.1×10^{7}

6.8 Results on CFD analysis and discussions

6.8.1 Temperature profiles

The results of temperature simulation show in Fig. 6-11. It can be found that the maximum temperature from fuel gas combustion is approximately 1,700 K at the outlet of gas burner. This maximum temperature is close to the theoretical flame temperature of biomass producer gas combustion.

The simulation of incinerator model A1 (commercial model) with high-moisture material model shows the temperature inside the primary chamber would be become highest at the exit of burner. However, the temperature at the front side of the incinerator still had the lowest value, equal to that of the ambient temperature. This phenomenon occurred because some of the combustion heat releasing from the gas burner is drafted into the secondary chamber by the influence of the exhaust fan, and the direction of the auxiliary air injected from the nozzle is dispersed perpendicularly onto the material's surface, causing the air flow to counter the combustion heat. Hence, a majority of the heat was smoldered in the backside of the combustion chamber.

When simulating the Model A2 of double-chambered incinerator, where the incline angle of the air holds were modified, it is found that the temperature between the material and the incinerator wall, including the front side, became higher compared to the A1 model simulation. When the airflow from the nozzles hits the material's surface, a majority of the air is directed toward the incinerator's front, and also forces combustion heat from the back to the front.

The simulation of Model A3, in which the burner incline angle is 25^{o} downward, also results in worse heat distribution, just as in Model A1. The position that has a high temperature is only in the back of the incineration, while the majority of the incinerator model has an ambient temperature at the beginning. Consequently, this model is also deficient for the actual incineration in terms of a great deal of fuel consumption.

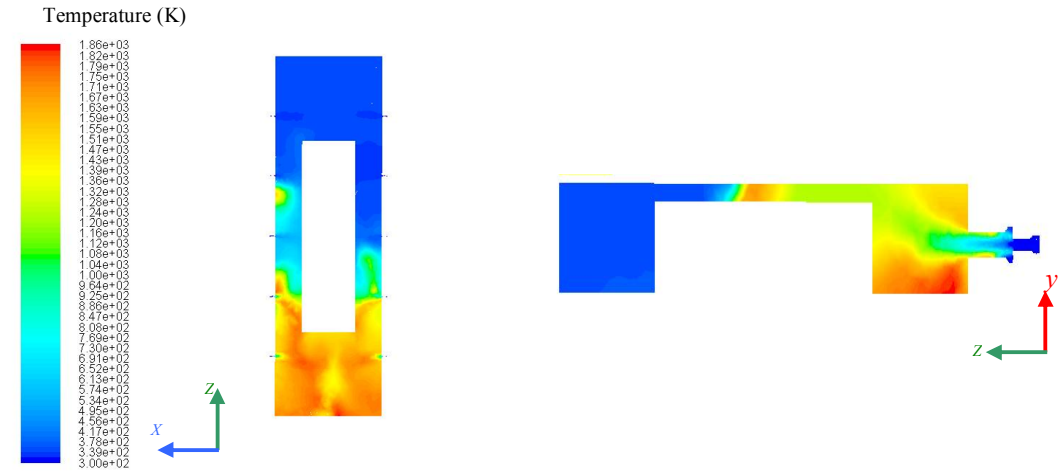

Model A1

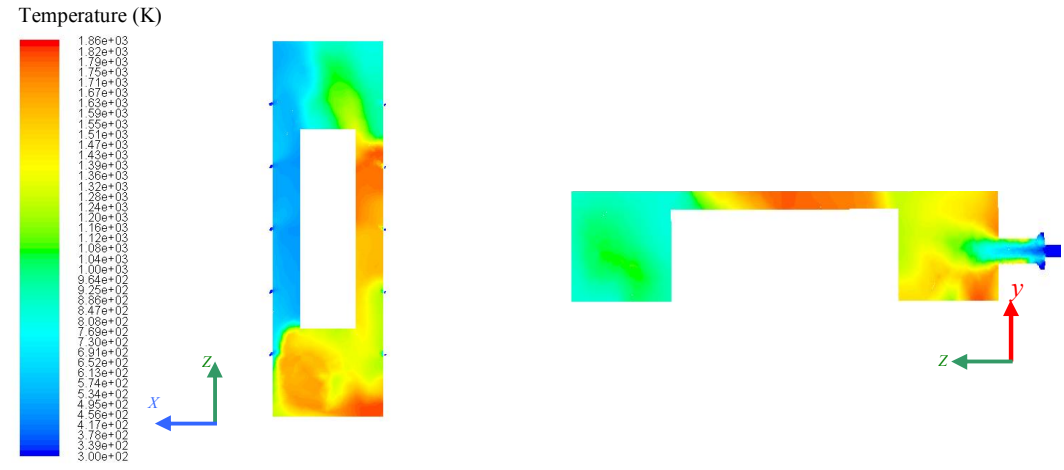

Model A2

Fig. 6-11 Temperature contours inside the primary chamber with a material model

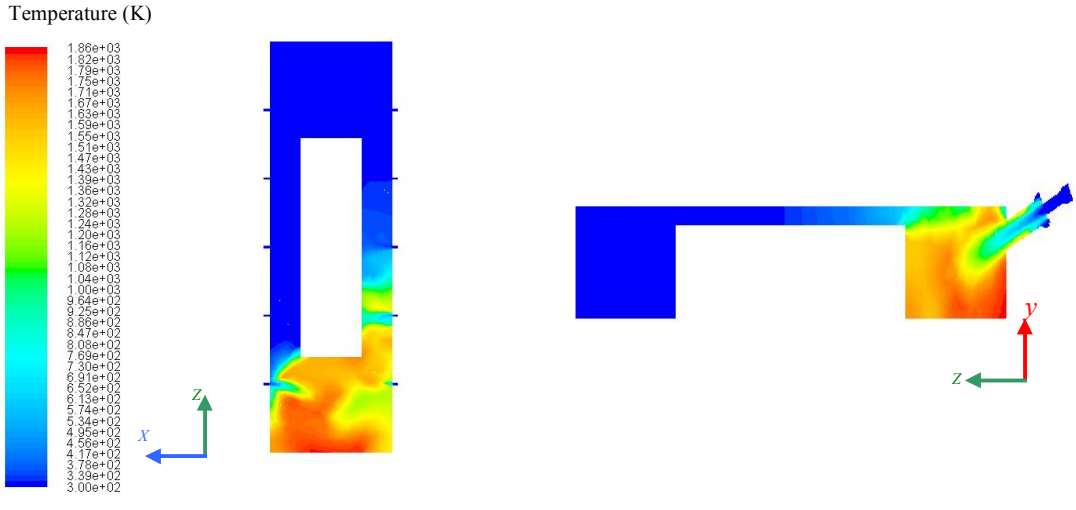

Model A3

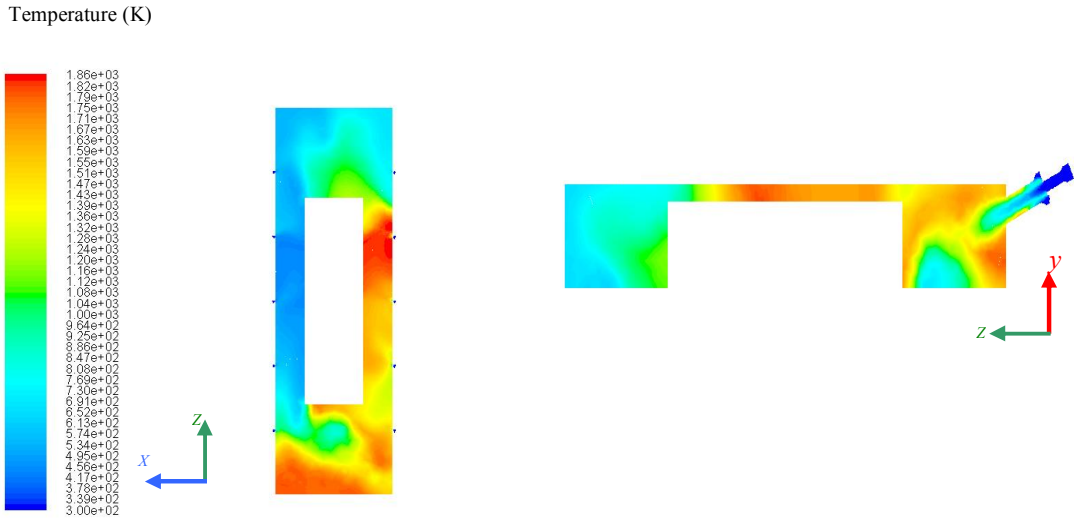

Model A4

Fig. 6-11 Temperature contours inside the primary chamber with a material model (continued)

The simulation results of Model A4, in which both the burner and air hold incline angle are modified, presented a good heat distribution. The average temperature beside the material is approximately 1,500 K, while the temperature towards the incineration's front is 900 K on average. In addition, because of the little space between material's top and the incineration's upper wall, a main obstacle is created against heat transferring throughout the material's topside. From the simulations results, as shown in Fig. 6-11, the distribution's contour of combustion heat between the material's top and the upper wall of models A2 and A4 is more efficient compared to models A1 and A3.

The simulation results on temperature contour inside the secondary chamber are shown in Fig. 6-12. The highest temperature occurring from combustion takes place in model A4, which the incline angle of burner and air nozzles are modified. The lowest temperature, on the other hand, occurs in the model A1 and A3, because an amount of excess air in primary chamber is drafted into secondary chamber, different from air flow of A4 that a majority of air is spread throughout the primary chamber and less of air will be flown into the secondary chamber, as described beforehand. Hence, influent excess air usually makes the secondary chamber's maximum temperature decrease and possibly becomes deficient in emission preventing.

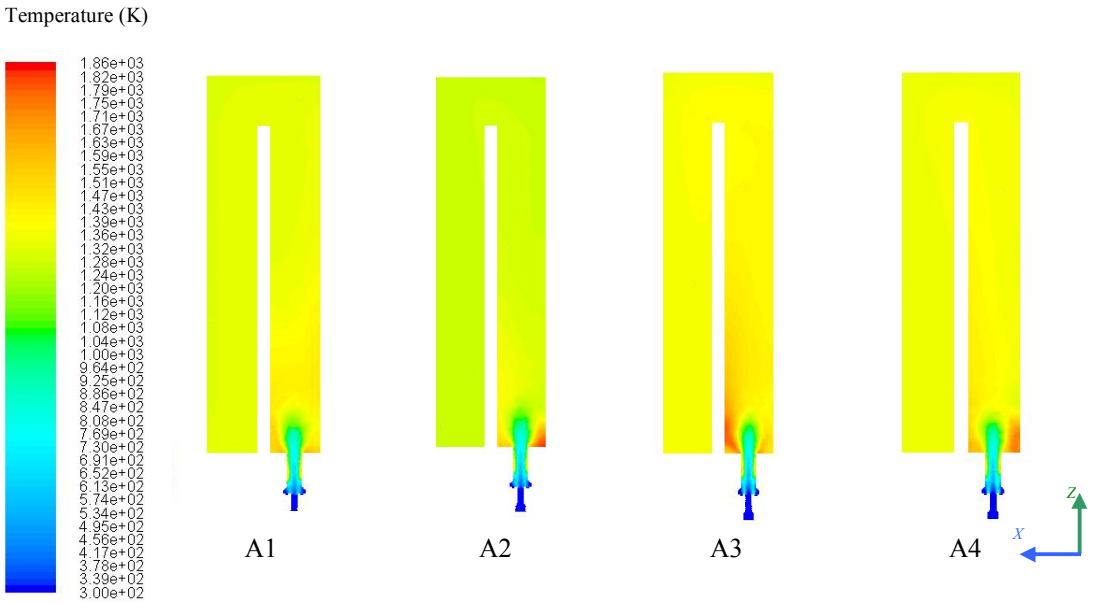

Fig. 6-12 Temperature contours inside the secondary chamber model

According to the temperature's simulation, it can be concluded that the adjusted air hold's angle essentially influenced heat transferring to the front of the incineration. The models in which the burners and air hold angles were modified performed better heat transfers so that the high-moisture material could reach the firing point and ignited faster, which can also reduce the overall operation time.

6.8.2 Turbulent intensity

Turbulent intensity is used to investigate the effectiveness of the air flow inside the incinerator, including the blending between producer gas and auxiliary air. Figure 6-13 shows the contour of turbulent intensity inside the primary chamber. It is found that the modified models (A2 and A4), in which the air nozzle angle is adjusted, presents better turbulent intensity compare to the commercial model (A1). This characteristic suggests that the modified models with adjusted air nozzles result in a more effective air and fuel gas blending.

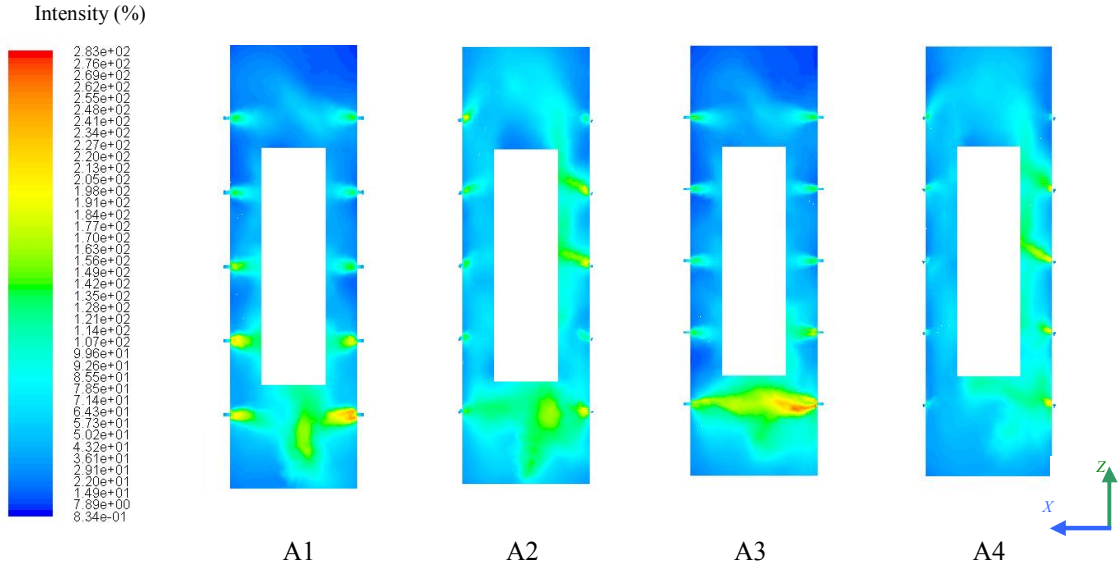

Fig. 6-13 Turbulent intensity (%) contour of the primary chamber

For the simulation of turbulent intensity inside the secondary chamber, which are shown in Fig. 6-14, high turbulent intensity for this chamber explain an effectiveness circulation of fluid flow. It is discovered that the modified model A4 results highest turbulent intensity, which is approximately 140%, while the commercial model (A1) presents in poor intensity. The high quantity of turbulent intensity usually takes place at the burner outlet because air and gas flow from the primary chamber is blended with the combustion product released from secondary burner, or it can be implied that combustion reaction is good in the modified model. Likewise, the better circulation of the secondary chamber also promote the residence time of toxic gas combustion.

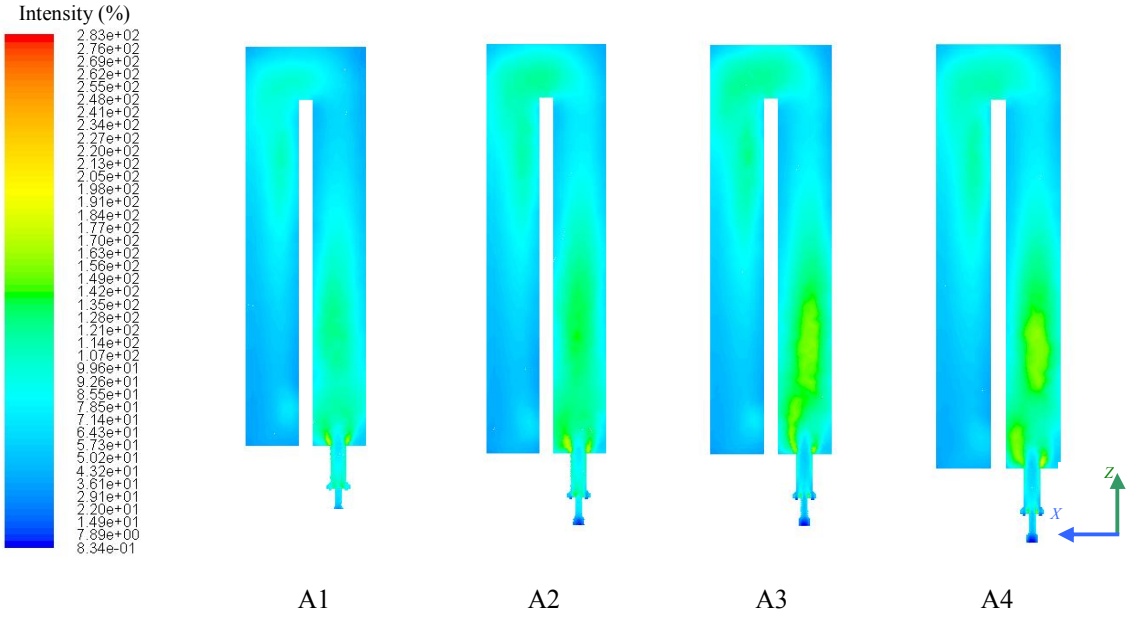

Fig. 6-14 Turbulent intensity (%) contour of the secondary chamber

6.8.3 Results on prediction of nitrogen oxide (NO) formation

As the beforehand explanation, the main constituent of biomass producer gas is nitrogen (N_2). Moreover, there is a number of nitrogen from injected auxiliary air with some unburnt oxygen content in excess air. Thus, the occurrence of pollution, such as a formation oxide of Nitrogen (NO), is also necessary to be considered.

Figure 6-15 shows the result contour of NO formation inside the incinerator model when only the primary burner is operated. It is found that the formation of NO achieved a maximum in the back of the crematory, which is equal to 245,000 mg/m^3. Then, the amount of NO formation becomes decrease at the middle position of primary chamber, which is 123,000 mg/m^3 on average. Finally, NO amount presents lowest at the incinerator's front.

The simulation explains the behavior of NO formation that the highest NO amount occurs at the burner outlet because this position has highest temperature occurring from fuel gas combustion. Thus, majority of nitrogen content in producer gas and air will form and become NO. At a same time, NO also happens at the air nozzles position, due to nitrogen content in excess air.

In addition, it can be found that the rate of NO formation becomes decrease in the secondary chamber at the connector between both chambers, and equal to zero in the stack. The reduction of NO in the secondary chamber can be explained by the low temperature in the secondary chamber, which then decreased the rate of NO formation.

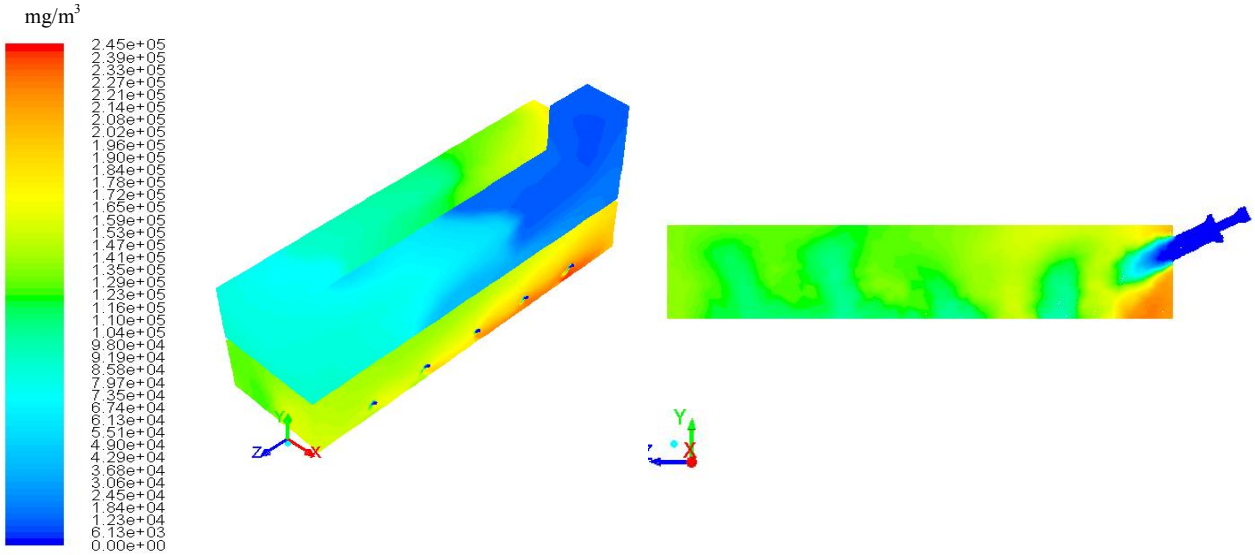

Fig. 6-15 NO prediction if operating only primary chamber

When both of primary and secondary chamber are ignited, the average NO formation inside the primary chamber is lower than the formation of NO when operate only primary chamber, which is approximately 70,000 mg/m^3. In addition, the NO concentration inside the secondary chamber and in the stack was approximately 20,000 mg/m^3, and then reduces gradually. Finally, the NO formation rate at the crematory's stack becomes 3,000 mg/m^3. This phenomenon can be described that the NO formation rate becomes decrease by this condition because some of

auxiliary air in the primary chamber is drafted and used for combustion at the secondary burner, thus, the formation retention time is not enough for the formation. At a same time, NO occurring in the primary chamber is also influenced to the secondary burner, and then, it will be decomposed during the combustion of secondary burner. Figure 6-15 presents the NO formation contour if the primary and secondary chambers are operated.

Although it is found some NO amount at the stack for this case, compare to the operating only primary burner, due to some of NO formation at the secondary burner position and is not destroyed completely. Nonetheless, formation of NO found in this case is lower compare to the rate of NO releasing if there is only primary chamber operation.

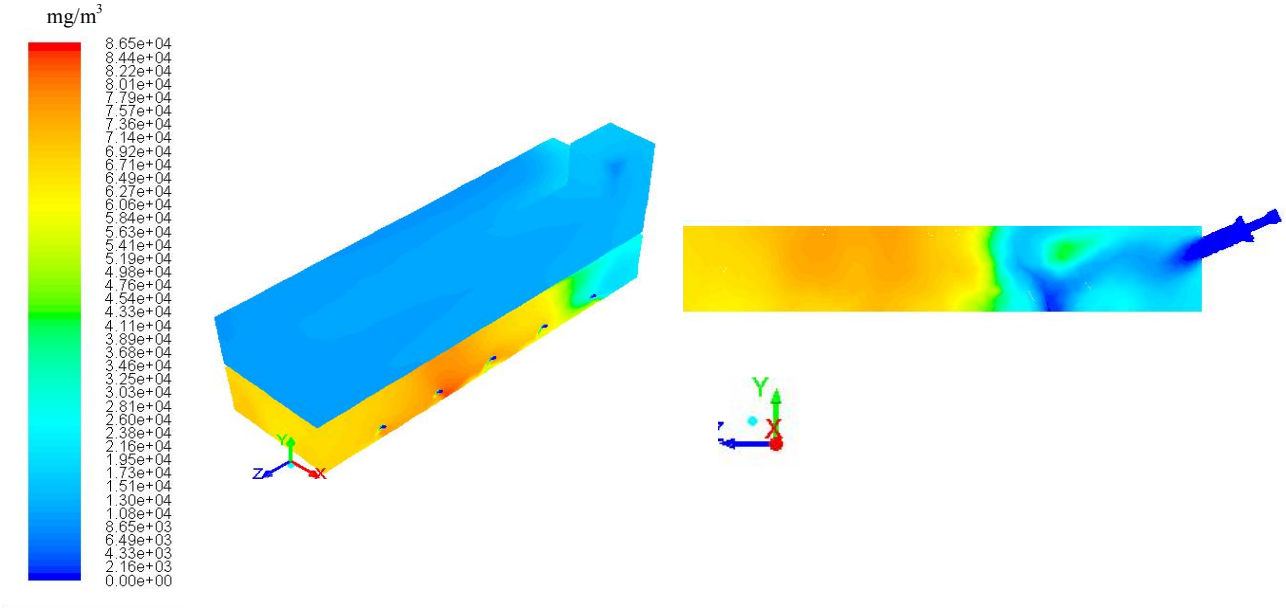

Fig. 6-16 NO prediction if operating both primary and secondary chamber

A relationship between gas burner's NO amount and fuel-air equivalence ratio (E.R.) is shown in Fig. 6-17. It is investigated that the formation rate of NO becomes highest when E.R. is appointed as 1.10, or it means starve air condition, which is approximately 97,500 mg/m^3. If decreasing E.R. number or increasing amount of air to the burner, the amount of occurring maximum NO slightly decreased.

The rate of NO formation concerning to the equivalence ratio, especially at the gas burner, can be found as presenting in Fig. 6-18. The results describe maximum rate of NO formation was 6.78 x 10^{-5} kmol/m^3-s when the E.R. was set as 0.9, which is the same position where the highest temperature occurred. On the other hand, the average NO formation rate was decrease when E.R. number became decrease [84]. This phenomena explains the higher amount of excess air fed to burner make the highest combustion temperature decrease, then, NO does not occur due to this temperature that lower than the formation point. However, it can find NO formation inside combustion chamber, because of nitrogen content in excess air. These results are in agreement with study of S. Sukumaran and S. C. Kong [85] that the major NO producing reactions in a biomass syngas burner are the oxidation of NH and N under slightly rich conditions and temperatures over 1,700 K.

Consequently, increasing amount of air at gas burner benefits for decreasing rate of thermal NO formation caused by gas combustion temperature. However, this operation sometimes causes of low combustion efficiency and other toxic gas, such as dioxin or gas origin of unpleasant smell, will take place.

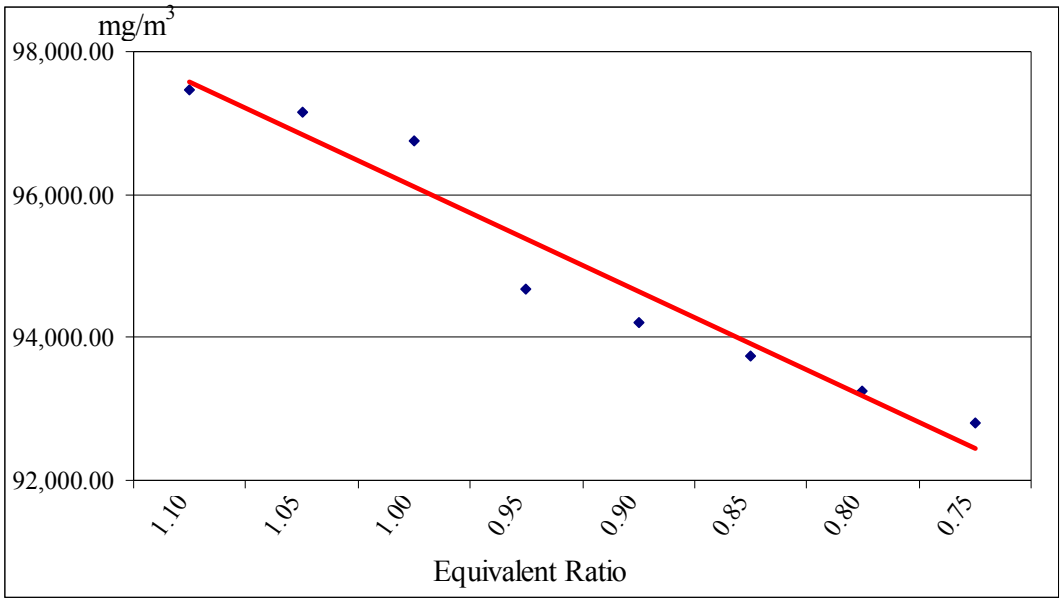

Fig. 6-17 NO prediction simulation results at any fuel-gas equivalent ratio

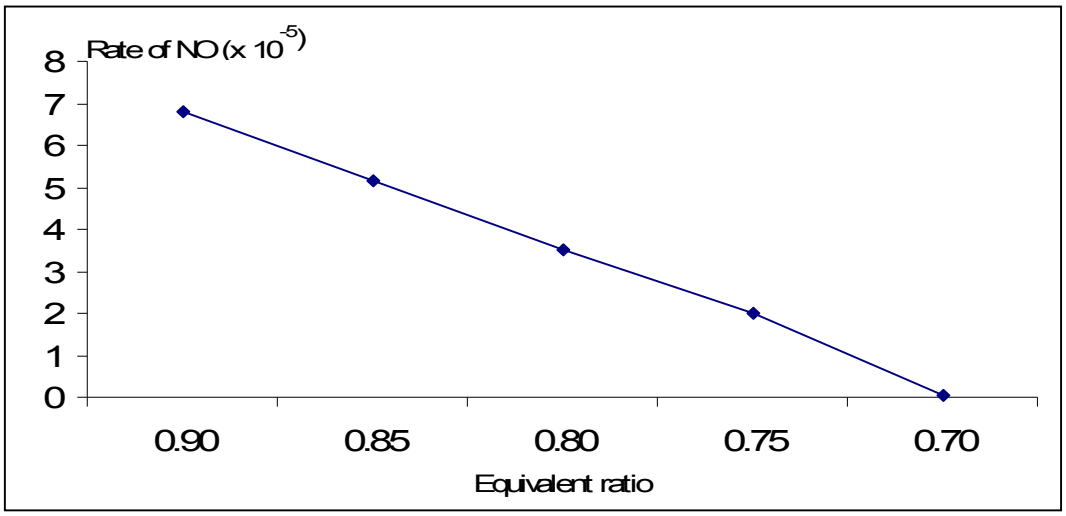

Fig. 6-18 Rate of NO formation at gas burner when adjusting any fuel-gas equivalent ratio

6.9 Analysis of combustion chamber's shape effect to residence time

In this research, study and analysis of the incinerator's secondary combustion chamber shape was also carried out. According to the constituents of combustion gas, especially high-moisture refuse incineration, contain dust particles, soot, toxic gas and an unpleasant odor. The secondary combustion chamber, therefore, is necessary to eliminate this matter by the proper residence time. The recommended residence time of the incinerator's secondary chamber must be at least 1 second to prevent emissions from being released into the atmosphere.

6.9.1 Differential equations

In order to analyze the residence time of chambers, standard $k-\omega$ models [102] were applied, which are represented in Eq. 6.76-6.77.

$$\frac{\partial}{\partial t}(\rho k)+\frac{\partial}{\partial x_i}(\rho k u_i) = \frac{\partial}{\partial x_i}\left[\left(\mu+\frac{\mu_t}{\sigma_k}\right)\frac{\partial k}{\partial x_j}\right]+G_k-Y_k-S_k \quad (6.76)$$

$$\frac{\partial}{\partial t}(\rho \omega)+\frac{\partial}{\partial x_i}(\rho \omega u_i) = \frac{\partial}{\partial x_i}\left[\left(\mu+\frac{\mu_t}{\sigma_\omega}\right)\frac{\partial \omega}{\partial x_j}\right]+G_\omega-Y_\omega-S_\omega \quad (6.77)$$

where G_k represents the generation of turbulent kinetic energy that arises due to mean velocity gradients, and G_ω is the generation of ω. Y_k and Y_ω represent the dissipation of k and ω due to the turbulence, whereas S_k and S_ω are defined source terms.

The turbulent viscosity was defined using a damping coefficient (α^*).

$$\mu = \alpha^* \frac{\rho k}{\omega} \quad (6.78)$$

6.9.2 Chamber's model implementation

Concerning the secondary combustion chamber's model, the shapes were classified into two types: rectangular and cylinder. The rectangular shape (Model A) is the same model as shown in Fig. 6-7. For the cylinder-type secondary chamber, the total volume was equal to 0.78 m^3, with a diameter of 1.0 m, and a height of 1.0 m. One of these types of chambers was located above the primary chamber (Model B), in which the gas flow (combustion gas and particle) released from the primary chamber was injected at the bottom of the secondary chamber, as shown in Fig. 6-19 (b). The other chamber was located beside the primary chamber (Model C), so that gas flow from the primary chamber would be injected beside the cylinder secondary chamber, as shown in Fig. 6-19 (c).

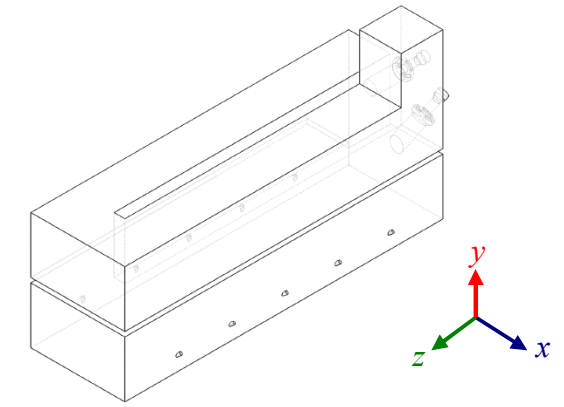

a) Rectangular chamber type (Model A)

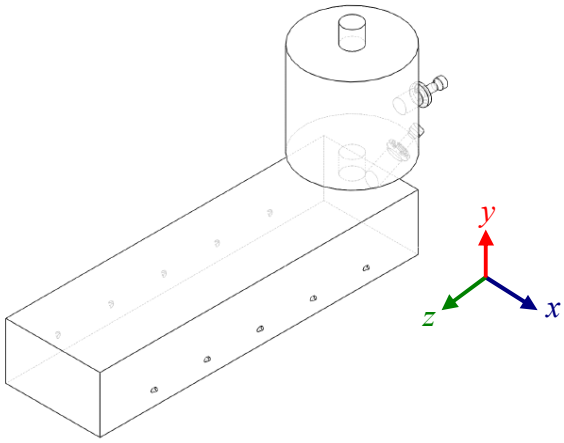

b) Secondary chamber located above the primary chamber (Model B)

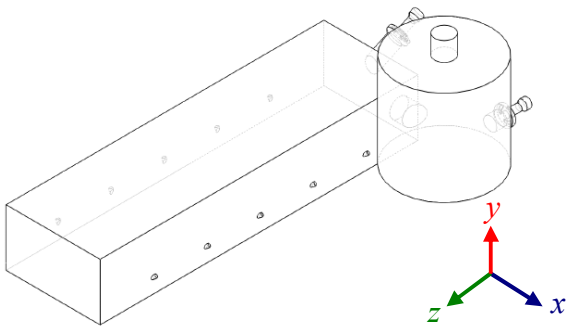

c) Secondary chamber located beside the primary chamber (Model C)

Fig. 6-19 Models for residence time analysis

6.9.3 Residence time analysis results

Simulation of the secondary chamber's residence time assumed that the dimension of particles released from the primary chamber has a 1 μ m diameter. The residence time observation occurred from when the particles were starting to exit the inlet of the secondary chamber until they reached the stack.

Figure 6-20 presents the results of the residence time of the rectangular-shaped secondary chamber. It was found that the residence time of the gas flow inside the chamber was 2.54 s on average, whereas the average residence time of the particle was 3.05 s. This chamber's type was beneficial due to its long length, allowing an increase in the residence time.

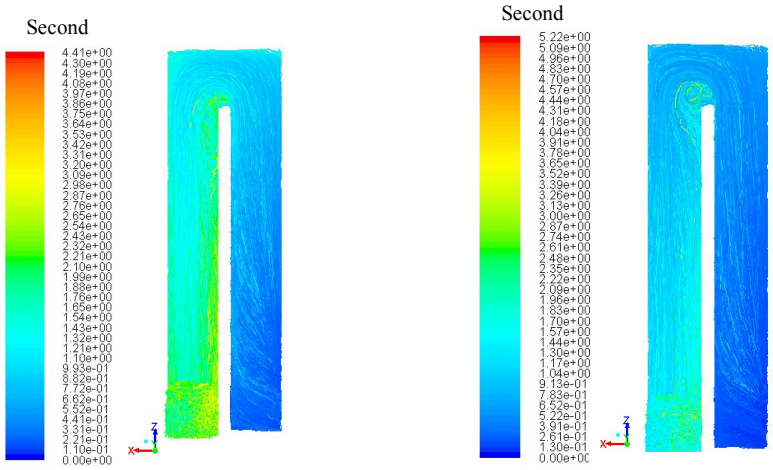

a) Particle residence time b) Gas residence time

Fig. 6-20 Simulation results of the residence time of the rectangular chamber type (Model A)

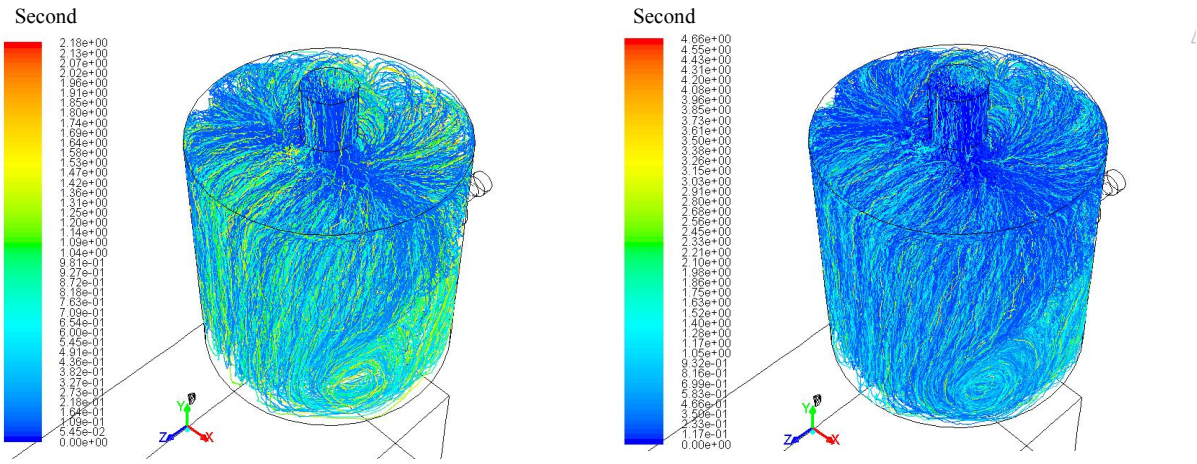

a) Particle residence time b) Gas residence time

Fig. 6-21 Simulation results of the residence time of the cylinder type (Model B)

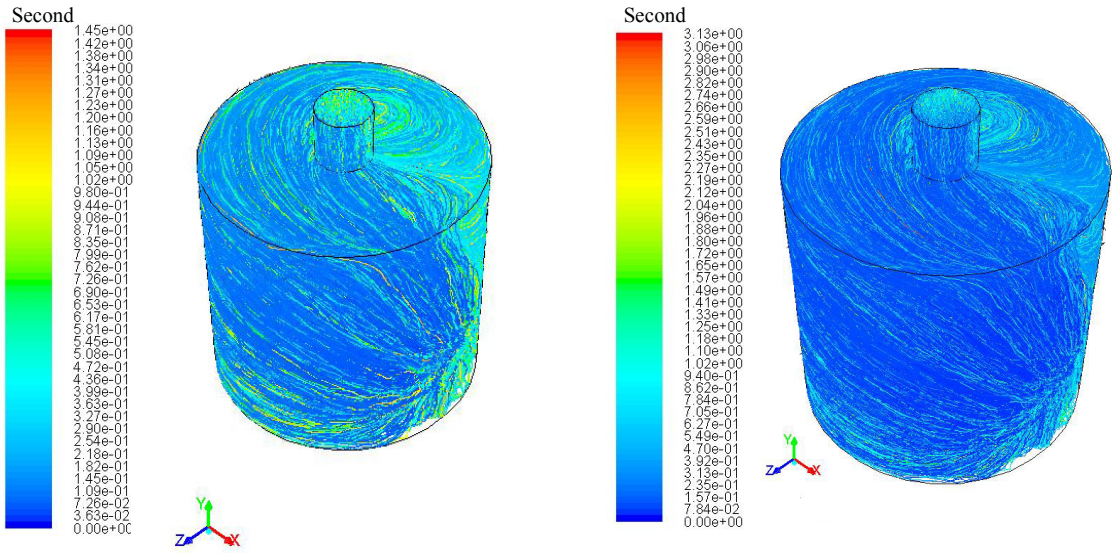

a) Particle residence time b) Gas residence time

Fig. 6-22 Simulation results of the residence time of the cylinder type (Model C)

For the cylinder-type chamber, it was investigated that if the secondary chamber was located above the primary chamber (Model B), the maximum residence time of particles occurred at 2.18 s, and the average particle's residence time was 1.20 s, as shown in Fig. 6-21. These residence time phenomena could explain why the majority of the flow inside the chamber presented a radial flow, and thus, both the released combustion particles and gas flow behavior were swirled causing a residence time increase.

Concerning the simulation results of Model C (Fig. 6-22), it was found that this chamber's type resulted in a shorter residence time compared with the residence time of Model B. For this model, the average residence time of particles and gas results were 0.70 and 1.02 s, respectively. These results occurred because the position of the chamber's inlet was located beside the main combustion chamber, forcing gas and the particle flow to be mixed. However, most particles and gas revealed only a few swirling flows before exiting the stack, and thus caused a shorter residence time.

Furthermore, the simulation of the chamber's dimensions were also carried out in this study in order to investigate the gas and particle flow behavior, and the changing of the residence time that is effected by several chamber's dimensions. Figure 6-23 shows a comparison of the residence times obtained from the simulation when changing the chamber's volume by increasing the chamber's height to 1.1, 1.2 and 1.3 m. The simulation results of Model B display a high residence time increase rate, particularly the residence time of gas that increased gradually when the chamber's height was lengthened, as well as the particle residence time. These phenomena can be explained by the increasing of the chamber's volume by extending the height, which allowed gas and particles to be maintained in the chamber for a longer time.

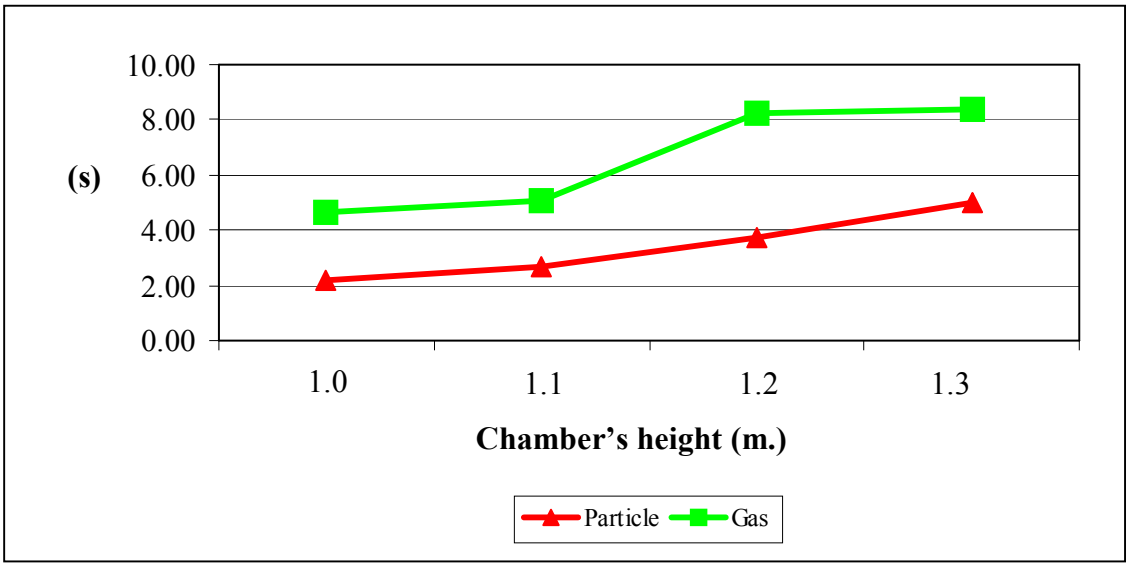

a) Model B

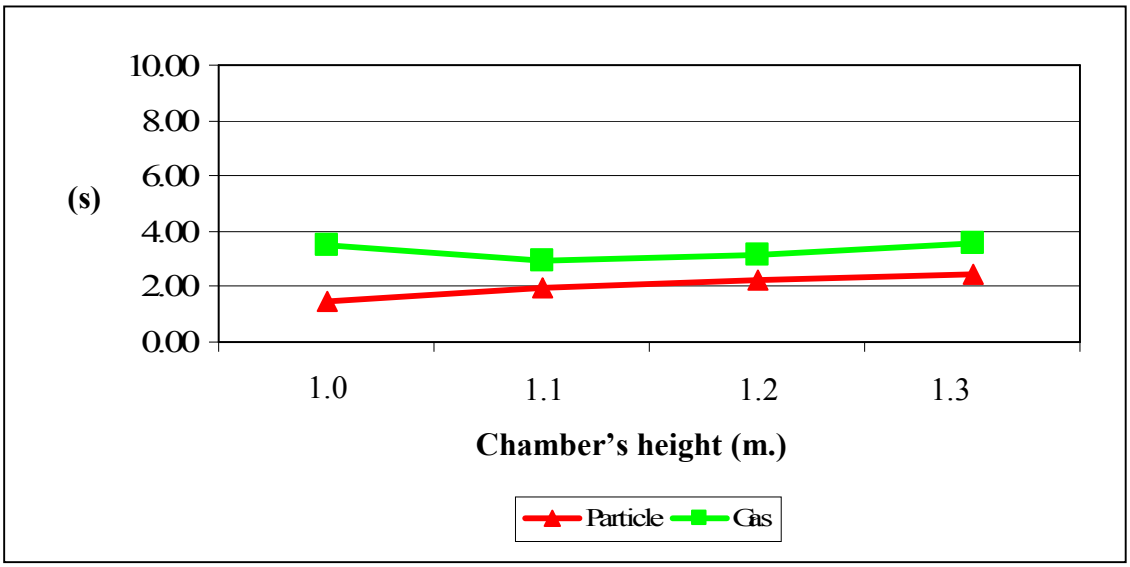

b) Model C

Fig. 6-23 Simulation results of the residence time when increasing the chamber's height

Concerning Model C, it could be observed that the majority of the residence time became rather constant, especially the residence time of gas. The particle residence time, on the other hand, resulted in a small increase, which reached a maximum of 2.5 s when the height was adjusted to 1.3 m. This model's results can be explained by the increase in the chamber's height, which affected the circulation of particles, thus, the simulated residence time of particles became higher. In contrast, most combustion gas flow behavior did not achieve a circulation flow. Consequently, the trend of the gas's residence time when simulated by Model C was fairly constant.

6.10 Chapter's conclusions

In this chapter, the significant parameters obtained from experiment were implemented for the actual scale of double-chambered incinerator by using CFD analysis. From the simulation result, it was found that the recent commercial double-chambered incinerator is rather deficient and not proper for biomass gas to be utilized as main fuel. Thus, some important parameter, such as position and angle of burner or air nozzle, is needed to be adjusted. The results of modified model show influences of air nozzle angle to the heat distribution throughout the primary chamber. At a same time, efficient flow circulation by turbulent intensity observing also promoted effective air and fuel gas blending.

Predictions of nitrogen oxide formation (NO) show NO formation during combustion process became high amount due to the nitrogen content in excess air and temperature occurring inside the combustion chamber. However, some of this NO may be reduced by simultaneously operating secondary chamber, to conduct for the repeat combustion condition, or reducing air injected to the gas burner. Nevertheless, there may be less amount of NO formation in the actual situation, because an evaporation of water content in high-moisture material was neglected in this simulation. In the actual procedure, an average temperature in the chamber will be reduced by this evaporated moisture, which becomes lower than the NO formation point.

Besides above parameters, one of the most significant values of high-moisture material's incinerator is the residence time. The analysis results show the rectangular-shape presents in best residence time occurring due to its longer length, whereas the cylinder type, in which the combustion gas and particle inlet are located at the chamber's base, results a rather efficient residence time.

By conclusion, a distinct advantage of using of CFD for combustion characteristics simulation is that it can reduce time for actual experiment conduction, as well as the construction cost reduction, because CFD analysis can simulate the result that similar to the actual situation. In addition, emission happening after combustion can be also predicted by this application, thus, it can save the budget for an investigation. At a same time, prediction of emission by this method instead of the actual can prevent the observer to avoid the harmful from toxic gas absorption.

Chapter 7
Conclusions

7.1 Summary of major conclusions

According to the facts, high-moisture refuse incineration recently uses petroleum fuel, which causes of serious environmental effects and high operation cost. Consequently, study for alternative and renewable energy sources to be used as a fuel for high-moisture refuse incineration is necessary. Especially, a double-chambered incinerator that consists of two main combustion chambers, the primary chamber is used for refuse elimination and the secondary chamber is used for toxic gas and dust elimination.

The results of biomass fuel and producer gas analysis show that average gross calorific value of fuel gas are between 4-6 MJ/m^3. In can be also investigated that the solid biomass contains higher heating value does not convert to high calorific value fuel gas. The quality of fuel gas usually depends on reactions inside the gasifier, especially, the temperature, porosity and height of reduction (char) zone. Moreover, if the temperature of the char bed is higher, rate of CO content in fuel gas becomes high and the quality of fuel is better. From the experimental results, it was investigated that combustion of biomass producer gas can achieve the highest temperature if adjusting the combustion equivalence ratio to be 0.9, or it means 10% of excess air input. The maximum temperature found was achieved approximately 750^oC. In contrast, the highest temperature of gas combustion will decrease if either increasing or decreasing equivalence ratio from 0.9 were carried out. Furthermore, adjusting of E.R. also relates to the flame length, which the length becomes longer if increasing E.R. or it means injecting more air to the burner.

The amount of excess air is necessary to be injected to the incinerator in order to combust high moisture waste. An adequate amount of excess air should be equal to 100% of waste's stoichiometric air, which results for high temperature taken place and low emission released. Too much excess air amount shown for worse temperature maintaining and also causes of more pollution, which was discovered by exhaust gas opacity. Furthermore, an evaluation on incinerator's energy balance shows the effectiveness of energy utilized for high-moisture material combustion. Although an incinerator's efficiency became low when operated both primary and secondary chamber, but nevertheless, this operation presents the benefit for preventing harmful toxic gas occurred from waste combustion, including unpleasant odors.

Using of Computational Fluid Dynamics (CFD) analysis also prefers more advantages in this research, in order to simulate an actual combustion behavior in the actual scale incinerator such as temperature, performance of fuel-air mixing. The simulation results show that the commercial model of incinerator used at present still has not good efficiency if biomass fuel gas will be used. Thus, modifying, such as angle of burner and air nozzle, will conduct for better outcome. An implementation of CFD supports the reason of double-chambered incinerator using that the formation rate of NO will decrease when operate both combustion chambers simultaneously. At a same time, the simulations on secondary chamber with a various shape shown the modified model, such as cylinder chamber shape, can prefer an acceptable residence time like a standard rectangular shape. However, the cylinder chamber shape has dominant benefit as a cheaper construction cost, and reducing the space needed for installation.

Finally, the research results exactly encourage the advantage of biomass energy source to be use for high moisture refuse incineration instead of petroleum fuel. Biomass energy is implied for a carbon-neutral and extremely promotes domestic fuel utilization, which fossil fuel cannot be. Accordingly, this research's output will be able to be applied for a several thermal application concerning, besides the waste incineration.

7.2 Highlights of study and further works

From the research, there is some recommended idea that must be considered, in order to develop the similarly further kind of this research.

1. Due to the experimental results, combustion efficiency inside the incinerator also mainly depends on the quality and continuity of biomass producer gas. For further research, it, therefore, is necessary to use the other of biomass fuel gas that has higher calorific value as an alternative fuel for high-moisture materials combustion.
2. This research used fresh meat as a sample of high-moisture refused, which is different from an actual condition. At the same time, the complex chemical reaction during the material combustion and organic substance decomposition was not emphasized in this research. Consequently, the future research should be considered for these criteria, then, the obtained results will be close to the actual situation.
3. By implementation of CFD for actual scale double-chambered incinerator, a standard k-epsilon viscous model was used, while the flow problem was solve by SIMPLE algorithm and first order upwind method, because these methods are reasonable for various kind of flow prediction. However, the demerits, such as poor results in swirling and rotating, may be found as a result. Thus, using of other viscous model, such as Reynolds stress model, can prefer more exact solution occurring. About the flow field problem, a second order or third order (QUICK method) are challenge for further research.
4. Using CFD analysis to predict rate of emission releasing was carried out base on temperature and elementary chemical combustion reaction. Nevertheless, there is another emission (i.e. prompt NO, dioxin furan and etc.) that needs complicate chemical reaction to estimate mentioned emission.

References

[1] Pollution Control Department, 2005, "Situation of Air Pollution from Crematory", Department publishing's document, Bangkok.

[2] Rajvanshi, A. K., 1986, "Biomass Gasification", Alternative Energy in Agriculture, Vol. II, pp. 83-102.

[3] The Committee on Natural Resources and Environment of Thailand, 2002, "Study on Air Pollution from Urban Crematorium and Problem Solving", Bangkok.

[4] Wongschitwan, P., 2010, Zero Pollution Cremation, <http://gotoknow.org/blog/babyr2r/352380>.

[5] Chawdhurya, M.A. and Mahkamovb, K., 2011, "Development of a Small Downdraft Biomass Gasifier for Developing Countries", Journal of Scientific Research 3(1), pp.51-64.

[6] Food and Agriculture Organization of the United Nations, 1986, "Wood Gas as Engine Fuel".

[7] Van der Aarsen, F.G., 1982, "Performance of a rice-husk fluidized bed pilot plant gasifier", 1st International Producer Gas Conference, Colombo, Sri Lanka.

[8] Schelaepfer, P. and Tobler, J., 1937, "Theoretischen und Praktische Untersuchungen uber den Betrieb von Motorfahrzeuge mit Holzgas", Bern.

[9] The Swedish Academy of Engineering Sciences, 1979, "Generator Gas-The Swedish Experience from 1939-1945". Translated by the Solar Energy Research Institute, U.S.A., SERI/SP-33-140.

[10] Solar Energy Research Institute, 1988, "Handbook of Biomass Downdraft Gasifier Engine Systems".

[11] Reed, T.B. and Levie, B., 1984, "A simplified model of the Stratified Downdraft Gasifier", International Bio-energy Directory and Handbook 1984, edited by Paul F. Bente, Jr., The Bio-Energy Council, Washington D.C., pp.379-389.

[12] Beenackers, A.A.C.M. and Van Swaaij, W.P.M., 1982, "Gasification of biomass, a state-of-the-art review", Press. 1st Europe Workshop on thermochemical processing of biomass, Birmingham, UK.

[13] Department of Alternative Energy Development and Efficiency, 2011, “Study and Research for 400 kW Rice Husk Gasification System”, Project Final Report, Bangkok, Thailand.

[14] Jayah, T. H., Aye, L., Fuller, R. J. and Stewart, D. F., “Simulation study of a down-draft wood gasifier used to produce thermal energy for tea drying”, Renewable Energy Transforming Business, pp. 639-646.

[15] Venselaar, J., 1982, “Design rules for down-draught gasifiers”, a short review, IT Bandung, Indonesia.

[16] Gunther, S., 1984, “Some Aspect on Producer Gas Operation of Internal Combustion Engines”, Proceedings of the Biomass Gasification Workshop, Chulalongkorn University, Bangkok, pp.85-86.

[17] Cuoci, A., Faravelli, T., Frassoldati, A., Grana, R., Pierucci, S., Ranzi, E. and Sommariva, S., 2009, Mathematical modeling of gasification and combustion of solid fuels and wastes, Chemical Engineering Transactions, Vol.18.

[18] Guo, J., 2004, “Pyrolysis of wood powder and gasification of wood-derived char”, Doctor Degree’s Dissertation, Universiteitsdrukkerij, TUE.

[19] Ramirez, J.J., Martinez, J.D. and Petro, S.L., 2007, “Basic design of a fluidized bed gasifier for rice husk on a pilot scale”, Latin American Applied Research, 37, pp.299-306.

[20] Prins, M.J., Ptasinski, K.J. and Janssen, F.J.J.G., 2006, ”More efficient biomass gasification via torrefaction”, Int. J. of Energy 31, Elsevier, pp.3458-3470.

[21] Arjharn, W., Hinsui, T., Liplap, P. and Vijaya, G.S., 2012, “Evaluation of electricity production from different biomass feedstocks using a pilot-scale downdraft gasifier”, Journal of Biobased Materials and Bioenergy, Vol. 6, No. 3, pp. 309-318.

[22] Chuchottaworn, J., 2012, “Energy and economic analysis of heat production from Pennisetum Purpureum cv. Pakchong1 Grass through gasification process”, Master Degree’s Dissertation, Chiang Mai University.

[23] Pianthong, K., 2012, “Gasification technology for ceramic industry”, Presented at the Seminar on renewable energy technology implementation in Thailand experience transfer from Europe, Bangkok, Thailand.

[24] Melgara, A., Pérez, J. and Horrilloc, A., 2009, “Biomass gasification process in a downdraft fixed bed gasifier: a real time diagnosis model based on gas composition analysis”, Rev. Fac. Ing. Univ. Antioquia No. 49, pp. 9-18.

[25] Manoonphol, W. and Phromma, N., 2011, "Characteristics of Heat Energy of Gasifier using Leaves and Dry Twigs as Fuel", Presented at the 25th Conference of the Mechanical Engineering Network of Thailand, Krabi, Thailand.

[26] Prins, M.J., 2005, "Thermodynamic analysis of biomass gasification and torrefaction", Doctor Degree's Dissertation, Technische Universiteit Eindhoven.

[27] Sharma, A.K., 2011, "Modeling and simulation of a downdraft biomass gasifier: 1. Model development and validation", Energy Conversion and Management 52, pp.1386-1396.

[28] McCabe, W.L., Smith, J.C. and Harriott, P., 1993, "Unit operation of chemical engineering", Fifth Edition, New York: MGH.

[29] Simpson, W.T., 1998, "Equilibrium moisture content of wood in outdoor locations in the United States and worldwide", Research note FPL-RN-0268, Forest Products Laboratory, United States Department of Agriculture.

[30] NIST, 2005, NIST Chemistry, <http://webbook.nist.gov>.

[31] Sharma, A.K.,2011, "Modeling and simulation of a downdraft biomass gasifier: 1. Model development and validation", Energy Conversion and Management 52, pp.1386-1396.

[32] Robert, A.F., 1970, "A review of kinetics data for the pyrolysis of wood and related substances", Combust Flame, 14, pp. 263-272.

[33] Sharma, A.K., Ravi, M.R., and Kohli, S., 2006, "Modeling product composition in slow pyrolysis of wood". SESI J., 16(1): pp. 1-11.

[34] Ducrane, E.D., 1998, "Modeling of gaseous pollutants emissions in circulating fluidized bed combustion of municipal refuse", Fuel: 77(13), pp.1399-1410.

[35] Giltrap, D.L., McKibbin, R. and Barnes, G.R.G., 2003, "A steady state model of gas-char reactions in a downdraft biomass gasifier". Solar Energy; 74, pp.85-91.

[36] Wang, Y. and Kinoshita, C.M., 1993, "Kinetic model of biomass gasification", Solar Energy; 51(1), pp.19-25.

[37] Kaviany, M., 1995, “Principles of heat transfer in porous media”, 2nd edition, New York: Springer-Verlag.

[38] White, F.M., 1991, “Viscous fluid flow”, 3rd edition, Singapore: McGraw Hill.

[39] White, F.M., 2003, “Fluid mechanics”, 5th edition, Singapore: McGraw Hill.

[40] Sharma, A.K., Ravi, M.R. and Kohli, S., 2006, “Modelling heat transfer in biomass gasifier”, In proceedings of 18th national & 7th ISHMT-ASME, Heat Transfer Conference. 315 (1315), IIT, Guawahati, India.

[41] Cengel, Y.A. and Ghajar, A.J., 2012, “Heat and Mass Transfer: Fundamentals and Applications”,4th Edition, McGrawhill, Singapore.

[42] Ragland, K.W., Arts, D.J. and Baker, A.J., “Properties of wood for combustion analysis”. Bioresour Technol 1901; 37: 161-8.

[43] Reid, R.C., Prausnitz, J.M. and Poling, B.E., 1988, “The properties of gases and liquids”. Fourth edition, New York: McGraw-Hill Company.

[44] Kerdsuwan, S., 2006, “Combustion and Emission Control”, King Mongkutt’s Institute of Technology North Bangkok, Bangkok.

[45] Floyd, H., 2007, “Practical Design of Waste Incineration”, Handbook of Environmental Engineering Calculations.

[46] Ontario Ministry of the Environment, 1986, “Incinerator Design and Operating Criteria Volume II - Biomedical Waste Incinerators”.

[47] Brunner, C. R., 1993, “Hazardous waste incineration”, McGraw-Hill Ryerson, Limited.

[48] Niessen, W. R., 1993, “Combustion and Incineration Process”, 3rd Edition, Marcel Dekker: New York.

[49] Kuo, K., 1986, “Principle of Combustion”, 2nd Edition, John Wiley and Sons.

[50] Turns, S.R., 2012, “An Introduction to Combustion: Concepts and Applications”, 3rd Edition, McGraw-hill, Singapore.

[51] Luiz de Sousa-Santos M., 2004, “Solid Fuels Combustion and Gasification”, CRC Press.

[52] F.J., Weinberg, 1975, The first half-million years of combustion research and today's burning problems, Progress in Energy and Combustion Science, 1: 1731.

[53] Delichatsios, M.A., 1993, "Transition from Momentum to Buoyancy-Controlled Turbulent Jet Diffusion Flames and Flame Height Relationships", Combustion and Flame, 92: pp.349-364.

[54] Jones, H.R.N., 1989, "The Application of Combustion Principles to Domestic Gas Burner Design", British Gas Teaching Fellow, University of Cambridge, London.

[56] Francis,W.E., 1964, J. Inst. "Gas Engineering 4", 399.

[57] Department of Department of Alternative Energy Development and Efficiency, 2010, "Study and Development of Biomass Gasification Unit for Agricultural Pumping System", Research Final Report.

[58] Jenkins, B. M., Baxter, L. L., Miles Jr., T. R. and Miles, T. R., 1998, "Combustion properties of biomass".

[59] Pavoni, J. L., Heer, J. E. and Hagerty Jr., D. J., 1972, "Handbook of Solid Waste Disposal Materials and Energy Recovery", Van Nostrand Reinhold.

[60] Lee, C. C. and Huffman, G. L., 1986, "Energy and Mass Balance Calculations for Incinerator", U.S. Environmental Protection Agency.

[61] Thavornun, S., 2007, "Study and Research on Crematory for Energy Saving", Research's report, Energy Policy and Planning Office, Ministry of Energy of Thailand.

[62] Bubpamala, W., 2007, "Research and Development of Human Crematory for Energy Saving", Master Degree's Dissertation: King Mongkutt's University of Technology North Bangkok.

[63] Kreith, F. , 1999, "Fluid Mechanics", Mechanical Engineering Handbook, Boca Raton: CRC Press LLC.

[64] Bureau of Mines, 1967, "Ringelmann Smoke Chart (Revision of IC 7718)", United States Department of the Interior.

[65] Gunther, S. ,1984, "Some Aspect on Producer Gas Operation of Internal Combustion Engines", Proceedings of the Biomass Gasification Workshop, Chulalongkorn University, pp.85-86.

[66] Bahadori, M.Y., Small Jr., J.F., Hegde, U.G., Zhou, L. and Stocker, D.P., 1995, "Characteristics of Transitional and Turbulent Jet Diffusion Flames in Microgravity", NASA Conference Publication 10174, Third International Microgravity Combustion Workshop, Cleveland, OH, pp. 327-332.

[67] Saito, M., Amagai, K., Okiwara, G.and Arai, M., 2001, "Combustion Characteristics of Waste Material Containing High Moisture", Fuel, Vol. 80, Issue 9, pp. 1201-1209.

[68] Saiyudthong, C., 2007, "Using CFD to Find Manning Roughness Coefficient of a Canal", Proceeding of The 12th National Convention on Civil Engineering, pp. 1-6.

[69] Anderson Jr., J. D., Degroote, J., Degrez, G., Dick, E., Grundmann, R. and Vierendeels, J., 2009, "Computational Fluid Dynamics: An Introduction", Third Edition, Springer-Verlag: Berlin Heidelberg.

[70] Doungsupa, N., 2004, "Simulation of Combustion in Ceramic Fiber Kiln Using Computational Fluid Dynamics", Proceeding of 11th Tri-University and Symposium Role of Asia in the Would, pp.192-195.

[71] Vorayos, N., 2002, "Numerical Modeling of Air Flow Inside Tobacco Curing Barn", Research's report, Department of Mechanical Engineering, Faculty of Engineering, Chiang Mai University.

[72] Hwang, C. C., 1993, "A Comparison of the Linear and Nonlinear k-l Turbulence Models in Combustors", Trans. ASME J. of Fluid Engineering, 115, pp. 93-102.

[73] Lin, C. A. and Lu, C. M., 1994, "Modeling three-dimensional gas-turbine combustor model flow using second-moment closure", AIAA Journal, Vol. 32, No. 7, pp. 1416-1422.

[74] Donghoon, S., Chang, K. R., and Sangmin, C., 1998, "Computational Fluid Dynamics Evaluation of Good Combustion Performance in Waste Incinerators", Journal of the Air & Waste Management Association, Vol. 48, Issue 4, pp. 345-351.

[75] Bubpamala, W., 2007, "Research and Development of Human Crematory for Energy Saving", Master Degree's Dissertation: King Mongkutt's University of Technology North Bangkok.

[76] Munson, B. R., Yong, D.F. and Okiishi, T. H., 1998, "Fundamentals of Fluid Mechanics", Third Edition, New York: John Wiley & Sons.

[77] Versteeg, H. K. and Malasekera, W., 1995, "An Introduction to Computational Fluid Dynamics", New York: John Wiley & Sons.

[78] Promvonge, P., and Silapabanleng, K., 2001, "Experimental Study of Combustion Characteristics in a Rice Husk Fired Vortex Combustor", Proceedings of IECEC 36th intersociety Energy Conversion Engineering Conference, Paper No. RE17, July 29-August 2, Savannah, Georgia, 2001.

[79] Courant, R., Isaacson, E., and Rees, M., 1952, "On the Solution of Non-linear Hyperbolic Differential Equation by Finite Differences", Communications on Pure and Applied Mathematics, Vol. 5, pp.243.

[80] Patanka, S.V. and Spalding, D. B., 1972, "A Calculation Procedure for Heat, Mass and Momentum Transfer in Three-Dimension Parabolic Flow", International Journal of Heat and Mass Transfer, Vol. 15, pp.1787.

[81] Ambatipudi, V., 2010, "SIMPLE Solver for Driven Cavity Flow Problem", Department of Mechanical Engineering, Purdue University.

[82] Patanka, S.V., 1980, "Numerical heat transfer and fluid flow", NY: Taylor & Francis.

[83] Guillaume, B., Gabriel, S., Laurent, Y.M., and Thierry, J. P., 2008, "Mesh Dependency of Turbulent Reacting Large-Eddy Simulations in a Gas Turbine Combustion Chamber", Quality and Reliability of Large-Eddy Simulations, Ercoftac Series, Vol. 12, pp. 319-330.

[84] Achawangkul, Y., Maruyama, N., Chaichana, C., Hirota, M., and Teeratitayangkul, P., 2014, "Computational Fluid Dynamics for biomass producer gas burner development to be used in the cremation process", Proceeding of The International Conference & Utility Exhibition (ICUE 2014) on Green Energy for Sustainable Development, Paper No. ICUE2014_079_O, CD-ROM, pp. 1-5.

[85] Sukumaran, S. and Kong, S.C., 2013, "Modeling fuel NOx formation from combustion of biomass-derived producer gas in a large-scale burner", Combustion and flame, vol. 160, pp. 2159-2168.

Appendices

Appendix A

Experimental Apparatuses' Drawings

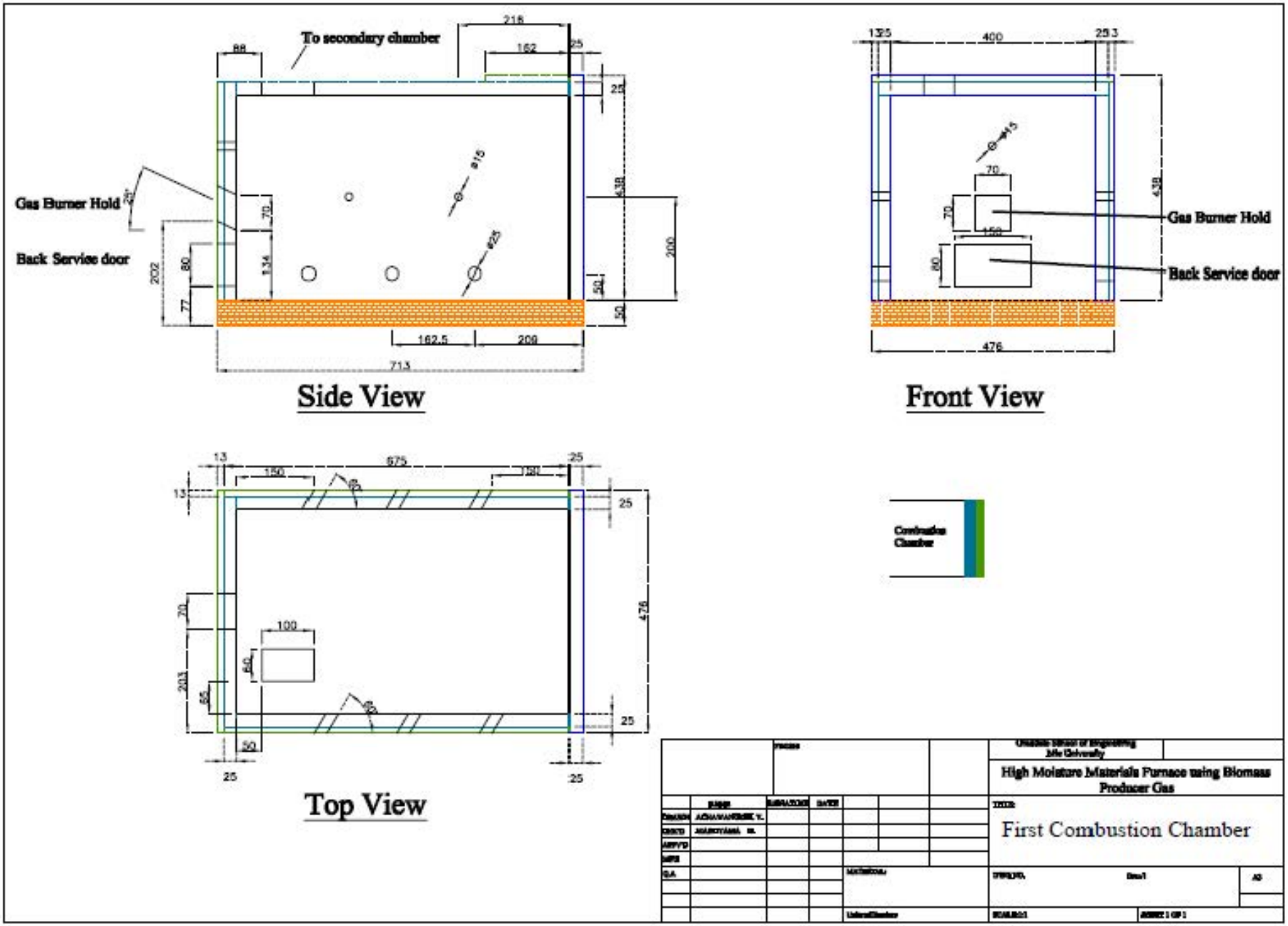
To secondary chamber
Gas Burner Hold
Back Service door
Side View
Front View
Gas Burner Hold
Back Service door
Top View
Combustion Chamber
High Moisture Materials Furnace using Biomass Producer Gas
First Combustion Chamber

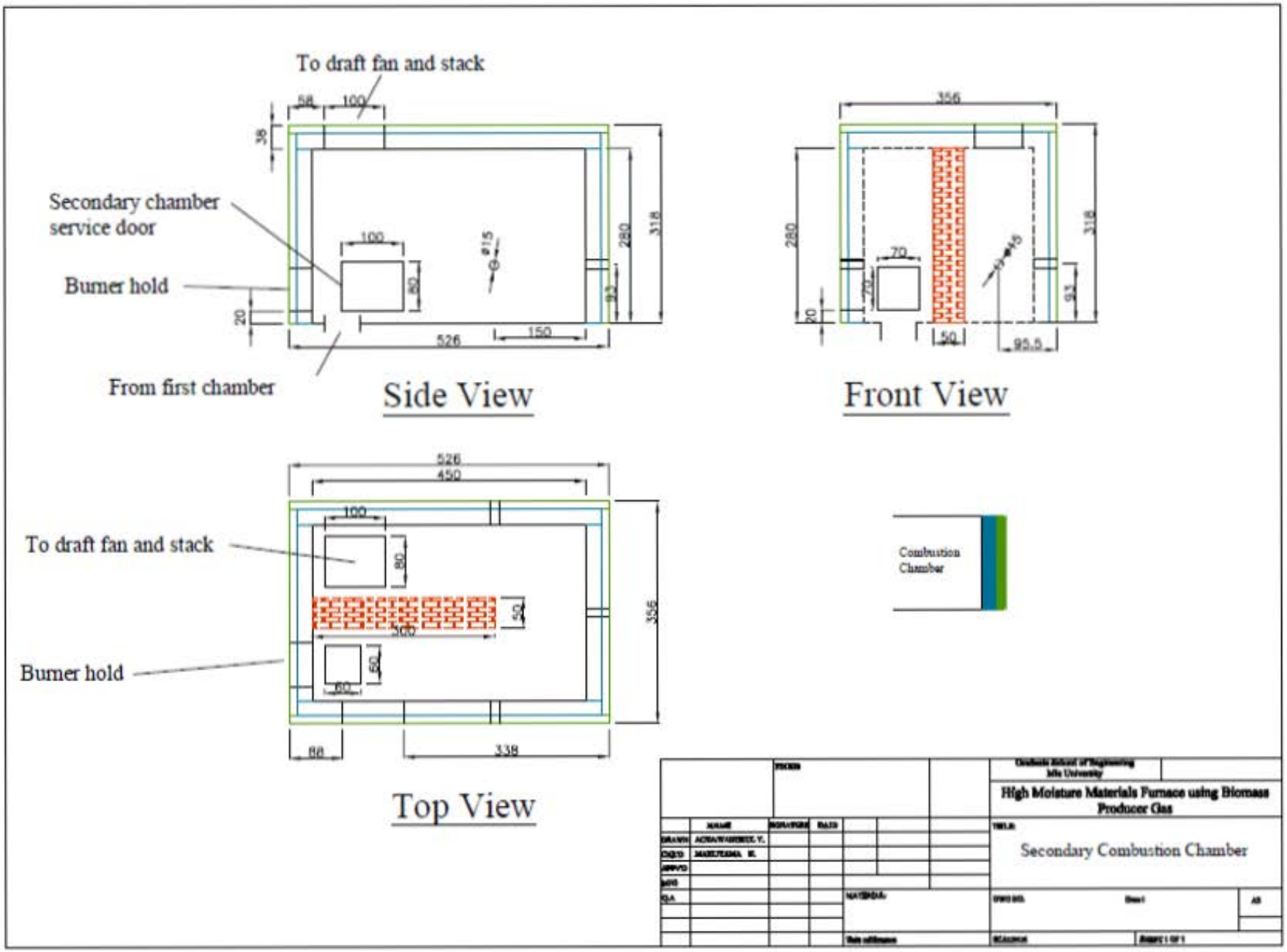
To draft fan and stack
Secondary chamber service door
Burner hold
From first chamber
Side View
Front View
To draft fan and stack
Burner hold
Top View
Combustion Chamber
High Moisture Materials Furnace using Biomass Producer Gas
Secondary Combustion Chamber

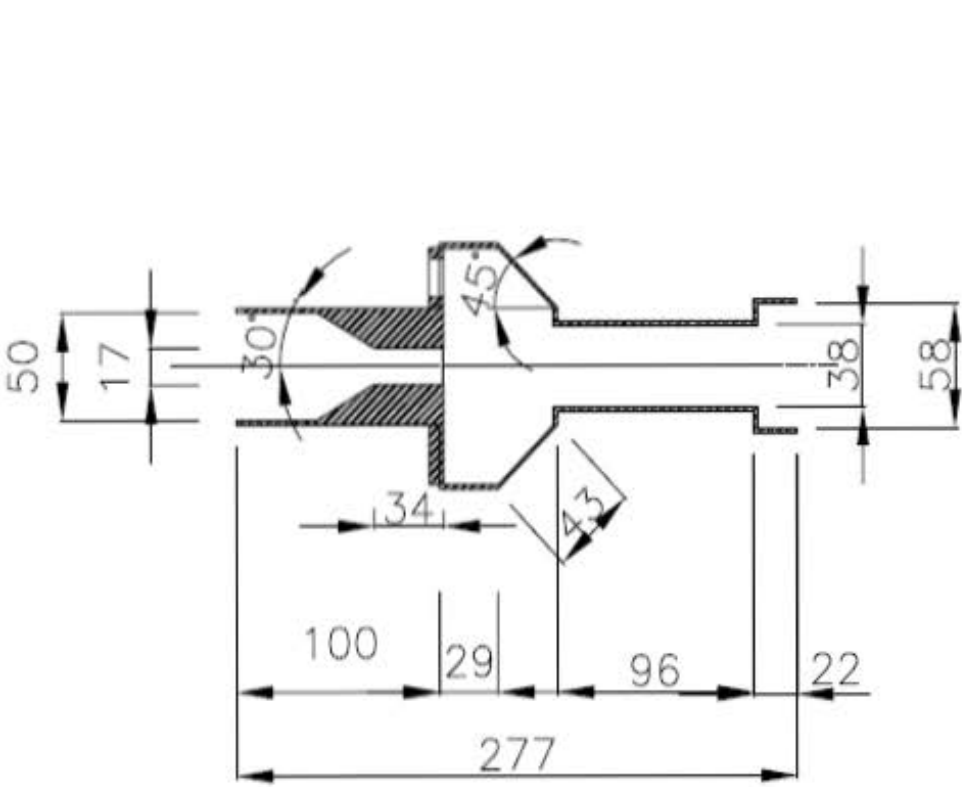

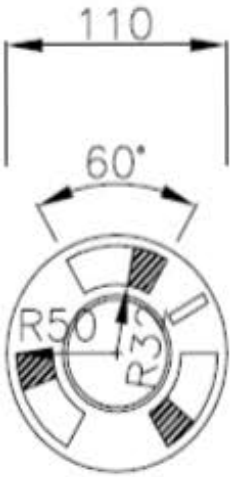

Sliding Shutter

						Chukwuka School of Engineering, Abia University
						High Moisture Materials Furnace using Biomass Producer Gas
	NAME	SIGNATURE	DATE			TITLE: Gas Burner
DRAWN	AGBATAROSOLU T.					
CHKD	AMAECHINA H.					
APPVD						
MFG						
Q.A				MATERIAL:		DWG NO. / Sheet / A3
						SCALE(1:1) / WEIGHT / SHEET 1 OF 1

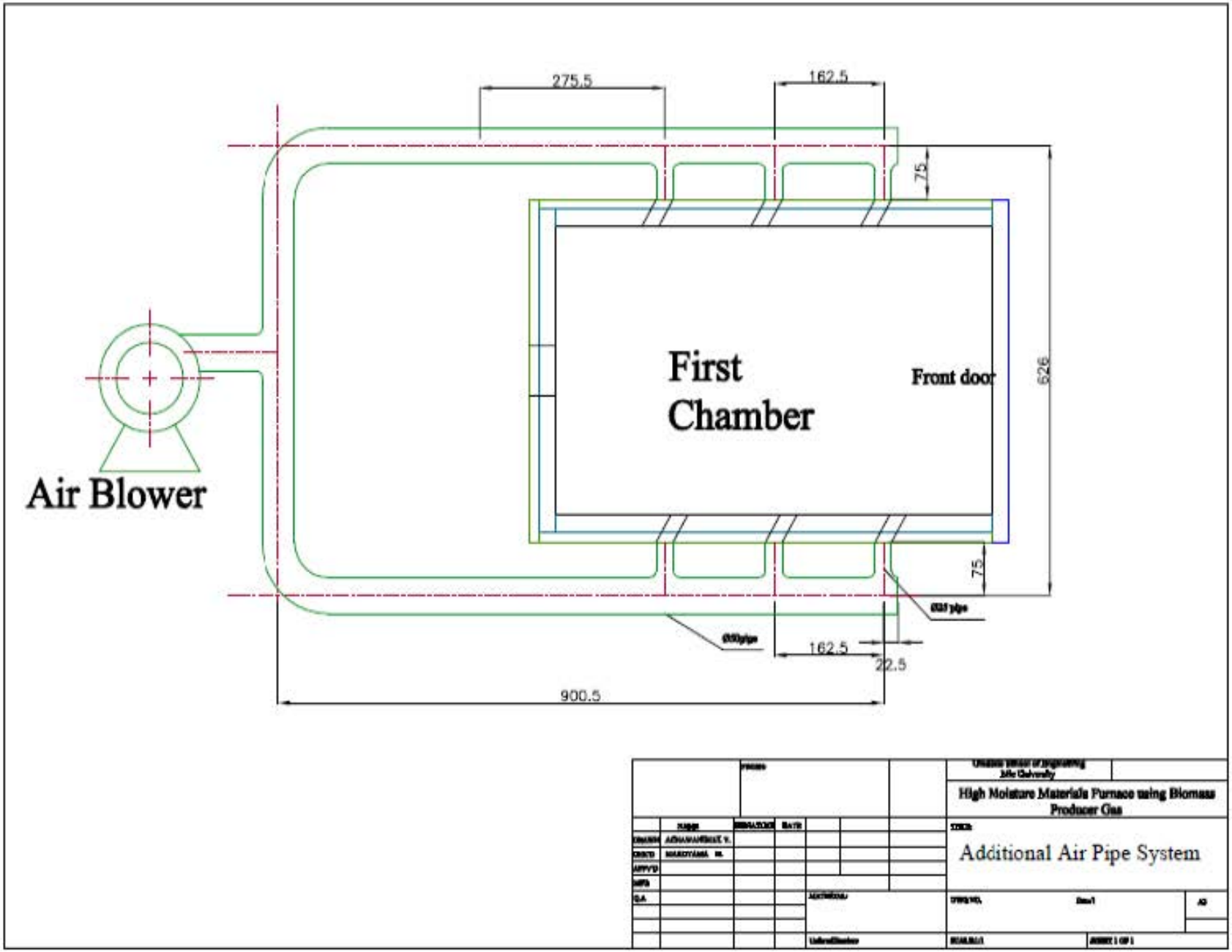
275.5
162.5
75
626
First
Chamber
Front door
Air Blower
75
162.5
22.5
900.5
High Moisture Materials Furnace using Biomass Producer Gas
Additional Air Pipe System

Appendix B

Specific Properties of Materials

Specific Properties of Materials

1. Incinerator's construction materials

1.1 SK30 refractory brick

Density, ρ , (kg/m^3)	1,920
Thermal Conductivity, k, (W/m K)	1.18
Specific Heat, c_p, (kJ/kg K)	0.79

1.2 Ceramic fiber

Density, ρ , (kg/m^3)	288
Thermal Conductivity, k, (W/m K)	0.13
Specific Heat, c_p, (kJ/kg K)	0.359

1.3 Metal sheet

Density, ρ , (kg/m^3)	7,854
Thermal Conductivity, k, (W/m K)	45.3
Specific Heat, c_p, (kJ/kg K)	0.434

2. Fresh chicken meat

2.1 Thermal conductivity at any temperature, k, (W/m K)

Temperature (K)	k, (W/m K)
198	1.60
233	1.49
253	1.35
273	0.48
293	0.49

2.2 Specific properties (at 0^{o}C)

Density, ρ , (kg/m^3)	1,050
Thermal Diffusivity, α , (m^2/s)	0.13×10^{-6}
Specific Heat, c_p, (kJ/kg K)	3.56
Latent heat of fusion (kJ/kg)	247

LIST OF PUBLICATIONS

1. Reviewed Journal Papers

5) Yaowateera Achawangkul, Naoki Maruyama, Chatchawan Chaichana, Masafumi Hirota, Akira Nishimura and Pimpawat Teeratitayangkul, **CFD analysis of double-chambered crematories using biomass producer gas as a fuel source**, *International Journal of Modern Engineering Research (ISSN: 2249-6645)*, Vol. 3, Issue 6, (2013), pp. 3493-3499.
6) Yaowateera Achawangkul, Naoki Maruyama, Chatchawan Chaichana, Masafumi Hirota and Pimpawat Teeratitayangkul, **Study and Evaluation for the Double-Chambered Incinerator Using Biomass Gas-Derived From Gasification**, *International Journal of Modern Engineering Research (ISSN: 2249-6645)*, Vol. 3, Issue 6, (2013), pp. 3818-3824.
7) Yaowateera Achawangkul, Naoki Maruyama, Masafumi Hirota, Chatchawan Chaichana and Twarath Sutabutr, **Analysis of the biomass gasification-based shape of the crematory's secondary chamber by using Computational Fluid Dynamics**, *International Organization of Scientific Research Journal of Engineering (ISSN: 2250-3021)*, Vol. 4, Issue 2, (2014), pp. 17-23.
8) Yaowateera Achawangkul, Naoki Maruyama, Chatchawan Chaichana and Masafumi Hirota, **Biomass gasification utilization for double-chambered crematory**, *Energy Procedia (ISSN: 1876-6102)*, Elsevier, in press.

2. Other Journal Paper

1) Naoki Maruyama, Shujun Hou, Masafumi Hirota and Yaowateera Achawangkul, **A New Bi-level Program Based on Unblocked Reliability for a Continuous Road Network Design**, *International Journal of Modern Engineering Research (ISSN: 2249-6645)*, Vol. 4, Issue 3, (2014), pp. 87-97.

3. Proceeding Papers (Reviewed)

1) Yaowateera Achawangkul, Naoki Maruyama, Chatchawan Chaichana and Masafumi Hirota, **Biomass gasification utilization for double chambers crematory**, Proceeding of 2013 International Conference on Alternative Energy in Developing Countries and Emerging Economies (2013 AEDCEE), (2013), pp. 423-427.
2) Yaowateera Achawangkul, Naoki Maruyama, Masafumi Hirota and Chatchawan Chaichana, **Energy balance evaluation for double chambers crematory using biomass producer gas as fuel**, Proceeding of The Fifth International Conference on Science, Technology and Innovation for Sustainable Well-Being (STISWB V), Paper No. MME11, CD-ROM, (2013), pp. 1-7.
3) Yaowateera Achawangkul, Naoki Maruyama, Chatchawan Chaichana, Masafumi Hirota and Pimpawat Teeratitayangkul, **Computational Fluid Dynamics for biomass producer gas burner development to be used in the cremation process**, Proceeding of The International Conference & Utility Exhibition (ICUE

2014) on Green Energy for Sustainable Development, Paper No. ICUE2014_079_O, CD-ROM, (2014), pp. 1-5.

4) Yaowateera Achawangkul, Naoki Maruyama, Chatchawan Chaichana, Masafumi Hirota, Surat Sedpho and Twarath Sutabutr, **Evaluation on environmental impact from the utilization of fossil fuel and biomass producer gas in the double-chambered crematories**, Proceeding of The 4th International Conference on Green and Sustainable Innovation 2014 (ICGSI 2014), to be published.

4. Poster Presentations

1) Yaowateera Achawangkul, Naoki Maruyama, Chatchawan Chaichana, Masafumi Hirota and Akira Nishimura, **Research and demonstrate for three stages rice husk gasification system**, Proceeding of The 1st International Symposium for Sustainability by Engineering at MIU, (2011), pp. 155-157.
2) Yaowateera Achawangkul, Naoki Maruyama, Masafumi Hirota, Chatchawan Chaichana and Pimpawat Teeratitayangkul, **Study for biomass producer gas utilization for high moisture materials combustion in double chambers incinerator**, Proceeding of The International Symposium on EcoTopia Science, Paper No. P-5-21, CD-ROM, (2013), p. 1.

5. Other Proceeding Papers

1) Yaowateera Achawangkul, Naoki Maruyama, Masafumi Hirota, Mayuraphan Sajjakulnukit, Peeraya Siriput, Natthapong Ngampradit and Thaweep Polsen, **Hydrogen Production by using Circulating Fluidized-Bed Reactor**, Proceeding of The 10th International Energy Conversion Engineering Conference (IECEC 2012), http://arc.aiaa.org/doi/abs/10.2514/6.2012-4053, (2012), pp. 1-11.
2) Yaowateera Achawangkul, Kulachate Pianthong, Decho Chanhom, Songkran Khamsri and Pisit Sanguantrakarnkul, **Study and Demonstration on Biomass Gasification System for Water Pumping and Irrigation**, Proceeding of The 3rd International Conference on Green and Sustainable Innovation 2012 (ICGSI 2012), CD-ROM, (2012), pp. 202-208.
3) Naoki Maruyama, Youhei Watanabe, Hiroaki Ito, Yaowateera Achawangkul and Masafumi Hirota, **Theoretical analysis for energy balance of material recycle using circulation type superheated steam evaporation system**, Proceeding of The Fifth International Conference on Science, Technology and Innovation for Sustainable Well-Being (STISWB V), Paper No. MME23, CD-ROM, (2013), pp. 1-6.
4) Naoki Maruyama, Youhei Watanabe, Hiroaki Ito, Yaowateera Achawangkul and Masafumi Hirota, **Theoretical analysis for energy balance of circulation-type superheated steam degreasing system**, Proceeding of The International Symposium on EcoTopia Science, Paper No. P-5-20, CD-ROM, (2013), p. 1.
5) Naoki Maruyama, Youhei Watanabe, Hiroaki Ito, Yaowateera Achawangkul and Masafumi Hirota, **Oily Waste Metal Recycle using Circulation-type a Superheated Steam Degreasing System**, Proceeding of The International Conference & Utility Exhibition (ICUE 2014) on Green Energy for Sustainable Development, Paper No. ICUE2014_134_O, CD-ROM, (2014), pp. 1-7.